JOHANNES GUTENBERG UNIVERSITÄT MAINZ

RHEOLOGY AND THERMODYNAMICS OF STARCH-BASED HYDROGEL–MIXTURES

DISSERTATION

zur Erlangung des Grades eines „Doktor der Naturwissenschaften“

im Promotionsfach Chemie

am Fachbereich Chemie, Pharmazie und Geowissenschaften
der Johannes Gutenberg-Universität
in Mainz

Natalie Ruß
geb. in Kirchheim-Bolanden

Mainz, April 2016

MAX-PLANCK-GESELLSCHAFT

“A Thing is a Thing, not what is said of that Thing.”

Abstract

The present work presents two different ways to achieve physically modified tapioca starch and the influence on mechanical properties of an aqueous starch paste is investigated. A completely cold soluble tapioca starch powder is produced by spray drying a previously gelatinized starch paste. Rehydrating the received white powder forms a viscous paste with significant loss in elasticity. Heating of a native tapioca starch suspension in contrast yields highly viscous paste with dominating elastic behavior. The combination of the spray dried tapioca starch with nongelling food hydrocolloids, such as xanthan gum, ι-carrageenan, and guar gum restores the mechanical properties and creates new starch-based thickening agents with stable structure. Rheological measurements of a gelatinized native tapioca starch paste compared to a rehydrated paste made from the spray dried starch show significant differences in viscosity and viscoelastic properties, which depend on temperature, amplitude, frequency, or shear rate. Further rheological, optical, and scattering investigations indicate weakening of the amylose network structure generated by the harsh shear and heat conditions during the spray drying process. The addition of water soluble hydrocolloids stabilizes the degraded gel structure by different mixing behaviors. According to the molecular nature of the added hydrocolloids, such as chain flexibility or charge distribution, different phase behavior in the starch-based composite system is induced. Thus, the stepwise replacement of starch by hydrocolloids influences the mechanical properties to various extents. The mixtures of spray dried tapioca starch and hydrocolloids have hydrocolloid dominated functional properties, and mixing the cold soluble tapioca starch with xanthan gum, ι-carrageenan, or guar gum on dry basis, a thickening effect with a weak gel character can be easily produced by hydration without heating. Depending on the desired application, the mechanical properties and texture can be controlled and tuned by the choice of hydrocolloid and by varying the mixture composition. Amylose and ι-carrageenan molecules are thermodynamically compatible, and a stable and well-mixed phase is formed. The mixture with xanthan gum and guar gum results in a phase separation where the hydrocolloid molecules separate into local domains. Phase separation is induced by thermodynamic incompatibility and mutual exclusion effects between amylose and xanthan or guaran molecules. The different phase behavior in the mixed systems is supported by confocal laser scanning microscopy and by covalent labeling of the hydrocolloids with specific fluorescence dyes.

Kurzfassung

In der vorliegenden Arbeit werden zwei Methoden der physikalischen Modifikation an Tapiokastärke und deren Einflüsse auf die mechanischen Eigenschaften einer wässrigen Dispersion präsentiert. Dazu wird zunächst eine vollständig kaltlösliche Tapiokastärke durch Sprühtrocknung einer zuvor gelatinisierten Stärkepaste hergestellt. Das erhaltene weiße Pulver bildet nach Resuspension eine schwach viskose Dispersion aus und zeigt einen deutlichen Verlust des Elastizitätsmoduls. Native Tapiokastärke bildet hingegen, nach ausreichender Wärmezufuhr, in wässriger Suspension eine hochviskose Paste mit dominierenden elastischen Anteil aus. Durch Zugabe von nichtgelierenden, wasserlöslichen Hydrokolloiden, wie Xanthan, ι-Carrageen oder Guar, können die viskoelastischen Eigenschaften der nativen Stärkepaste zurückgewonnen werden wodurch die Herstellung von neuen und stabilen stärkebasierten Verdickungsmitteln ermöglicht wird. Rheologische Untersuchungen der Viskosität und der viskoelastischen Eigenschaften einer gelatinisierten nativen Stärkepaste im Vergleich zu einer rehydrierten Paste der sprühgetrockneten Stärke, zeigen in Abhängigkeit von Temperatur, Amplitude, Frequenz und Scherrate deutliche Unterschiede. Durch zusätzliche rheologische und optische Analysen, sowie verschiedenen Streuungsversuchen kann eine deutliche Schwächung des Amylosenetzwerks, verursacht durch die hohe Scher- und Hitzebelastung während des Sprühtrocknungsprozesses, aufgezeigt werden. Der Einsatz der wasserlöslichen Hydrokolloide stabilisiert die Gelstruktur durch unterschiedliche Mischungsverhältnisse. Je nach molekularer Beschaffenheit der Hydrokolloide, wie Kettenflexibilität oder Ladungsverteilung, kann in den stärkebasierten Kompositsystemen verschiedenes Phasenverhalten generiert werden. Dabei können die mechanischen Eigenschaften des Mischsystems durch schrittweises Ersetzen von sprühgetrockneter Stärke unterschiedlich stark beeinflusst werden. Die Mischungen aus sprühgetrockneter Tapiokastärke und Hydrokolloiden zeigen deutlich Hydrokolloid dominierte funktionelle Eigenschaften, wodurch ein Verdickungseffekt mit schwachem Gelcharakter bereits ohne Wärmezufuhr induziert werden kann. Je nach gewünschter Anwendung können so die mechanischen Eigenschaften des Mischsystems durch die Wahl des entsprechenden Hydrokolloids und durch die Mischungskomposition angepasste werden. Zwischen Amylose- und ι-Carrageenmolekülen kann eine gewisse thermodynamische Kompatibilität gefunden werden, wodurch eine gemischte Phase mit stabiler Netzwerkstruktur aufgebaut wird. In der Mischung mit Xanthan und Guar hingegen, resultiert eine Phasenseparation, in der sich die Hydrokolloidmoleküle in lokalen Domänen separieren. Diese Phasenseparation ist durch molekulare Inkompatibilität und gegenseitige Ausschlusseffekte bedingt. Mit Hilfe von konfokaler Laserscanning Mikroskopie und durch das kovalente Färben der Hydrokolloide mit Fluoreszenzfarbstoffen, kann das unterschiedliche Phasenverhalten in den Kompositgelen nachgewiesen werden.

Content

List of Figures

List of Tables

List of Abbreviations

A	Deformation area [m^2]
α	Cone angle [°]
χ	Flory-Huggins exchange parameter
CLSM	Confocal laser scanning microscopy
CMC	Carboxyl methyl cellulose
c, c^*	Concentration, critical concentration [$molm^{-3}$]
δ	Phase shift [°]
DLS	Dynamic light scattering
DMSO	Dimethyl sulfoxide
DSC	Differential scanning calorimetry
DP	Degree of polymerization
D_s	Diffusion coefficient [m^2s^{-1}]
ΔG_m	Gibb's free enthalpy of mixtures [J]
ΔH_m	Mixtures enthalpy [J]
ΔS_m	Mixtures entropy [JK^{-1}]
$\frac{\partial W}{A\partial t}$ / $\frac{\partial N}{A\partial t}$	Quantity of heat *W* or particles *N* per area *A* and time *t*
$\frac{\partial T}{\partial x}$ / $\frac{\partial c}{\partial x}$	Temperature T or concentration c gradient
E_a	Activation energy [J]
FITC	Fluorescin-5-isothiocyanat
$\vec{F}$	Shearing force [N]
f	Frequency [Hz or $rads^{-1}$]
γ	Shear strain [dimensionless]
$\dot{\gamma}$	Shear rate [s^{-1}]
GG	Guar gum
$G(q,t)$	Correlation function of intensity as function of wave vector q and time t
G	Shear modulus [Pa]

G'	Storage modulus [Pa]
G''	Loss modulus [Pa]
ιC	ι-Carrageenan
$I(q,t)$	Scattering intensity as function of wave vector q and time t
J_W	Heat/energy flux [$Js^{-1}m^{-2}$]
J_N	Material/particle flux [$mols^{-1}m^{-2}$]
K	Power law consistency coefficient [Pa]
λ_s	Thermal conductivity coefficient [$JK^{-1}m^{-1}s^{-1}$]
LM	Light microscopy
LCST	Lower critical solution temperature
M	Molecular weight [$gmol^{-1}$]
N	Power law flow behavior index [dimensionless]
NA	Numerical aperture
η	Viscosity [Pas]
η_{app}	Apparent viscosity [Pas]
η_{cold}	Cold viscosity [Pas]
$\eta_{initial}$	Initial viscosity [Pas]
η_{peak}	Peak viscosity [Pas]
η_0	Zero shear viscosity [Pas]
$[\eta]$	Intrinsic viscosity [mLg^{-1}]
φ_i, λ_i	Volume fraction *i* [dimensionless]
PPI	Pseudoplastic index [dimensionless]
R	Ideal gas constant [$JK^{-1}mol^{-1}$]
R	Plate radius [mm]
R_h	Hydrodynamic radius [nm]
ρ	Density [Kgm^{-3}]
SDTS	Spray dried tapioca starch
SEM	Scanning electron microscopy
σ	Shear stress [Pa]

σ_0	Yield stress [Pa]
$\tan\delta$	Loss factor [dimensionless]
T	Temperature [K]
T_{endset}	Endset temperature [°C]
T_m	Melting temperature [°C]
T_{onset}	Onset temperature [°C]
$T_{pasting}$	Pasting temperature [°C]
T_{peak}	Peak temperature [°C]
TS	Native tapioca starch
UCST	Upper critical solution temperature
$\vec{v}$	Velocity [ms^{-1}]
VTP	Viscosity-temperature profile
ω	Angular frequency [$rads^{-1}$]
WD	Working distance
XG	Xanthan gum
XRD	X-ray diffraction

1 Introduction

Starch is one of the most widely used functional and flexible food stabilizers for both thickening and gelling. Since early history, humans have always eaten starchy foods derived from seeds, roots, and tubers and they developed agricultural production of grain crops such as barley, rice, wheat, or corn [1]. Today, the largest industrially produced crops that are cultivated for starch extraction are cassava (tapioca), corn (maize), potatoes, and wheat; on a more limited industrial scale, rice, peas, sweet potatoes, and mung beans are also produced [2]. Starch in its native form is a versatile product and the raw material for production of many modifications, sweeteners, and ethanol. It has many applications in the nonfood industry, e.g. as a component of many paper grades or as polymeric material. These starch-based polymeric materials play a significant role due to the fact that starch can be produced from a wide variety of sources, is annually renewable and inherently biodegradable. In blends with synthetic polymers, starch can be used in packaging, as disposables, or as tablet coating [3]. A more common use of starch is their wide applications in the food industry in order to thicken, gel, add stability, replace, or extend the use of more costly ingredients. Starch is also favored for its availability, low cost and unique properties. For some applications starches are inherently unsuitable and thus have to be modified chemically or physically to enhance their positive attributes and to minimize their defects. In addition, the admixture of proper hydrocolloids can also overcome the shortcomings of native starches, and these combinations have been used in processed foods since at least 1950 [4]. Nevertheless, the structure and functional properties of starch are still not fully comprehended as each starch is unique in terms of its granule organization and the structure of its constituent polymers. In addition, the behavior of starches from different sources is limited and not all granules of a single starch preparation behave identically. In particular, the interaction that takes place in a starch–hydrocolloid mixture and what happens when starch and hydrocolloid are heated together are not yet understood. The investigation of such composite systems is currently a difficult undertaking on account of the complexity of the systems, the variety of granular structures, starch polymers and hydrocolloid molecules as well as a strong dependence on composite paste preparation. Obviously, there is a need for more systematic and fundamental work on structural formation and rheological properties in mixed starch–hydrocolloid gels, to provide the basis for preparing and controlling the structure and texture of processed formulated products that contain starch.

This work focuses on the rheology and phase behavior of tapioca starch-based hydrogel–mixtures. Compared to other starches, tapioca starch is a unique native

material with distinct properties. The low amylose, low lipid and low protein content, combined with the high molecular weight of its amylose, make tapioca a unique native starch for direct use in food and industrial applications and an excellent starting material for modification into special products [5]. To obtain tapioca starch pastes, a starch–water suspension has to be heated up to 95 °C, while stirring intensively. Many applications in the food industry or kitchen require a thickening effect at ambient conditions, either to simplify the handling or to protect heat- sensitive flavors or spices. Therefore, the central idea behind this work is to provide a basis for the production of a cold soluble tapioca starch, which disintegrates at room temperature. At the same time the typical characteristics of a tapioca starch paste are maintained, such as high adhesiveness, clear and transparent appearance, smooth texture, and lack of special flavors. To accomplish this, first a cold soluble pregelatinized tapioca starch is produced by spray drying an already gelatinized paste. Then, by mixing this physically modified (spray dried) starch with the appropriate cold soluble thickening agents, it is possible to tune and adjust the mechanical properties of the rehydrated modified starch paste. The mechanical properties of the resulting starch–hydrocolloid mixtures strongly depend on the physicochemical properties of the added polymers. Therefore, three hydrocolloids with distinctly differing flexibility and charge have been chosen to study the limiting cases of mixtures with very stiff or very flexible polymer chains: xanthan gum as a highly charged polysaccharide with a stiff molecular structure, ι-carrageenan, as a charged polyelectrolyte but with a sufficiently flexible backbone, and guar gum, as a neutral hydrocolloid with a flexible coil conformation.

However, to date rehydrated solutions of spray dried tapioca starch pastes and their mixtures with other cold soluble polysaccharides have not been investigated, though there is an increasing market interest in products of physically modified starches. In addition, the consumer’s growing demand for healthy products with natural ingredients has steadily increased and encouraged the development of formulations without synthetic food additives. In the field of starch modification, there is always the challenge of adjusting the texture and functional properties according to different applications or products. In particular, pregelatinized starches produced by physical modification are used as a thickening agent in pie fillings, puddings, sauces, and baby foods to generate a pulpy texture [6]. This work explores one possibility of how to produce a physically modified tapioca starch where the mechanical properties and texture can be controlled and adapted according to the desired application in a wide frequency and amplitude range. By mixing the cold soluble tapioca starch with xanthan gum, guar gum, or ι-carrageenan on a dry basis, a thickening effect with a weak gel character can be easily produced by hydration without heat addition. The choice of hydrocolloid and the variation of mixture composition both enable a concrete adjustment on a widespread range of applications and processes.

Chapters 2, *3*, and *4* serve as an introduction and provide a basis for the relevant background. Starting with a brief overview of food biopolymers in general, the reader is introduced to the chemistry and functional properties of starch and nonstarch polysaccharides (*Chapter 2*). Some basics concerning thermodynamics and phase behavior in mixed polysaccharide systems are given in *Chapter 3*; *Chapter 4* leads into fundamental considerations on rheology, especially relevant in the case of fluid foods, food gums, and gels. In *Chapter 5* the materials used, sample preparation, methodologies and performed experiments are presented and discussed.

Chapter 6 starts with the presentation of the gelatinization process, formed gel structure and observed viscoelastic properties of the native tapioca starch. Furthermore, the influence of the spray drying process on gel structure and viscoelastic properties is discussed. Compared to the initial paste, rehydrated pastes made from such modified starches lose some of their elastic properties, due to degradation of the starch components, which results in weaker network structures. Chapter 6 investigates the molecular consequences of a spray drying process on a gelatinized tapioca starch paste and highlights the macroscopic alterations of the viscoelastic properties.

The initial viscoelastic properties can be regained and adjusted by mixing the spray dried starch with other cold soluble thickening agents and is a fundamental part of *Chapter 7*. The mechanical properties of the starch-based mixtures can be tuned and designed by successive addition of hydrocolloids and are followed analytically by rheological measurements. The interaction that takes place in a composite gel between the investigated hydrocolloids and the native tapioca starch allow conclusions to be drawn for the mixed systems with the spray dried starch. Based on the results, a phenomenological model describing the different phase behaviors in the investigated starch–hydrocolloid mixtures is presented in *Chapter 8*. The addition of flexible ι-carrageenan is supposed to result in the formation of a well-mixed system with strong intermolecular interaction between the different polymers. On the other hand, the mixture with xanthan gum and guar gum results in a separation into local domains and a mutual exclusion of starch and hydrocolloids.

2 Food biopolymers

Food biopolymers and their interaction in mixtures are mainly responsible for the structure–properties relationship in food [7]. The main constructing materials of food are carbohydrates, proteins, lipids, and enzymes, which are entrapped in water, the main medium, solvent and plasticizer (figure 2.1). Water represents one of the major components and determines the texture of food products, containing 0% in e.g. cooking oils or up to 87% in milk or 90% in several fruits [8]. The interaction of water with food constituents has high impact on food processing and quality.

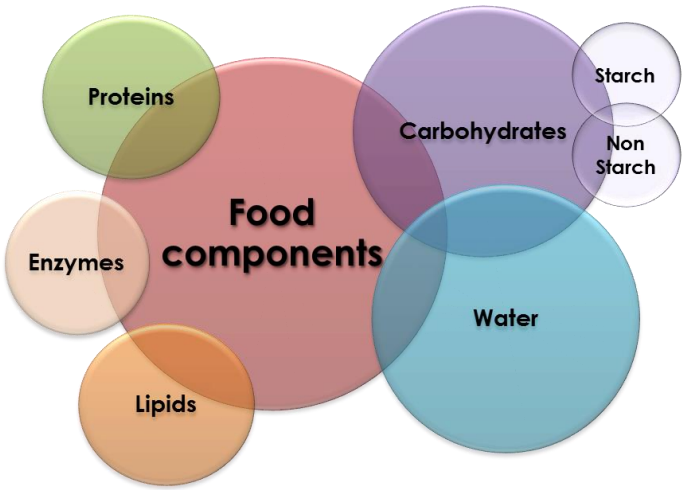

Fig. 2.1 Schematic presentation of food composition.

After water, carbohydrates are the most abundant and widely distributed food components. They include mono-, di-, and oligosaccharides, like sugars, and polysaccharides [9]. Polysaccharides can be separated into two groups: starches and nonstarch polysaccharides both of which belongs to the group of *hydrocolloids* [10]. Proteins, lipids, and enzymes complete foods and make them to a multicomponent molecular system. Thus interaction between components is more significant than the chemical and physical properties of the single components. Food structures are mainly arranged by noncovalent, nonspecific interaction of proteins and polysaccharides in an aqueous medium [11]. Most biopolymers form physical gels, structured by weak interaction (hydrogen, electrostatic, hydrophobic). In this work carbohydrates and their interplay with water are investigated, with main focus on starch and other polysaccharides as thickening and gelling agents. They are presented in more detail in the following section. Water presents a universal plasticizer and solvent for naturally occurring organic materials and is an exceptional solvent due to its strong polarity

which enables interaction with itself as well as with other chemical groups by hydrogen bonding [12].

2.1 Hydrocolloids and hydrogels

Nowadays hydrocolloids are widely used in a variety of industrial sectors to perform a number of functions. In food products they are used as thickening, gelling, emulsifying or stabilizing agent as well as to control the crystal growth of ice and sugar [13]. Even though they are often used only in concentrations less than 1%, they have significant influences on the textural and organoleptic properties of food [14]. Changes in modern and fast lifestyle and the always growing pursuit of dietary and healthy food raise the request of readymade meals, functional food and high fiber, low fat food products. Consequently, the increasing demand for hydrocolloids used in food products for example, as fat replacers, stabilizers or texturizers, lead to an always growing hydrocolloid market (valued at $4.4 billion and a total volume of about 260.000 tons [14]).

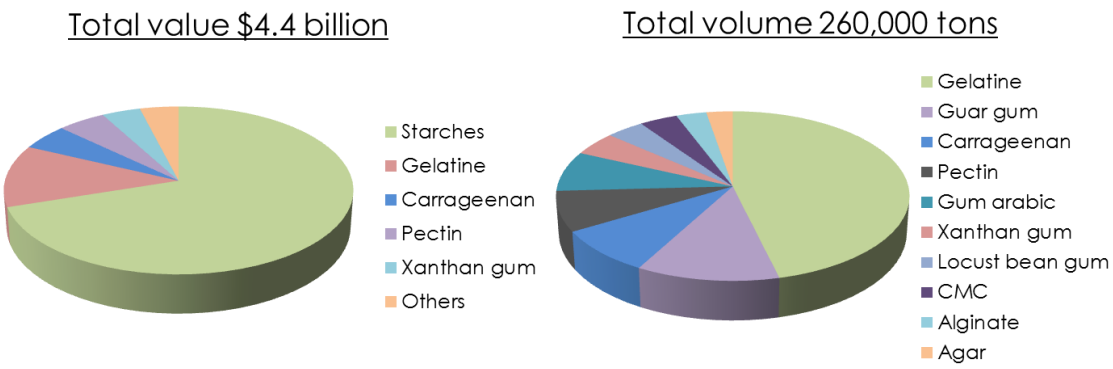

Fig. 2.2 Value and volume of world market of individual hydrocolloids. According to [14].

Hydrocolloids consist of long-chain polymers, which have thickening and gelling properties while dissolving in water. The extent of thickening varies with the molecular composition and nature of the hydrocolloids. Due to the high amount of hydroxyl groups they show a huge affinity to bind water molecules, but possess also slight hydrophobic properties [15]. While all hydrocolloids have the ability to thicken only a few are also able to form a gel. At the molecular level, gelation is the formation of a continuous network of polymer molecules consisting of a framework of polymer chains. In most biopolymer gels, the polymer chains form extended junction zones by means of side by side associations of a physical nature, in contrast to the typical single covalent bonds found in chemically crosslinked networks. These physical junction zones can be formed by simple point crosslinks, extended crosslinks, where at least two chains are bound or by a formation of multiple helical structures (figure 2.2).

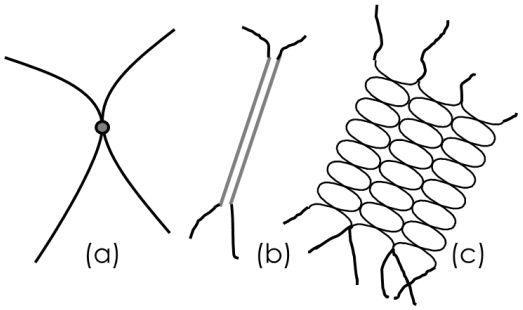

Fig. 2.3 Junction zones found in physical gels. a) Point crosslink, b) Extended crosslinks by intermolecular cooperative binding between adjacent segments, c) Multiple helical structures by complex associations. Modified according to [16].

The bonds involved in these junction zones are generally noncovalent such as hydrogen bonds, hydrophobic or ionic interaction [17]. Consequently, in physical gelation the formation and breakdown of the junction zones are usually reversible, the crosslink functionality is very high, and the junction zones have a finite lifetime [18]. The formation of these kinds of transient networks is determined by the chemical composition of the polymer and thus by the stiffness and occupied volume in the solution and by the solvent which constitute the gelling system [16].

2.2 Starch and tapioca starch

Starch occurs in the form of tiny white granules in various sites of plants, for example in cereal grains (maize, rice, wheat, barley, oat, sorghum), in roots (sweet potato, cassava, yam), in tubers (potato), in stems (sago palm) and in legume seeds (pea, bean) and was designed by nature as a plant energy reserve. Therefore, glucose is immobilized by forming a condensation polymer in which glucose chains are linked together by the elimination (condensation) of water and act as long-term energy storage system [19]. Industrially, the main important crops which are cultivated for starch extraction are: cassava for tapioca starch, corn for maize starch, potato or wheat (table 2.1).

Tab. 2.1 Global starch production volumes 2006. Values are in million tons. According to [2].

	Maize	**Wheat**	**Potato**	**Tapioca**	**Other Starches**
South America	1.49	0.03	–	0.76	–
Europe	5.55	3.57	1.99	–	0.10
Asia Pacific	17.83	0.54	0.44	7.12	0.54
North America	25.92	0.56	0.12	0.01	0.20
Rest of the World	0.64	0.27	–	0.03	0.02
Total	54.43	4.96	2.56	7.92	0.86

Besides some applications in the nonfood industry, such as in the paper industry or as biodegradable polymeric materials, starches have their main application in the food industry with the purpose to thicken, gel, stabilize or replace and extend more costly ingredients. There, they are favored due to their availability, low costs and unique properties, which are summarized in more detail in the following sections.

2.2.1 Chemical structure and starch composition

When thinking of the structure of starch two levels of composition have to be considered: the *molecular and chemical structure* and the *microscopic arrangement* into starch granules and how they interact in bulk. All together develop the functional and texturizing properties of different starches depending on botanical source and production process.

Molecular and chemical structure. All starches consist of long-chain polymers of α-linked glucose units, making them digestible by animals in contrast to the β-linked glucose units in cellulose (figure 2.4a).

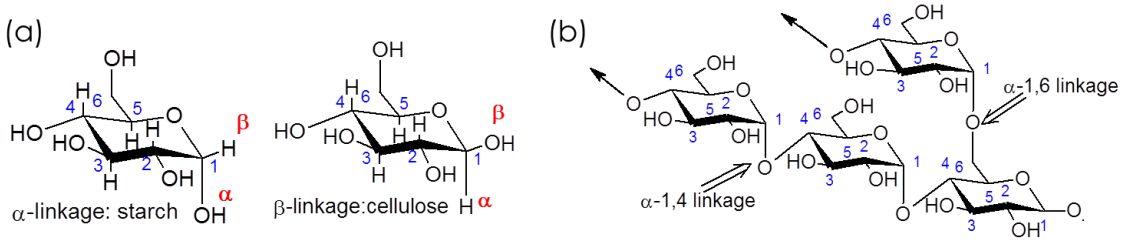

Fig. 2.4 (a) Glucose units linked via horizontal oriented hydroxyl groups (α-linkage) in starch compared to linkages via equatorial oriented hydroxyl groups (β-linkage) in cellulose. (b) Different α-linkages in starch. Linear polymer chains are produced by 1,4-linkage and branching points by 1,6-linkages.

For polymerization the glucose units in starch provide three reactive sites, namely C_1, C_4 and C_6 and two different linkages can be made (figure 2.4b). The reaction between C_1 and C_4 yields linear and elongated polymer chains, whereas the linkage between C_1 and C_6 produces branching points and the beginning of a new linear chain [2]. Regarding this molecular composition two main components of starch can be separated: amylose, which consists of more 1,4-linkages with only a few branching points and side chains; and amylopectin with a highly branched structure. Both, 1,4-linkages and 4–5% 1,6-linkages can be found in amylopectin, resulting in one of the largest natural polymers with molecular weights up to 10^8 g/mol [20]. The α-1,4-linked glucose units enable the formation of a helical configuration, which are typical for the linear and flexible amylose molecules (figure 2.5a). However, the conformation of amylose in aqueous solution is still a matter of debate, and besides a continuous helical conformation, an interrupted helix or even a random coil structure, is assumed. The branching points along an amylopectin chain lead to a cluster formation with helical

side chains (figure 2.5b) [21]. Typical molecular weights of extracted amylose are in the region of 10^5 to 10^6 g/mol and in aqueous solution they can behave as flexible coil with a typical hydrodynamic radius of 7–20 nm [22]. The branching of amylopectin is not random and a bimodal population of chains with two main populations exhibiting a peak DP around 12–14 and ~45 was found [23]. Current models of amylopectin structure depicted short chains of 10–20 units arranged in clusters on longer chains, with the longer chain spanning more than one cluster (figure 2.5b). A consequence of the branching is, regarding its molecular weight, that the amylopectin molecules are relatively compact.

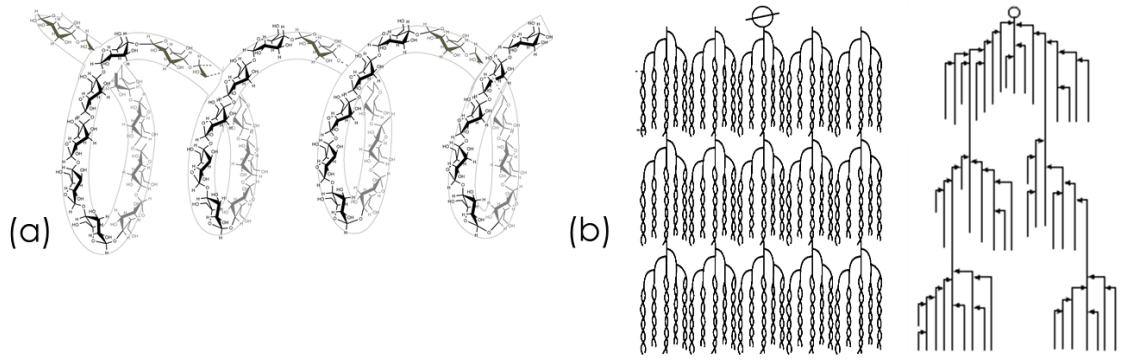

Fig. 2.5 (a) α-1,4-linked glucose units and helical formation in amylose, adapted by [24]. (b) Cluster formation with helical side chains in amylopectin, adapted from [25] and cluster model with short chains arranged in clusters on longer chains, adapted from [26].

Depending on the botanical source the ratio between amylose and amylopectin and their degree of polymerization varies significantly (table 2.2), which determines their different functional properties and allows a target use for different starches. Besides amylose and amylopectin commonly other substances such as lipid (including phospholipids and free fatty acids), phosphate monoesters and proteins/enzymes can be found in starches [27].

Tab. 2.2 Amount and DP of amylose and amylopectin in different starch raw materials. According to [2].

	Amylose (%)	Amylopectin (%)	DP amylose	DP amylopectin
Maize	25–28	72–75	2000	2 000 000
Waxy maize	< 1	> 99	–	2 500 000
Potato	19–21	79–81	10 000	3 000 000
Rice	17–19	81–83	1000	2 000 000
Tapioca	17	83	5000	3 000 000
Wheat	25	75	8000	2 500 000

Microscopic arrangements to starch granules. Starch occurs naturally as water insoluble granules whose form is characteristic of its botanical origin. Amylose and amylopectin are densely packed to these semicrystalline starch granules, which occur in all shapes and sizes from 0.1 to at least 100 µm depending on the botanical source (table 2.3).

Tab. 2.3 Granular size and shape of different starches. Modified according to [2]

	Source	Granular size distribution (µm)	Shape
Maize	Cereal	3–26	Polygonal round
Potato	Tuber	5–100	Oval, spherical
Rice	Cereal	3–8	Polygonal, spherical
Tapioca	Root	4–35	Oval truncated, 'kettle drum'
Wheat	Cereal	1–40	Round lenticular

Starch granules consist of alternating amorphous and semicrystalline concentric layers (figure 2.6a), representing growth rings produced during the biosynthesis of the plant [28]. The semicrystalline, dense layers consist of alternating crystalline and amorphous lamellae (figure 2.6b); the less dense amorphous layers contain more water. The crystalline lamellae are made up of amylopectin double helices which are packed in a parallel fashion; whereas the amylopectin branching points are located in the amorphous lamellae (figure 2.6c).

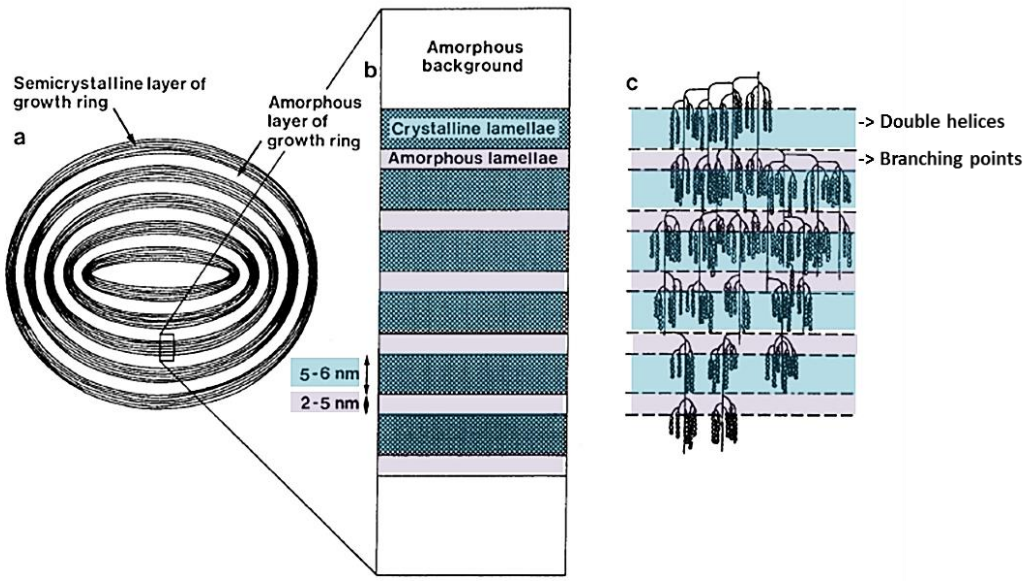

Fig. 2.6 Starch granule structure. (a) Single granule with amorphous and semicrystalline layers. (b) Semicrystalline layer consisting of crystalline and amorphous lamellae. (c) Amylopectin within the semicrystalline layer. Adapted from [29]

The amylopectin double helices can be arranged in three forms of packing, A-, B-, and C-types, which determine the crystallinity and type of the corresponding starch [30]. In

general, most cereal starches exhibit the A-type pattern, some tuber starches and cereal starches rich in amylose the B-type pattern and legume starches yield the C-type pattern. Many authors investigated the cluster formation of amylopectin and fine architecture of starch granules of different botanical sources by X-ray diffraction which are reviewed in detail by Pérez et al. [31], Jane [27] or Tester [32].

However, the detailed starch granule structure is still under discussion and especially the exact location of amylose within the granule remains unclear. It is suggested that amylose is radially oriented as individual chains and randomly interspersed amongst amylopectin in both crystalline and semicrystalline regions [31]. Jane [27] summarized the organization of a starch granule with the recent advances in understanding the granule structure with a schematic picture (figure 2.7).

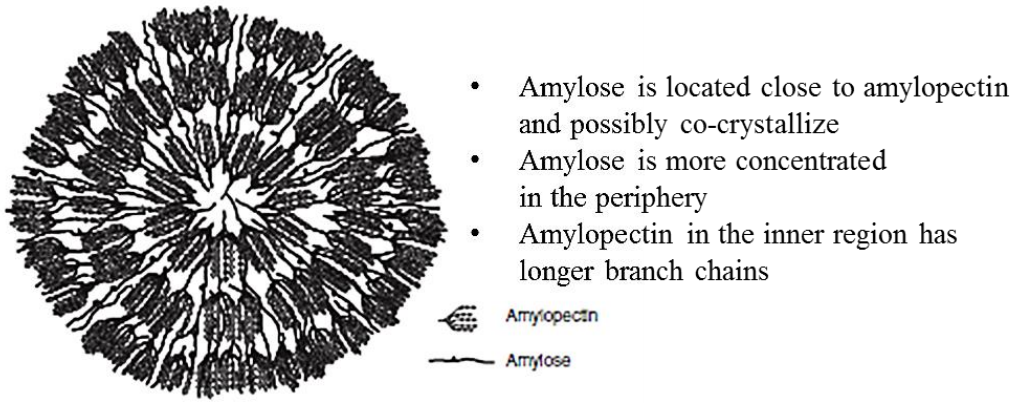

Fig. 2.7 Schematic organization of a starch granule proposed by [27].

The radial oriented arrangement of crystallites can also be observed under polarized light. Native starch granules show a dark birefringence cross, which is well known as Maltese cross and can be for example seen for native tapioca starch in figure 2.8.

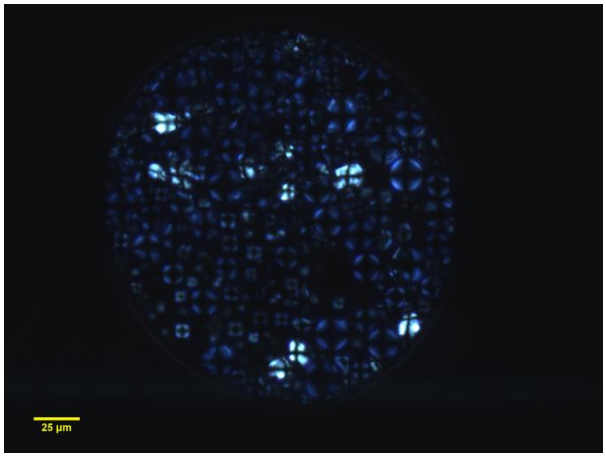

Fig.2.8 Native tapioca starch granules observed by light microscopy under polarized light.

2.2.2 Gelatinization, pasting, and melting

All native starches require a hydrothermal treatment to disrupt the ordered structures in the starch granules in order to make use of the hydrocolloid properties of the starch polymers. Heating of granules in excess water causes large changes in the rheological properties of a starch–water suspension and influences the behavior and functionality of

starch containing systems. When starch granules are heated in excess water progressively, a point is reached where the polarization cross starts to disappear and the granules begin to swell irreversibly [33]. This disruption of granular structures is called *gelatinization* and can be defined as the collapse of molecular orders (breaking of hydrogen bonds) within the granules, accompanied by irreversible changes in properties such as water diffusion inside the granules and granular swelling, endothermal crystallite melting, birefringence loss, starch solubilization, and viscosity development [33]. At the same time amylose is preferentially solubilized, whereas solubilization of the high molecular weight amylopectin is rarely observed [26]. The breakage of the hydrogen bonds in the amorphous regions produces initially absorption of a huge amount of water, which acts as plasticizer. As the temperature increases, more hydration and swelling in the amorphous regions as well as partially hydration and melting of the crystallites, occurs [34]. Disruption of amorphous and crystalline structures results in an irreversible loss of the granular order and is followed by leaching of starch molecules, mainly presented by amylose, although low molecular weight amylopectin may also solubilize depending on the nature of the starch and the density of amylopectin crystallites [30]. The process of *pasting* follows gelatinization and occurs with continued heating in excess water and involves continued granule swelling, additional leaching of dissolved starch molecules, and disruption of the fragile, swollen granules. During cooling the released molecules rearrange and form, depending on amylose content, a weak or strong gel/paste consisting of a continuous phase of dissolved starch polymers and a discontinuous phase of granule remnants. This setback and the molecular process are known as *retrogradation*. The first, short-term part of retrogradation involves the network formation by entanglement or junction zone formation between amylose molecules; embedded within this network are swollen granule remnants, which reinforce the interpenetrating matrix [35]. In the long term the amylopectin retrogradation occurs, which is due to the huge molecule size a much slower process and may proceed for several days. All these phenomena will be discussed in more detail in chapter 6.1 using the example of tapioca starch. Gelatinization and retrogradation can be seen as nonequilibrium melting and chain ordering/recrystallization processes, facilitated by the solvent. Marchant and Blanshard [36] already proposed in 1978 that gelatinization has to be a semi-cooperative process by a temperature induced melting of the crystalline regions, which leads to greater freedom and mobility of the polymer chains in the amorphous zones and enables further swelling and hydration by disentanglement of the chains. The terms, *starch gelatinization* and *starch melting*, have to be differentiated regarding the amount of available water. Gelatinization occurs in excess water and yields to a starch paste or gel, whereas melting corresponds to the loss of crystallinity in the granule at low moisture.

2.2.3 Tapioca starch

Tapioca starch is obtained from the roots of the cassava plant and can be found in the equatorial regions. Depending on the region, the cassava plant is also known as manioc (Brazil), yucca (Central America), tapioca (India and Malaysia) or cassava (Africa, Southeast Asia) [5]. The expression cassava is generally applied to the roots of the plant, whereas tapioca is the name given to the starch. Tapioca starch is a unique native material with, compared to other starches, distinct properties, which enables direct use in food and industrial applications but is also an excellent starting material for modifications into specialty products. Despite being a poor source of proteins, vitamins or minerals, the cassava root represents a good energy source due to its high starch content and is currently used as a staple food in many regions [5]. The roots contain up to 26% starch [2], which is extracted and converted into a white powder by different washing and drying processes. Their starch granules are smooth, spherical grains with diameters ranging from 4 to 35 µm [37] (cf. A1). Often, they show one or more spherical truncations and fissures which cross the hilum (figure 2.9).

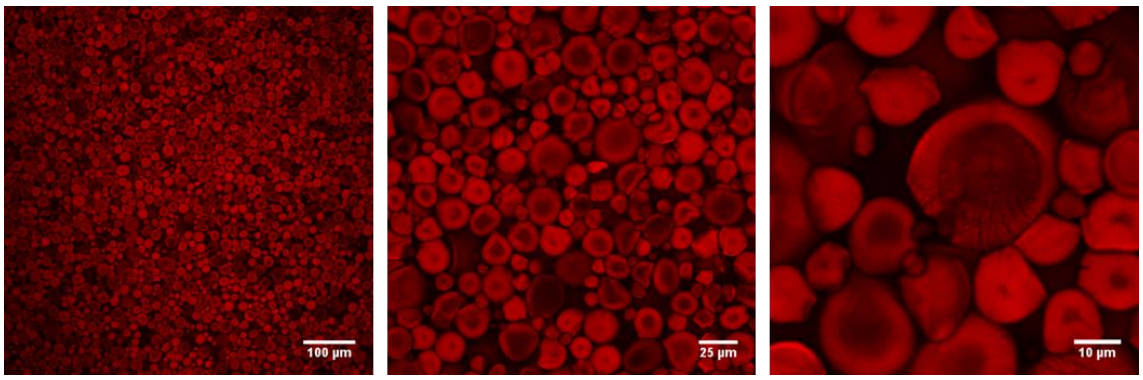

Fig. 2.9 CLSM images of native tapioca starch granules, stained with rhodamine B, showing smooth, spherical grains with truncations and fissures. Objective: 20×, image size: 707.11×707.11 µm^2, electronic zoom: 0, 4 and 8.5.

In contrast to other starches, tapioca starch possesses a low level of residual materials such as proteins, phosphorous, ash or lipids and has an exceptional low amylose content in comparison to other starch sources (table 2.4). No significant variation of amylose content (17 to 20%) has been found in tapioca while, for example, in corn or rice it may vary from 0 to 70% or 0 to 40%, respectively [5]. The amylose molecules in tapioca starch are not exclusively linear and show higher molecular weights than in other amylose containing starches. Amylopectin in tapioca starch possesses many branching points and short side chains, which enables a very densely packed and crystalline organization within the starch granules, resulting in a very strong resistance against disintegration.

Tab. 2.4 Tapioca starch in comparison to other starches, adapted from [37].

Source	Granule diameter (µm)	Amylose content (%)	Amylose average DP	Phosphorus (%)	Ash (%)	Protein (%)	Lipid (%)
Tapioca	4–35	17	3000	0.01	0.2	0.10	0.1
Potato	5–100	21	3000	0.08	0.4	0.06	0.05
Maize	2–30	28	800	0.02	0.1	0.35	0.7
Wheat	1–45	28	800	0.06	0.2	0.40	0.8

Due to the low amount and high molecular weight of amylose in tapioca starch, its pastes exhibit a low setback after gelatinization. At concentrations lower than 10% only very viscous pastes with a weak gel character are formed. After gelatinization, tapioca starch possesses special and well appreciated properties such as high adhesiveness, a clear and transparent appearance, smooth texture and, most important, no off–flavors. Additional advantages are the low price of tapioca starch and its very long shelf life as well as moisture and heat resistance in dry form.

The greatest diversity in use of tapioca starch is in the food industry. One very famous application is in form of tapioca pearls for example in bubble tea, where spherical pearls are formed of a mixture of gelatinized and ungelatinized starch. Other food applications generally use tapioca starch as thickening and stabilizing agent with special emphasis to its lacking off–flavor, desired for example in baby foods or Asian style noodles. Due to the almost absence of lipids, tapioca starch is an excellent raw material for the dextrinization process. Tapioca starch dextrins are used as coating material of confections or in low fat products [5].

2.3 Starch modification and spray drying

2.3.1 Starch modification

Native starches have many disadvantages and are often unsuitable for most applications which is why they have to be modified to enhance their positive attributes and facilitate their handling. Principle reasons for starch modification are to increase the solubility in cold water and to modify the cooking characteristics, to decrease retrogradation and gelling tendency, to increase freeze–thaw stability or to improve gel/paste properties such as texture, clarity or adhesion [38]. In general, there are three different ways of modifying native starches: genetic, chemical or physical.

From an ethical point of view, the most discussed route is the biotechnological modification of crops by controlling the genetic composition of the plant, which

influences the synthesis of the starch. This genetic modification can dictate the ratio of amylose and amylopectin, amylopectin branching patterns and chain lengths as well as phosphate, lipid and protein content [6]. The most prominent genetic modified starches are the waxy starches, containing very low to almost no amount of amylose, which leads to low viscous and adhesive pastes with lower tendency to retrograde.

Chemical modification of starch commonly involves esterification, etherification, oxidation, cationization or crosslinking [39]. The main purpose of these chemical reactions is to strengthen or weaken the granular structure or to shorten the chain length distribution. However, various chemical modification routes have been proposed and established in the food industry. But these chemically modified starches are strictly regulated and have to be declared on the ingredient list of each food product to ensure the safety of the consumer.

Physical modification is more consumer friendly and has a steadily increasing interest in the market trend [2]. Some main processes can be distinguished which apply a physical modification on native starch. Heat–moisture, annealing or pH treatments induce rearrangements of the starch components within the granular structure, yielding changed gelatinization profiles. Applied mechanical forces lead to starch granule disruption and adjust the particle size distribution. Cold water soluble starch is prepared by pregelatinization of a starch slurry, followed by drum or spray drying which will be described in detail in the following paragraph.

2.3.2 Spray drying

Spray drying is a process to convert liquid materials into powders and commonly used in the food industry for preservation, ease of storage, transport and handling [40]. The main advantages of spray drying are that powders with a narrow particle size distribution can be achieved and the characteristics of the dried products such as size, density or moisture content, can be predetermined.

The basic principle of spray drying is the formation of droplets from the bulk liquid followed by the removal of moisture from the liquid droplets by heat application. The first step involves the surface enlargement of the liquid by atomizing it into small droplets with an diameter of 1–25 µm [41], which creates a bigger working surface. Almost simultaneously to the atomizing step, the solvent is evaporated by the drying gas. This solvent removal bases on two transport effects (figure 2.10): heat transport into the droplet following Fourier's law and solvent diffusion from the droplet to the surrounding environment after the first Fick's law [42]. Fourier's law describes the heat transport across a temperature gradient from the surrounding gas into the droplet with lower temperature $\frac{\partial T}{\partial x}$, where x defines the droplet radius and λ_s the thermal conductivity coefficient. The material transport is related to the first Fick's law of diffusion and

solvent molecules diffuse along a concentration gradient $\frac{\partial c}{\partial x}$ from the droplet with high concentration to the environment, where the diffusion coefficient D_s describes the proportionality. The decreasing droplet size by atomization increases the temperature and concentration gradient, yielding a higher heat and material flux and consequently a rapid and amplified drying process of the droplets.

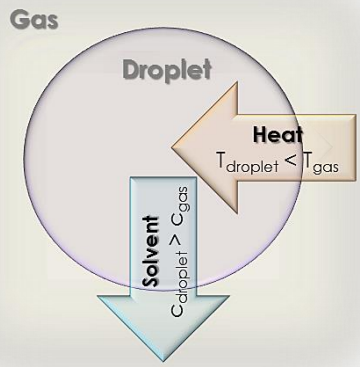

Fourier's law (heat transport):

$$J_W = \frac{\partial W}{A \partial t} = -\lambda_s \frac{\partial T}{\partial x} \qquad (2.1)$$

Fick's law of diffusion (material transport):

$$J_N = \frac{\partial N}{A \partial t} = -D_s \frac{\partial c}{\partial x} \qquad (2.2)$$

Fig. 2.10 Heat transport and solvent diffusion during evaporation.

Figure 2.11 presents a typical set up of a spray drier and the drying process. First the liquid sample is pumped by a peristaltic pump to a two feed spray nozzle, where a low humidity nitrogen blast atomizes the feed into small droplets. In the drying chamber the sprayed droplets are mixed with preheated drying gas and the water is evaporated. The drying gas is forwarded by suction of the aspirator through the whole system. Drying of the droplets continues inside the drying chamber, until the desired particle characteristics are achieved. The particles are transported via the drying gas into the cyclone, where the separation of particles from the drying gas takes place. Cyclones are usually cylindrical in the upper part while the bottom is conical. Powder and drying air tangentially enter the cyclone at same velocity and sink in a spiral path down to the bottom, while the powder is precipitated at the cyclone wall. The powder hits the cyclone wall due to centrifugal forces and is dragged down by gravity, while the clean air moves up from the bottom to the top of the cyclone along the centerline [40]. The most difficult challenge of spray drying is the correct adjustment of the spraying parameters, corresponding to the feed material and the desired characteristics. Sample concentration, drying temperature, atomizing pressure, pump velocity or aspirator rate influence the product yield, size distribution, and morphology of the dried particles.

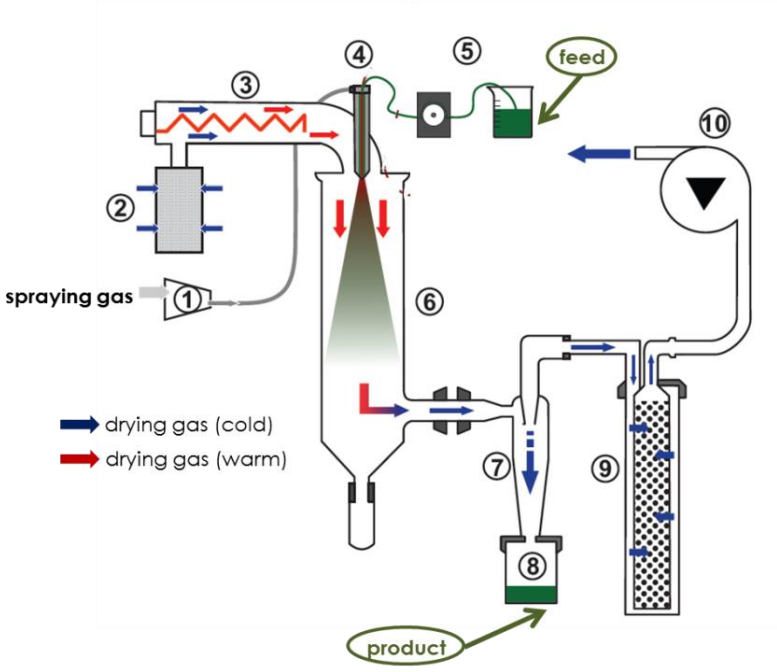

Fig. 2.11 Schematic diagram of a laboratory spray drying system; 1 compressor, 2 inlet filter, 3 heating coil, 4 spray nozzle, 5 peristaltic pump, 6 drying chamber, 7 cyclone, 8 dry product, 9 outlet filter, 10 aspirator. Reprinted from http://chobotix.cz/research-2/encapsulation-technologies/spray-drying/

2.4 Nonstarch polysaccharides

From a general point of view, nonstarch polysaccharides are especially important in the domain of water soluble polymers, where they play an important role as thickening, gelling, emulsifying, hydrating, and suspending polymers. Due to the presence of many hydroxyl groups in the molecule, polysaccharides have a tendency to form cooperative intra- and interchain hydrogen bonds, causing some insolubility or at least the presence of aggregates when solutions are prepared [15]. Due to their stereoregularity, they are often able to form helical conformations in solution; their ordered and helical conformation has a semi-rigid character and its stability depends on temperature and ionic concentration.

2.4.1 Xanthan gum

Xanthan gum is a heteropolysaccharide produced by fermentation, using the bacterium *Xanthomonas campestris* [43]. Dissolved in cold water, xanthan produces highly viscous solutions with a weak gel character. The primary structure consists of a cellulose like backbone of β-1,4-linked glucose units, substituted alternately with a trisaccharide side chain. This side chain is composed of two mannose units separated by a glucuronic acid (figure 2.12).

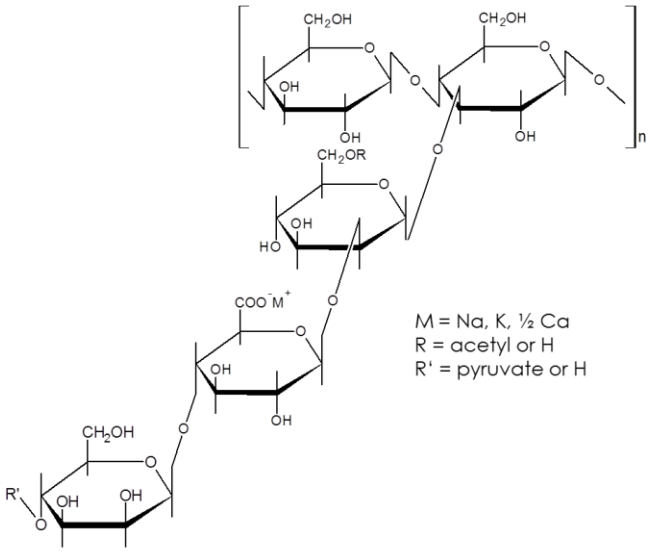

Fig. 2.12 Haworth formulae of xanthan gum. The backbone consists of *β*-1,4-linked glucose units with a trisaccharide side chain whose terminal mannose unit is linked fifty–fifty to a pyruvate group and the nonterminal residue usually carries an acetyl group. Redrawn from [44].

Due to the carboxyl group on the side chain, xanthan gum represents highly charged polysaccharide molecules with a very rigid polymer backbone. It has a high molecular weight of about 2 500 000 g/mol with a narrow distribution and low polydispersity. Via XRD measurements xanthan's secondary structure could be elucidated as a helical conformation, where the backbone is stabilized by the side chains [45]. Due to the concentrated charges along the side chains, they repel each other and fold towards the backbone, resulting in electrostatic stiffening. In solution, xanthan gum gives a weak gel like network. 1984, Norton et al. presented [46] a model where helical chain segments arrange side by side and are connected by disordered sequences to a three dimensional network (figure 2.13a). However, Nordqvist and Vilgis [47] [48] proposed a simple model, considering that xanthan molecules behave like charged and rigid rods, which undergo a nonequilibrium jamming transition above a critical concentration c^*, as it could be shown for neutral systems in [49]. In a salt free solution and at low xanthan concentrations, the charged rods repel each other according to the Coulomb interaction, but are still able to diffuse and xanthan acts as simple thickener. At larger concentrations, the competition between electrostatic repulsion and decreasing distance between the xanthan molecules creates frustrated conformations and it is more and more difficult to remain separated from each other. At a critical concentration c^*, which depends strongly on the molecular weight, this repulsion gets so strong that their motion is strongly hindered and they undergo a so called jamming transition and form a logjam; the rods get frozen at arbitrary positions with random orientations. This immobilization is based on multiple compromises between energy minimization and entropy maximization. At one hand, the molecules should maintain a large distance due to the

electrostatic repulsion; on the other hand they are kept together by the increasing density. Consequently, above a critical concentration a salt free xanthan dispersion is characterized by a solid-like and weak gel behavior.

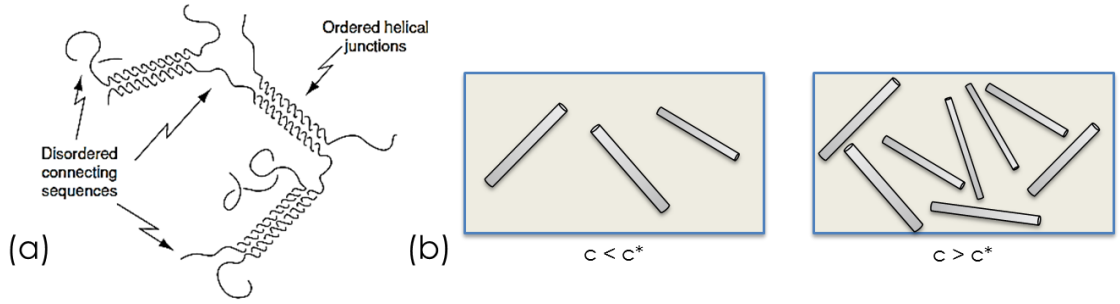

Fig. 2.13 Thickening models for xanthan gum. (a) Side by side association of helical chain segments, connected by disordered regions. (b) Xanthan as rigid, highly charged polyelectrolyte; left: at low concentration the rods are able to move unhindered, right: at higher concentration the molecules strongly hinder each other and freeze at an arbitrary position and orientation.

In a mixture with other polysaccharides, the rigid and randomly oriented xanthan gum molecules reduce the mobility and diffusion of the co-solute. The physical consequences of these hindering effects have been recently demonstrated for mixed systems of xanthan gum and agarose [50], [51].

2.4.2 Carrageenan

Carrageenan is obtained from red seaweeds and represents a commonly used polysaccharide with a wide polydispersity. Three primary types can be distinguished: κ-, ι- and λ-carrageenan. κ- and ι-carrageenan form thermally reversible gels, whereas λ-carrageenan is nongelling [52]. From molecular point of view, carrageenan consists of a backbone of repeating units of galactose and 3,6-anhydrogalactose, both sulphated and nonsulphated and linked alternatingly by α-1,3- and β-1,4 glycosidic bonds. The three types differ in amount and location of ester sulphate groups and the proportion of 3,6-anhydrogalactose (figure 2.14). The distribution and amount of ester sulphate groups and content of anhydrogalactose determine the functional properties and gelling ability. Upon cooling a hot aqueous solution containing various salts, κ-carrageenan forms brittle and firm gels, ι-carrageenan soft and elastic gels and λ-carrageenan only thickens. This work only investigates ι-carrageenan, due to the known synergy with starch [52].

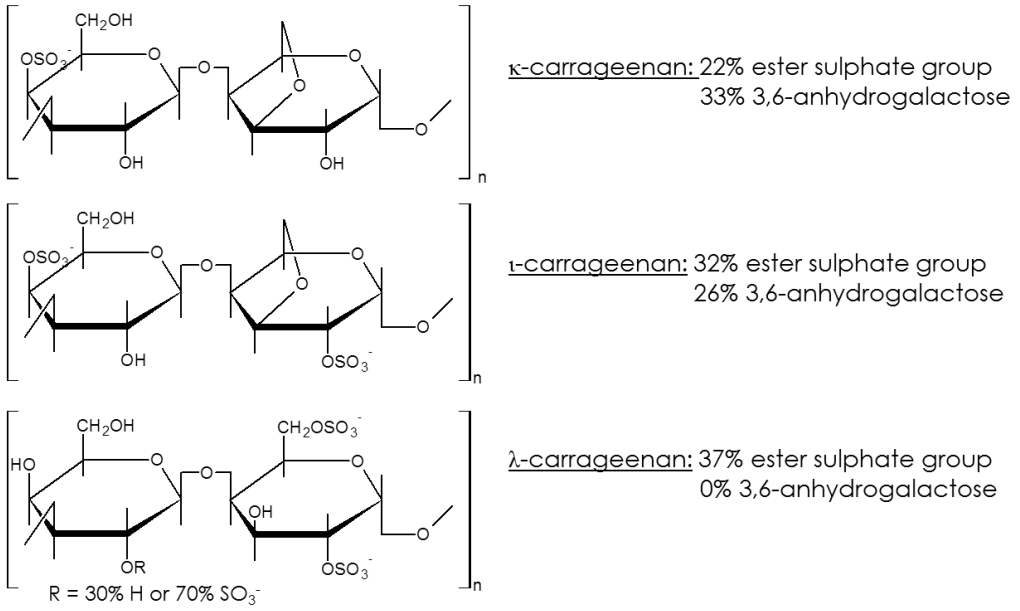

Fig. 2.14 Haworth formulae of different carrageenan types.

In comparison to xanthan gum, ι-carrageenan is also a charged linear polyelectrolyte but with a sufficiently flexible backbone with molecular weight ranging from 200 000 to 800 000 g/mol. Consequently, in aqueous solution, carrageenan molecules are distributed as random coils with intrinsic chain flexibility and are expanded by polyelectrolyte effects [53]. The linear architecture and chain flexibility are particularly pronounced in ι-carrageenan due to its high ester sulfate content.

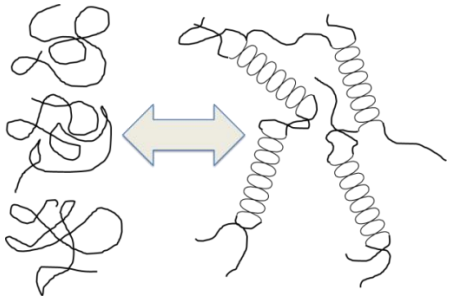

Fig. 2.15 Conformational transition of carrageenan during thermal treatment.

ι-Carrageenan is supposed to undergo a thermally induced disorder–order transition from random coil to double–helix conformation during cooling (figure 2.15). The double–helical junction zones are connected by disordered carrageenan chains, resulting in a quasi-permanent network, where each carrageenan chain passes through several independent helical regions, each with a different chain [54].

2.4.3 Guar gum

Guar gum is obtained from the seeds of *Cyamopsis tetragonolobus* and belongs to the family of the seed gums, which are also often combined to the galactomannans. Galactomannans (carob, guar, locust bean, tara, etc.) are neutral polysaccharide, whose

main chains are made of β-1,4-linked mannopyranosyl (M) units with different degrees of substitution of galactopyranosyl (G) units [15]. The M/G ratio depends on the botanical source and determines the solubility and rheological properties of the different seed gums. Guaran is the functional polysaccharide in guar gum, whose galactopyranosyl side groups are substituted on the average to every second main chain unit, i.e. an average galactose to mannose ratio of 1:2 and molecular weights between 50 000 and 800 000 g/mol [8] (figure 2.16).

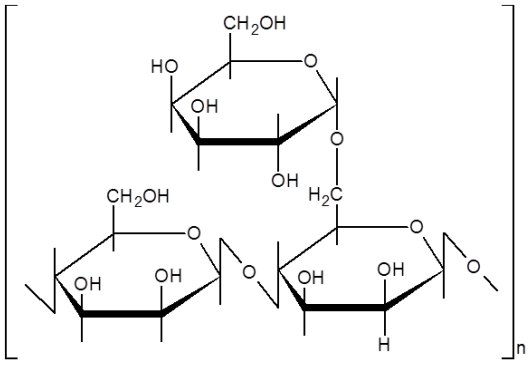

Fig. 2.16 Haworth formulae of guaran.

The high substitution ratio in guar gum enhances the solubility by leading to a lower crystallinity and promoting the penetration of water and enables a fully hydration in cold water [55]. When guar gum is dissolved in water, the long mannose chain unfolds and forms an open, flexible nonordered random coil conformation. At low concentration these coils are well separated and able to move unhindered within the solution. As the concentration rises, the polymer chains will come into contact, resulting in mutual entanglements and an exponential increase in viscosity [55].

2.5 Starch–hydrocolloid mixtures

Starch–hydrocolloid combinations are widely used in processed foods to customize and design paste properties according to the desired application and customer demands. Native starches, generally, do not have ideal properties for food product preparations, thus they are often chemically modified (cf. 2.3.1) to improve processing conditions and paste textures. The mixture with other food hydrocolloids may enhance the texture and can be used to achieve specific flow properties or to reduce costs. In addition, providing a “clean label”, the use of terms such as modified starch, which scare many customers, can be avoided.

In general, starch–hydrocolloid systems have been widely studied in literature and recently, BeMiller [4] summarized more than 250 reports on different starch–hydrocolloid mixtures and analytical methods in a detailed review. He demonstrated the complexity of these systems, containing different starch components, hydrocolloids and water, and that due to a variety of starch granules, starch polymers, and hydrocolloid

molecules, several mechanisms are likely to operate and vary with different starches, hydrocolloids, and methods of preparations and measurements. It is well known, that already low concentrations of other food hydrocolloids alter drastically the pasting and gelling properties of starch dispersions. Modifications of the macroscopic properties in starch–hydrocolloid mixtures are thought to arise from changes during granule swelling and amylose leaching as well as from starch–hydrocolloid interaction in the continuous phase [56] [57] [58] [59] [60] [61]. Different hydrocolloids have different effects on the pasting and gel properties of a given starch due to their structural disparity in chemical structure, ionic charges, shapes, flexibility/stiffness or molecular weight [4]. In this work the main focus was on the ionic charge and the polymer chain flexibility of the added hydrocolloids. Xanthan gum and ι-carrageenan, both highly charged polyelectrolytes, differ significantly in chain stiffness. The polymer chains of xanthan gum have a more rigid structure while those of ι-carrageenan are rather flexible; guar gum in contrast represents a neutral polysaccharide with an overall flexible conformation. In conclusion, all mixtures between starch and other food biopolymers are supposed to result in thermodynamic incompatibility leading to phase separation [62] or in the formation of co-polymer networks by synergistic interaction between starch and hydrocolloid molecules [58] [63]. The phase behavior of such polysaccharide mixtures will be discussed in more detail in the following chapter.

3 Phase behavior in mixed polysaccharide systems

Foods are always multicomponent physical systems and thus different interactions have to be considered for understanding the microscopic and macroscopic properties of the complete structure. Various interactions play a role in the investigated starched based biopolymer gels: starch–starch, starch–solvent, starch–hydrocolloid, hydrocolloid–hydrocolloid, and hydrocolloid–solvent. The following chapter gives an overview of the fundamental physical behavior of polymers in solution and in mixed phases which can be transferred to the present biopolymer based hydrogel–mixtures. Starting with a single polymer in solution and its interaction with the solvent, polymer–polymer interaction and finally a multicomponent system are presented.

3.1 Polymers in solution

The shape of an isolated polymer in solution is determined by its molecular conformation and depends on the chemical constitution and conformation within the molecule. The simplest chemical structure of polymers is that of a long chain of identically linked chain units. The more or less free rotation around chain bonds allows the macromolecule to distribute in space as much as the neighboring chain units will allow and it adopts the conformation of a three dimensional random coil. Locally, polymer chains are not completely flexible and are restricted by rigid bond angles between the units, by large substituents or helical chain segments. Such semi-flexible or rigid chains resist to coil and curl wormlike, which can be seen as elastic wires with flexible energies [64]. This is a model of polymer shape without accounting any specific interaction or structure details. There is no fixed arrangement of the coil but rather a set of conformations defined by the combination of bond angles and enthalpic interaction that minimize free energy. Any change to that arrangement will increase the free energy [65]. During dissolving, different interactions arise, which influence the shape of the polymer molecule. In thermodynamically good solvents, the interaction between polymer and solvent are more favored than those between the pure components. Thus the coil dimension is much bigger then in theta or poor solvents for the same constitution and molecular weight. With increasing polymer concentration the coils will compress until they reaches their unperturbed dimension at the critical entanglements concentration c^* and start to overlap and interpenetrate, resulting in entanglements with other polymer chains (figure 3.1). This entangled solution restricts the flow and movement of the polymers and can be thought as temporary networks [16].

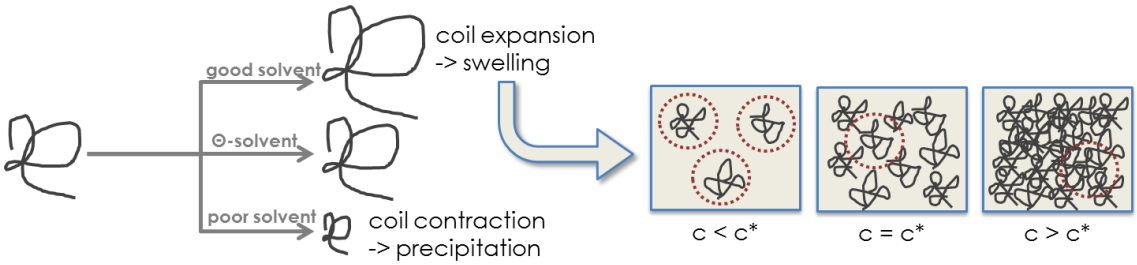

Fig. 3.1 Solvent influences on coil dimension and their overlap in concentrated solutions.

3.2 Thermodynamics of polymer mixtures

A polymer solution consists of the polymer and at least one solvent and represents in the simplest case a two component system. To understand the thermodynamics of polymer solutions the *Gibbs–Helmholtz equation* for mixed systems has to be considered:

$$\Delta G_m = \Delta H_m - T\Delta S_m \tag{3.1}$$

Hereby ΔG_m describes the Gibbs' free enthalpy, ΔH_m the enthalpy and ΔS_m the entropy of the mixture; T defines the absolute temperature of the system. Thus, a condition for polymer–solvent miscibility is that the free energy of mixing is negative, $\Delta G_m < 0$. To describe the polymer–solvent interaction in solution in a quantitative way, a lattice model can be used (figure 3.2). Three lattice model restrictions have to be considered. Both mixing components have the same size and during mixing no volume contraction or expansion occurs. Only combinatorial entropy is included, i.e. only given by the number of rearrangements during mixing and it is only valid for nonpolar molecules since e.g. hydrogen bonds between polymer and solvent are not encountered. In addition, it is a mean-field model and only average interaction is taken into consideration.

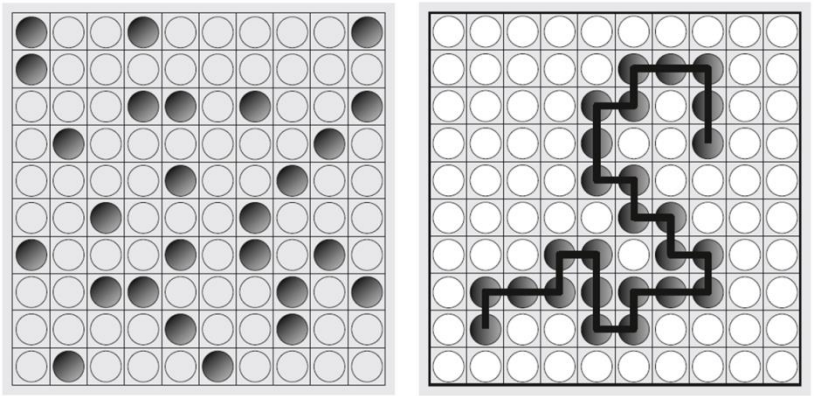

Fig. 3.2 Lattice model of dissolved low molecular weight solute molecules (left) and of a dissolved polymer (right). Dark dots: solute, light dots: solvent. Reprinted from [66].

For solutions of low molecular molecules the solute molecules (dark dots) are placed randomly onto a lattice and the gaps are filled with white solvent molecules. According to equation 3.1 the Gibb's free enthalpy of mixing is given as:

$$\Delta G_m = RT(\varphi_1\varphi_2\chi + \varphi_1 \ln \varphi_1 + \varphi_2 \ln \varphi_2) \tag{3.2}$$

The first term describes the enthalpic contribution composed of thermal energy RT, volume fraction φ_i of solvent and solute and the Flory–Huggins exchange parameter χ and describes the solute–solvent interaction. Positive values of χ indicate endothermal interaction ($\Delta H_m > 0$) between solvent and solute. The second and third term count the entropic contribution, derived from the amount of position possibilities of the molecules in the entire system. The ideal entropy of mixing for this system is always positive and promotes the mixing of solute and solvent by increasing the disorder. Consequently, for small values of χ, mixtures are stable due to a lower free Gibb's enthalpy compared to the single components' free enthalpy, making mixing energetically favorable [66].

In a polymer solution, the solute molecules are much larger than the solvent molecules and the polymer is represented as a chain of monomers adjacent to one another on the lattice (figure 3.2). In contrast to small molecules on the lattice, the possibilities of placing the polymer molecule is reduced since the monomers of the polymer have to be in a continuous chain. The number of possible mixed configurations determines the entropy of mixing so the entropy of mixing for a polymer into solvent is much lower than for a corresponding small molecule solution. For large polymers, mixing entropy is negligible and the free energy of mixing is determined solely by enthalpic interaction. Analogous to the low molecular solvents the free energy of mixing a solvent and a polymer can be approached by the *Flory–Huggins equation*:

$$\Delta G_m = RT\left(\varphi_1\varphi_2\chi + \varphi_1 \ln \varphi_1 + \frac{\varphi_2}{X_N} \ln \varphi_2\right) \tag{3.3}$$

The first term in the equations describes again the enthalpic interaction, the second is the contribution of the solvent 1 to the entropy of mixing, and the third is the contribution of the polymer 2 to the entropy of mixing, where X_N defines in addition the degree of polymerization [66]. Here the χ parameter allows classifying the character of a solvent. If $\chi > 0.5$, the polymer is hardly soluble and the solvent is regarded as poor. Values of $\chi < 0.5$ characterize good solvents and correspond to an exothermic or a small endothermic enthalpy of mixing. The condition $\chi = 0.5$ marks the borderline between good and poor solvent, and is referred to as θ-condition. The state of a polymer at these conditions is characterized by the absence of long range interaction and the polymers exhibit their unperturbed dimension. The contribution of the polymer to the entropy of mixing decreases as polymer molecular weight increases, and becomes negligible for high polymers since restriction of distribution on the lattice. Thus,

dissolving a polymer is always from an entropic point of view inferior compared to a same concentration of low molecular molecules.

It is possible to extend this approach to mixtures of two polymers and a solvent and the miscibility of the polymers can be estimated. Here, there need to be additional two exchange parameter terms for the enthalpy of polymer 3–solvent 1 interaction χ_{12} and polymer 2–polymer 3 interaction χ_{23}. For polymers with infinite molar mass the entropic contribution is very small and the miscibility or immiscibility of the polymers is mainly determined by the mixing enthalpy and the polymer 2–polymer 3 exchange parameter χ_{23}. In order to achieve a negative value for ΔG_m, as a condition of miscibility, the Flory–Huggins exchange parameter has to be negative and enthalpic contribution of mixing captures negative or small positive values. In practice, however, most polymer–polymer–solvent ternary mixtures separate into two phases with different compositions [65].

3.2.1 Phase separation

Unfavorable polymer–solvent interaction in a binary system limits miscibility and lead to liquid–liquid phase separation into polymer rich and polymer poor domains. Something similar is found by mixing dissimilar macromolecules in one solvent, which usually leads to phase separation and develops two liquid phases where each polymer is enriched in one of the two phases. This is caused either by thermodynamic incompatibility of the polymers or by the formation of insoluble interpolymer complexes [67]. Two main types of phase separation can be distinguished. If polymer 1 and polymer 2 strongly interact with each other, complexes are formed which can either precipitate or form a stable suspension of fine particles. This referred to as associative phase separation. In contrast if polymer 1 and polymer 2 do not interact and the mixture separates into regions enriched in one type of polymer and depleted in the other, it is known as segregative phase separation (figure 3.3). This repulsion between the polymers results from the fact that molecules tend to be surrounded by molecules of their own type. Generally, interaction between polymers is unfavorable resulting in mutual exclusion. This type of segregative interaction is known as polymer immiscibility or incompatibility. Polymer incompatibility usually results in a separation in which the polymers are in different phases (segregative), while interpolymer complexing leads to the accumulation of both polymers in the same phase (associative) [59]. Another reason for the formation of segregative separation may a very low affinity of one polymer for the solvent. In addition attraction between the two polymers forms soluble or insoluble complexes.

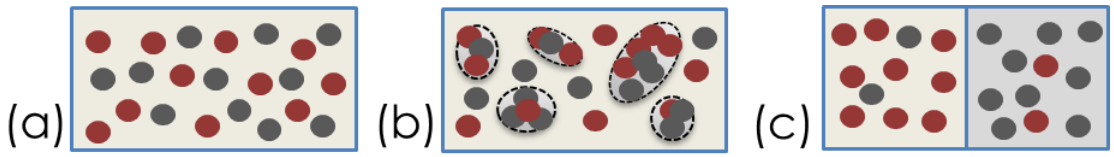

Fig. 3.3 Mixture of two aqueous solutions of polymers a) fully miscible, b) associative phase separation, and c) segregative phase separation. Modified from [65].

For a binary system the phase separation and the critical transitions can be visualized by a phase diagram (figure 3.4a). Polymer blends can exhibit a wide range of phase behavior. Three regions of different degree of miscibility can be distinguished: the single–phase miscible region between the two binodals, the four metastable regions between binodals and spinodals, and the two–phase separated spinodal regions bordered by the spinodals.

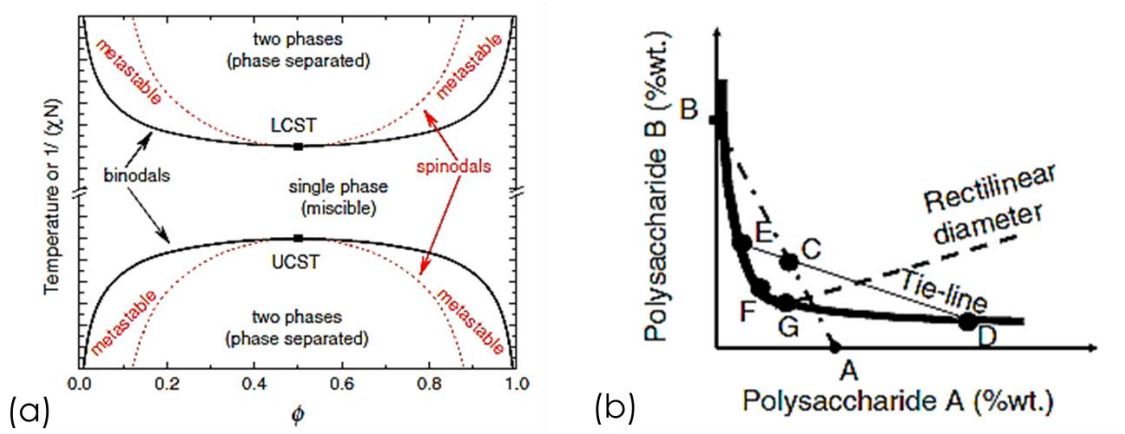

Fig. 3.4 Phase diagram of a) binary liquid mixture with the progression of binodals and spinodals, according to [68] and b) mixed polysaccharide–polysaccharide solution, according to [67].

Two critical solution temperatures, the lower LCST (at high temperatures), and the upper UCST (at lower temperatures) are specified. For low molecular weight components usually these two critical points can be separated while for polymers only one critical point is accessible and typically shows either the LCST (mostly) or the UCST. The spinodal represents the threshold for phase separation, where the thermodynamic conditions are given by:

$$\left(\frac{\partial^2 \Delta G_m}{\partial \varphi^2}\right)_{T,p} = 0 \tag{3.4}$$

Phase separation takes place when a single–phase system undergoes a change in composition or is forced by a change in temperature or pressure to enter the metastable or two–phase region. The transition from the single–phase to the metastable region is produced by a slow demixing through nucleation and growth of the phase separated domains. Whereas in the unstable region of the phase diagram, a spontaneous demixing

into phase separated two–phase regions occurs by spinodal decomposition and two interpenetrating phases are formed [68]. For polymer solutions, binodal and spinodal do not stay symmetric for the components and are relocated depending on the strength of the polymer interaction and degree of polymerization [66]. By holding the system in the unstable domain, phase separation goes on and eventually leads to a bulk phase separation. Figure 3.4b shows a typical phase diagram where polysaccharide A concentration is plotted versus polysaccharide B concentration. The slid line represents the binodal and the region below corresponds to the single–phase mixed solution while above the binodal a two–phase system locates. During mixing a polysaccharide solution A and a polysaccharide solution B, a mixture of composition C can be obtained. This mixed solution spontaneously breaks down into two liquid phases, phase D and phase E. Phase D is rich in polysaccharide A and E is rich in polysaccharide B. Point F represents the phase separation threshold, i.e. the critical concentration required for phase separation. The tie line connects the points of coexisting equilibrium phases and the rectilinear diameter crosses the mid tie line and point G, where both coexisting phases have the same composition [11]. The morphology of phase separated systems depends on the interfacial tension between the polymers, the volume ratio, the viscoelasticity of the components, and the processing history, i.e. temperature, time and type of flow, which in turn, determine the rheological properties of the blend [69].

3.2.2 Thermodynamic incompatibility of polysaccharides

According to equation 3.3, thermodynamic incompatibility of polymers can be ascribed to the low entropy of their mixing since in an equilibrium state complete miscibility of a polymer mixture requires that $\Delta G_m < 0$. In general, the driving force of demixing and the transition of a single–phase state to a two–phase state is the entropy and for polymers due to the large molecular size and rigidity always very low. Thus, the sign of ΔG_m and the formation of a stable one–phase system, always depends on the interaction between the two polymers and on the value of the mixing enthalpy ΔH_m (i.e. exothermal or endothermal). Consequently, dissimilar polysaccharides are incompatible and do not form a single–phase when there is no attraction (attraction: $\Delta H_m < 0$) between them and the entropy difference $T\Delta S_m$ does not exceed the enthalpy of mixing ΔH_m [67]. Thus, the mixing process can only give complete compatibility when the entropy difference between the two–phase and single–phase state is larger than the mixing enthalpy. In general polymer immiscibility can be explained by unfavorable interaction between the polymer species. The miscibility of polymers in solution decreases enormously with increasing polymer concentration and demixing is predicted when the polymer chains start to entangle and cross the coil overlap concentration [70]. The phase behavior of these ternary systems of solvent 1, polymer 2, and polymer 3 is also strongly affected by the polymer–solvent interaction and immiscibility is increased

when the affinity of one of the polymer to the solvent is significantly different from that of the other [71]. In consequences, molecularly homogeneous mixtures of biopolymers can be only achieved if ΔH_m is negative, i.e., the attractive forces between different macromolecules are equal to or larger than those between the same type of macromolecules. This in turn means that biopolymer compatibility corresponds to formation of soluble interpolymer complexes. Consequently, the incompatibility of biopolymers occurs under conditions that inhibit interaction between macromolecules of different types and promote association between macromolecules of the same type. The chemical composition and structure of polysaccharides play therefor an important role in the incompatibility and the formation of phase separation. Branched polysaccharides for example exhibit lower excluded volume, higher solubility, and higher phase separation thresholds than linear polysaccharides of the same molecular weight [67].

3.2.3 Immiscibility of amylose and amylopectin

Although amylose and amylopectin are chemically similar and only glucose units are involved in the formation of their polymer chains, Kalichevsky and Ring reported already 1987 [71] that even moderately concentrated aqueous solutions of amylose and amylopectin exhibit immiscibility. Usually, it would be expected that such polymer chain homologues are thermodynamically compatible and form transparent single-phase systems. But due to the branching points and side chains of amylopectin, huge differences between molecular length and flexibility between amylose and amylopectin molecules are observed, which prevent their mutual recognition of having the same chemical nature. Also differences in regularity of chains promote the self–association of either amylose or amylopectin. In addition the tendency of amylose to form complexes with lipids increases the differences for both polymers in solubility and rigidity [62]. It has to be noted that for starch the thermodynamic quality of water as solvent also plays an important role. At ambient temperature, water is considered to be rather a poor solvent for starch. As the temperature increases, the thermodynamic quality of water as solvent increases and breaking the hydrogen bonds, which keep starch self–associated, becomes easier at high temperatures. In fact, solubilization of starch in neutral, aqueous systems always requires heating, while good solvents like DMSO already dissolves starch at ambient temperatures. During subsequent cooling, the decreased affinity of water to starch promotes starch–starch interaction which is the driving force for bulk phase separation. The phase separation of amylose and amylopectin shows an UCST behavior, which means that a transition from single to a two phase system occurs by lowering the temperature [69]. The complexity of starch's phase behavior increases even more by the admixture of other polymers, such as hydrocolloids.

3.2.4 Excluded volume of macromolecules

The excluded volume of macromolecules determines the phase separation conditions and the minimal concentration at which this occurs and arises from the impenetrability of molecules by each other. Macromolecules in concentrated solutions have in addition to the external excluded volume between different molecules, an internal excluded volume [64]. The repulsive long range intractions along one chain lead to the exclusion of one chain segment for all other segments of the same chain, resulting in an expansion of the polymer coil which gets perturbed. In contrast, if repulsive and attractive intractions of one chain balance each other, the internal excluded volume disappears and the coil gets unperturbed. This impenetrability and mutual repulsion of chain segments also occurs between chain segments of different molecules, leading to intermolecular excluded volume effects and a mutual repulsion of macromolecules at short range. In diluted solutions, one molecule captures a certain volume and decreases, depending on its excluded volume, the amount of free available volume of solution for another molecule [72]. For spherical macromolecules, the radius of the excluded volume equals the diameter of the sphere leading to an eightfold greater excluded volume than that of the molecule itself [73]. For nonspherical macromolecules, such as linear rigid polysaccharides, the excluded volume is even significantly greater and increases with rigidity and size of the molecule. The excluded volume effects describe the occupancy by the macromolecules and reflect the mutual competition for space in the solution. Due to the excluded volume, the molecules mutually concentrate each other leading to a more concentrated mixed solution. Changes in the excluded volume can arise from conformational transitions or association and dissociation of molecules [62]; the association, gelation, crystallization, and complex formation of macromolecules for example reduces the excluded volume and may diminish the increasing pressure during rising concentration.

3.3 Multicomponent biopolymer gels

The structures of gelled mixtures of several polysaccharides can be idealized and divided into different types of interaction (filled, mixed, and complex gels) [16] [74].

Filled gels consist of a phase separated network containing one or several independent continuous phases filled by dispersed particles. These filled gels may be either a single–phase or a two–phase gel. Consisting of a single–phase, the gel contains a polymer network and other polymers (fillers) in the form of molecules or molecular aggregates of the solute. Two– or more–phase gels are formed by a continuous network filled with dispersed particles. A gelatinized starch gel or paste (figure 3.5a) can be understood as such a filled two–phase gel. This gel consists of a continuous amylose network,

interpenetrating the swollen granule remnants, mainly containing amylopectin, which act as filler particles reinforcing the amylose network [75].

Mixed gels (figure 3.5b) consist of two or more independent networks that both span the entire system and interpenetrate throughout each other. Interpenetration on molecular level is more unlikely due to thermodynamic incompatibilities of polysaccharides and constrains more on topological interaction.

Fig. 3.5 Schematic models of the idealized structures in multicomponent gels. (a) Filled phase separated gel showing the example of a starch gel. (b) Mixed gel with two interpenetrating independent networks. (c) Complex gel with direct association between the polymer networks. Reprinted from [16].

Complex gels (figure 3.5c) make up the third group of this classification. In this case, direct associations between two polymers occur and a subsequent network formation can be obtained. It is suggested that intermolecular binding between two polysaccharides contributes to the formation of a permanent network [76]. But this implies some stereochemical similarity between the polymers and certain recognition as being of the same chemical nature.

Mixtures of different gelling agents can influence the physical and macroscopic properties in synergistic, additive or antagonistic ways. The synergistic effect of single–phase mixed solutions of hydrocolloids bases on the excluded volume of the macromolecules, resulting in mutual concentrating of each other, and may increase the rate of gelation or elasticity modulus. In two–phase systems, synergy results from increasing concentration of the continuous phase, rich in stronger gelling agent.

4 Rheology

In this chapter a general introduction into rheology is given and the mechanical properties of viscoelastic fluids and solids are presented in detail. Rheology contains the study of deformation and flow of materials and bases on the response to an applied stress on macroscopic level. Especially, for food systems rheology is an important analyzing method, because flow and deformation behavior defines the food structure during production processes or preparations in the kitchen and may simulate the physiological in mouth, stomach, and intestine digestion [77]. The aim of rheological characterization is to quantify the functional relationship between deformation or stresses, and the resulting rheological properties such as viscosity, elasticity, or viscoelasticity.

4.1 General basics about rheology

Mechanical properties such as viscosity, elasticity, and viscoelasticity can be explained by starting with a simple model for a steady laminar flow in purely viscous medium (figure 4.1a). A material is located between two plates; while the upper plate with the area A is moved with the force $\vec{F}$ in random direction, the sample between the plates is deformed. The ratio of force $\vec{F}$ and area A is defined as a stress tensor $\bar{\bar{\sigma}}$ and can be separated according to the direction of force application: parallel application to the surface normal A causes elongation or compression, while perpendicular forces provoke shearing with shear stress σ (figure 4.1b).

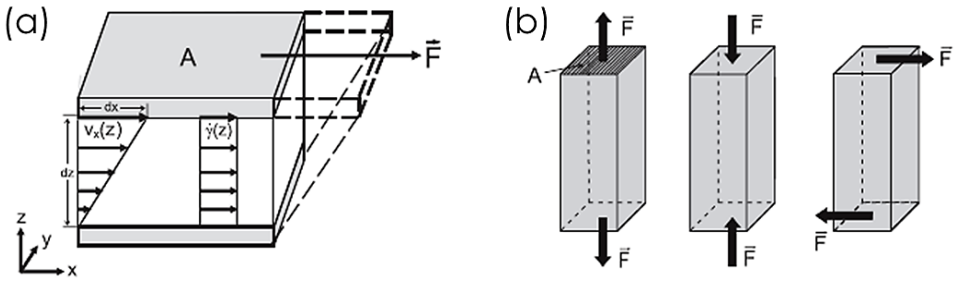

Fig. 4.1 (a) velocity distribution $v_x(z)$ and shear rate $\dot{\gamma}(z)$ acting in the two–plate model. (b) Force $\vec{F}$ direction separation into elongation, compression, and shearing. Modified according to [78].

The horizontal displacement dx can be specified in dependence to the shearing gap dz, which defines the shear deformation γ. During continuous shearing, a gap dependent

velocity gradient $v_x(z)$ establishes in shear direction x and can be transferred into the gap independent shear velocity or rate $\dot{\gamma}$:

$$\dot{\gamma}(z) = \dot{\gamma} = \frac{1}{dt}\frac{dx(z)}{dz} = \frac{dv_x}{dz} \tag{4.1}$$

4.1.1 Viscous, elastic, and viscoelastic deformation

The deformation behavior of materials can be divided in three properties and those combinations: viscosity, elasticity, and viscoelasticity.

Viscous deformation: Ideal fluids can be described by the *Newton equation* (4.2) which is valid for a steady laminar flow, separated by infinitesimal thin and incompressible layers which slip one below the other due to internal friction:

$$\frac{F}{A} = \sigma = \eta \cdot \dot{\gamma} \tag{4.2}$$

Ideal fluids show direct proportionality between shear stress σ and shear rate $\dot{\gamma}$, where the viscosity η acts as proportional constant. Viscosity is the internal friction of a fluid or its tendency to resist flow. The case that the viscosity is independent on the shear rate is called linear regime and a zero shear rate viscosity η_0 can be measured. When η becomes a function of $\dot{\gamma}$, the behavior is called nonlinear. Newtonian fluids are mechanically represented by a dash pot, because after load removal the fluid stays completely deformed.

Elastic deformation: Deformation of an ideal elastic material is completely reversible after load removal and has an ideal elastic response. This behavior is illustrated by a spring, which fully recovers its initial state and can be described by *Hook's law* (4.3):

$$\sigma = G \cdot \gamma \tag{4.3}$$

The shear stress σ behaves proportional to the shear deformation or strain γ. They are related to each other by the shear modulus G, i.e. the stress response is in phase with the excitation.

Viscoelastic flow and deformation: All materials possess both viscous and elastic behavior and depending on which part dominates they show viscoelastic flow or deformation properties on different time scales. Viscoelastic flow behavior describes viscous on long time but elastic deformation on short time scale. Viscoelastic solids show delayed deformation which recovers slowly. Ideal viscoelasticity can be described by combining Newton's and Hook's law in two different models. The *Maxwell model* refers to viscoelastic flow behavior and connects the dash pot and spring in series, i.e. the total stress charges each element in equal measure and total strain is obtained as sum of the individual deformations; shear or deformation velocity behave also additive (figure 4.2). Solids with additional viscous properties can be described by the *Kelvin-Voigt model*. Thereby, dash pot and spring are arranged in a parallel way and each

element is deformed to same extent (figure 4.2). The total stress of the system results as sum of Hook's and Newton's equation:

$$\sigma_{total} = G \cdot \gamma + \eta \cdot \dot{\gamma} \tag{4.4}$$

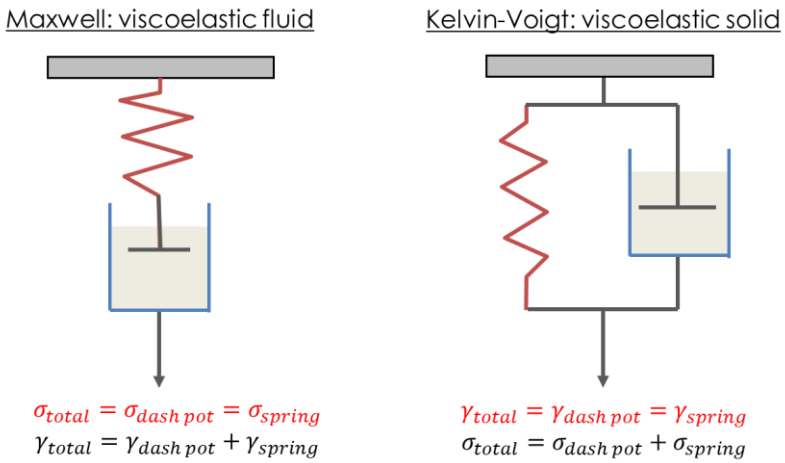

Fig. 4.2 Maxwell model for fluids with elastic components and Kelvin–Voigt model for solids with viscous components.

4.1.2 Steady and dynamic measurements

In the steady shear measurements a shear rate $\dot{\gamma}$ is applied and shear stress σ or directly the viscosity η are measured as response under steady state conditions. In oscillatory shear, not only the applied strain or shear rate, but also the direction of shear changes permanently in a sinusoidal manner with the angular frequency $\omega = 2\pi f$. These oscillatory measurements are called dynamic measurements due to the continuously changing strain. In dynamic measurements the strain amplitude γ_0 follows a sinusoidal excitation and the torque is measured. The sinusoidal displacement is given by the following equation:

$$\gamma = \gamma_0 \sin(\omega t) \tag{4.5}$$

Here, γ defines the deformation strain, γ_0 the amplitude of the sinusoidal movement, and ωt the excitation frequency. When this deformation is forced on a sample, the stress responses to this excitation with a phase lag after a few oscillations (figure 4.3). The resulting stress, with a phase shift, is given by equation (4.6):

$$\sigma = \sigma_0 \sin(\omega t + \delta) \tag{4.6}$$

After derivation of equation 4.5 an expression for the shear rate can be obtained:

$$\dot{\gamma} = \omega \gamma_0 \cos(\omega t) \tag{4.7}$$

The shear stress can be separated into two contributions, the term $\sin(\omega t)$ in phase and the term $\cos(\omega t)$ 90° out of phase [79]:

$$\sigma = \sigma'(t) + \sigma''(t) = \sigma'_0 \sin(\omega t) + \sigma''_0 \cos(\omega t) \tag{4.8}$$

The sinusoidal varying stress is usually expressed as a complex quantity and can be split into the shear storage modulus $G'(\omega)$ and the shear loss modulus $G''(\omega)$ [79]:

$$G^* = \frac{\sigma^*}{\gamma^*} = G' + iG'' \tag{4.9}$$

$$G'(\omega) = \frac{\sigma'_0}{\gamma_0} = \frac{\sigma_0}{\gamma_0}\cos(\delta) \tag{4.10}$$

$$G''(\omega) = \frac{\sigma''_0}{\gamma_0} = \frac{\sigma_0}{\gamma_0}\sin(\delta) \tag{4.11}$$

In equation 4.9 the real part G' reflects the elastic and the imaginary part G'' the viscous part of the complex modulus G^*. Thus, the shear stress consists of one part following Hook's law and of one part following Newton's law. In a purely viscous response strain and stress are out of phase ($\delta = 90°$) and in a purely elastic response strain and stress are in phase ($\delta = 0$). More complex materials where the angle between strain and stress ranges between 0° and 90° are called viscoelastic materials [78].

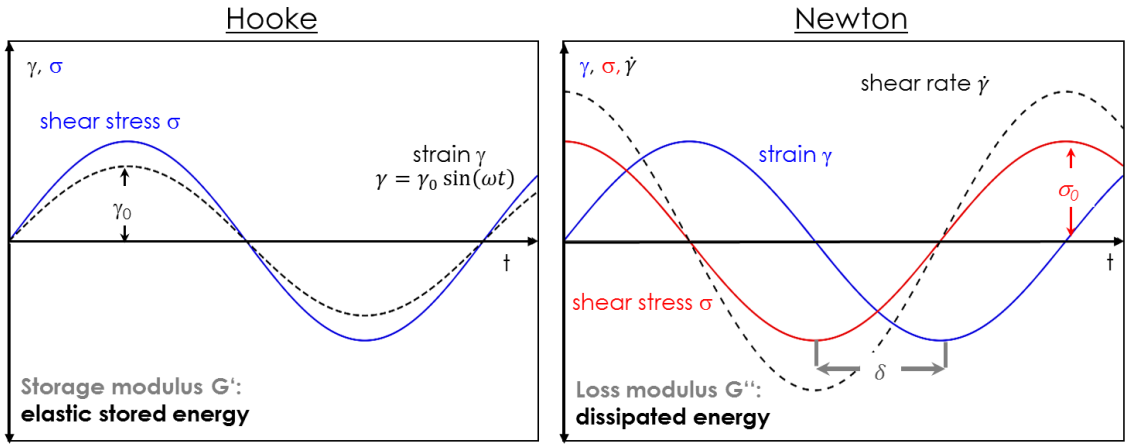

Fig. 4.3 Storage modulus G' expresses the elastic part of a viscoelastic material where shear stress responds directly in phase to an applied strain. The storage modulus counts the stored deformation energy during the shearing process, which is completely available after load removal and allows the material to recover completely. Loss modulus G'' defines the viscous part of the sample by delayed response of shear stress (phase shift). The loss modulus represents the dissipated and lost deformation energy which was needed to change the sample structure or was released to the environment. Viscoelastic materials range between those two limiting cases.

Each periodic or dynamic measurement at a given frequency provides simultaneously two dependent quantities, either $G'$and G'' or $\tan\delta$, which is known as loss factor and defines the ratio of viscous and elastic part, i.e. the angle between excitation and response:

$$\tan\delta = \frac{G''}{G'} \tag{4.12}$$

Table 4.1 summarizes five limiting cases of material behaviors and their mathematical properties:

Tab. 4.1 Material behaviors and their mechanical properties. According to [78].

Ideal viscous flow behavior	**Viscoelastic fluids**	**Ideal Viscoelastic materials**	**Viscoelastic gels or solids**	**Ideal elastic deformation behavior**
$\delta = 90°$	$90° > \delta > 45°$	$\delta = 45°$	$45° > \delta > 0°$	$\delta = 0°$
$\tan\delta \to \infty$	$\tan\delta > 1$	$\tan\delta = 1$	$\tan\delta < 1$	$\tan\delta \to 0$
$G' \to 0$	$G'' > G'$	$G'' = G'$	$G'' < G'$	$G'' \to 0$

4.2 Properties of fluid foods

Foods can be classified into different groups, such as solids, gels, homogenous fluids, suspensions of solids in liquids, and emulsions [80]. Fluid foods do not retain their shape after deformation and in addition, those containing significant amounts of dissolved high molecular weight polymers and/or suspended solids exhibit non-Newtonian flow behavior, i.e. viscoelastic properties. Already a small amount of a dissolved polymer can increase the viscosity and alters the flow characteristics of the solvent.

4.2.1 Fluid flow behavior

The major flow behaviors of fluids can be monitored in a shear diagram of shear rate versus shear stress (figure 4.4a) or in a flow curve where shear rate is plotted versus viscosity (figure 4.4b). As a function of shear rate, materials can possess three main mechanical responses, Newtonian, shear thinning, and shear thickening, subdivided depending on the presence of a yield stress σ_0 or zero shear viscosity η_0.

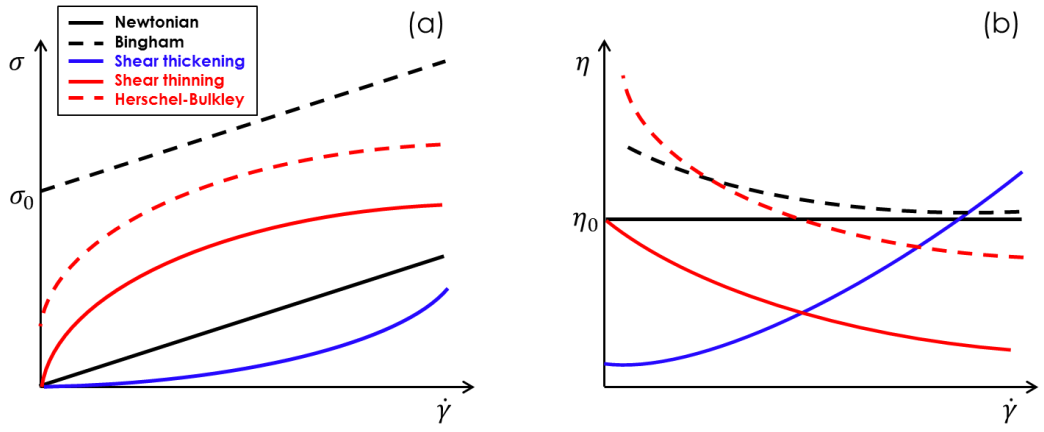

Fig. 4.4 Shear diagram of shear rate $\dot{\gamma}$ versus a) shear stress σ and b) viscosity η for five different types of fluid flow behaviors.

Newtonian behavior: For Newtonian fluids the shear rate is directly proportional to the shear stress and the viscosity stays constant during the whole shear rate range. The flow behavior of Newtonian fluids is described by the simple Newton equation (4.2). Some materials have to overcome a certain threshold value of stress before they start to flow, the yield stress σ_0 which defines the transition from reversible to irreversible elastic deformation. Such materials which demand a yield stress in order that the viscosity stays constant with increasing stress or shear rate are called *Bingham plastic fluids* and are described be the following equation:

$$\sigma = \sigma_0 + \eta'\gamma \tag{4.13}$$

The stress diagram (figure 4.4a) shows Newtonian fluids and Bingham plastics as straight lines where the Newtonian plot begins in the origin and the Bingham plot at σ_0. Due to the constant proportionality of shear stress and rate for the Newtonian fluid its flow curve (figure 4.4b) runs parallel to the abscissa; that of the Bingham plastic only after overcoming the yield stress.

Shear thinning/thickening behavior: Shear thinning fluids show a decreasing shear stress or viscosity with increasing shear rate, i.e. an increasing shear rate gives a less than proportional increase in shear stress. Shear thickening behavior shows the opposite way, i.e. an increasing shear stress gives a more than proportional increase in shear rate. To describe the shear rate–shear stress relation more parameters are needed. The *power law model* describes the data of shear thinning and shear thickening fluids [81]:

$$\sigma = K\dot{\gamma}^n \tag{4.14}$$

$$\log\sigma = \log K + n\log\dot{\gamma} \tag{4.15}$$

where K defines the consistency coefficient as the shear stress at 0.1 s^{-1} and n the dimensionless flow behavior index and reflects the similarity to Newtonian flow ($n = 1$ and $K = \eta$). For $n < 1$ the fluid is shear thinning and for $n > 1$ it is shear thickening with increasing shear rate. The logarithmic coordinates are often used to directly identify a linear dependence. In the stress diagram (figure 4.4) the curves of shear thinning or thickening can begin at the origin and show a zero shear viscosity in the flow diagram; but they can also exhibit a yield stress which can be included in the power law and is known as *Herschel-Bulkley* model [81]:

$$\sigma = \sigma_{0H} + K_H\dot{\gamma}^{n_H} \tag{4.16}$$

Shear thinning is supposed to occur when during shearing particles deform or orientate according to the flow and minimize the flow resistance. Such minimization depends on the material nature (figure 4.5). Anisotropic particles orientate in parallel fashion along the flow direction; isotropic particles arrange into parallel layers which are able to slide against each other, and deformable particles like droplets adopt the deformation by shearing. Aggregates of particles may be destroyed by the shearing force and are

separated in those primary particles. The shear thinning behavior of polymers is generated by their entanglements. During shearing the polymer molecules straighten along the shear direction, partially disentangle and minimize the flow resistance. Extreme shear conditions may lead to a disruption and destroying of the polymer chains, resulting in a degradation of the chemical structure [78].

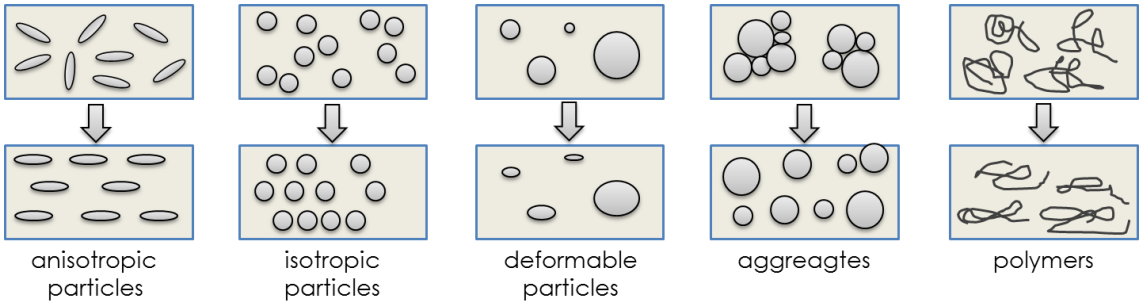

Fig. 4.5 Structure changes of different dispersions during shearing.

Polymer solutions can show at low shear rates a constant viscosity, the plateau value η_0 is called zero shear viscosity (figure 4.4b) and after reaching a critical shear rate the sample shows shear thinning. At low shear rates releasing entanglements caused by shearing and their reformation caused by Brownian motions balance each other and a constant density of entanglements is reached, provoking the zero shear viscosity. At higher shear rate, the time becomes insufficient for reformation of all released entanglements, consequently the density number of entanglements decreases with increasing shear rate and the sample shows shear thinning. This regime follows the power law and can extend over several decades in shear rate. The critical shear rate where shear thinning starts is the reciprocal of the characteristic relaxation time needed to form new entanglements [82]. The value of η_0 in the low shear range significantly depends on the polymer concentration. Already shown in 3.1, polymer solutions have to reach a critical concentration *c** to form a constant density of entanglements. Thus, low concentrated polymer solutions without effective entanglement density behave ideal viscous and the viscosity is directly proportional to particle concentration (figure 4.6a).

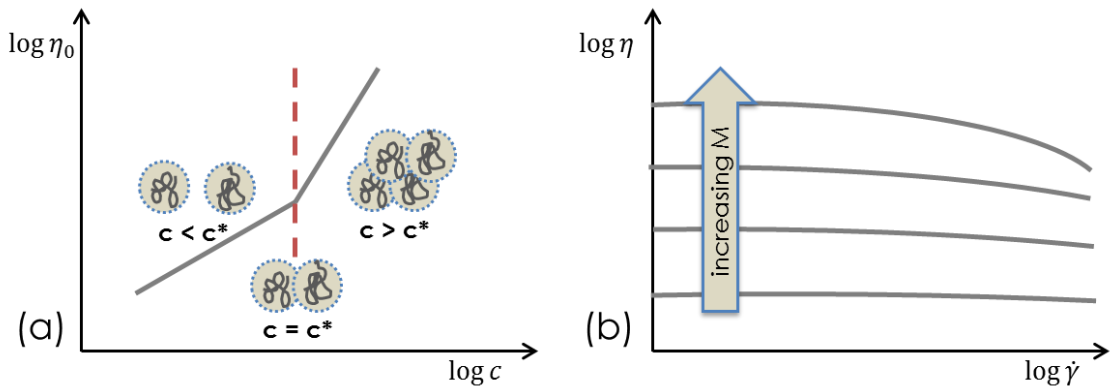

Fig. 4.6 Zero shear viscosity in dependence of a) polymer concentration and b) molecular weight. Modified according to [78].

Concentrated polymer solutions with constant entanglement density show an increasing zero shear viscosity with increasing concentration and increasing molecular weight (figure 4.6b). The effective entanglement density depends either from the polymer concentration as well as from their chain length, i.e. molecular weight. With increasing molecular weight, the number of effective entanglements increases and thus the zero shear viscosity increases. In diluted solutions the intrinsic viscosity may help in addition to characterize the polymer solution. The intrinsic viscosity $[\eta]$ of a polymer in solution depends only on the dimension of the polymer chain, i.e. the hydrodynamic volume and is related to the molecular weight and to the radius of gyration [80].

Time dependent behavior: Viscosity and shear stress of fluids may also depend on the duration of a constant shear. Shear thinning or thickening is not only produced by increasing shear rate but also by long reigning deformation with constant shear. Shear thinning by time is called thixotropic and shear thickening is known as antithixotropic behavior. (Anti)thixotropy can be identify by measuring shear stress in dependence of first ascending order of shear rate and immediately followed in descending order. For thixotropic fluids, the received curves do not coincide thus the values of the second run are lower than the one of the first run. Antithixotropic materials in contrast show higher shear stress values in descending order of shear rate than for the ascending order [81].

4.2.2 Effect of temperature

Temperature has a great effect on viscosity and other mechanical properties of fluid foods, especially on the apparent viscosity at a specific shear rate or on the consistency index, K, of the power law in equation 4.14. The effect of temperature on the apparent viscosity η_{app} at a specific shear rate or the consistency index K can be for example described by the *Arrhenius relationship* [81]:

$$\eta_{app} = \eta_{\infty A} \exp\left(\frac{E_a}{RT}\right) \tag{4.17}$$

$$K_{app} = K_{\infty} \exp\left(\frac{E_a}{RT}\right) \tag{4.18}$$

$\eta_{\infty A}$ and K_{∞} define the frequency factor or in general the pre-exponential factor, E_a the activation energy for the elementary flow, and RT the thermal energy as product of gas constant and temperature. The whole expression $\exp\left(-\frac{E_a}{RT}\right)$ corresponds to the Boltzmann factor and gives the probability of the molecules to overcome the energy barrier. With increasing temperature the energy of the whole system consequently increases and more and more energy is available to move molecules and to cross the energy barrier for the elementary flow which leads according to equation 4.17 to a decreasing viscosity.

4.2.3 Polyelectrolytes

Polyelectrolytes are water soluble polymers with ionic groups either on main chain atoms, as in the case of ι-carrageenan, or on side chains, as in the case of xanthan gum. Whereas for uncharged polymers in solution a random coil conformation can be found, polyelectrolytes have, depending on their charge, a more extended conformation due to electrostatic repulsion. Reduced viscosity:

$$\eta_{red} = \frac{\eta_{sp}}{c} \tag{4.19}$$

where $\eta_{sp} = \frac{\eta - \eta_0}{\eta_0} = \eta_{rel} - 1$ (4.20)

with $\eta_{rel} = \frac{\eta}{\eta_0}$ (4.21)

of polyelectrolytes increase strongly with increasing polymer concentration, pass through a maximum, and then decline [64]. This maximum of η_{red} is most pronounced in the absence of an added low molecular salt and decreases with increasing salt concentration.

Polyelectrolytes are little dissociated at both, high polyelectrolyte concentration without added salt and low polyelectrolyte concentration with high concentration of added salt. The lower the polyelectrolyte concentration, the more polymer groups will dissociate and the more they will repel each other. As a result, molecule dimensions and therefore reduced viscosities increase strongly with decreasing polymer concentration. Addition of salt increases the ionic strength outside the coils relative to the interior, and osmotic effects cause water to quit the polymer coil which therefore contracts.

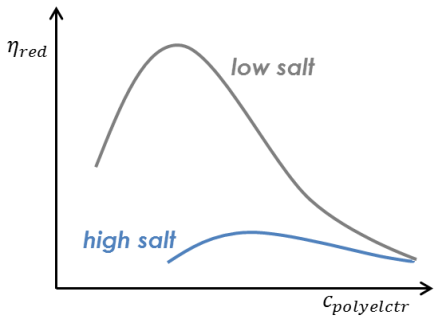

Fig. 4.7 Reduced viscosity as function of polyelectrolyte concentration in aqueous solution with various salt concentrations. Modified according to [64].

In addition the added counterions may reduce the electrostatic repulsion within the coil. Both effects reduce the coil diameter, and therefore the reduced viscosity, compared to the coil dimension in salt free solutions. For diluted, salt free polyelectrolyte solutions a proportionality of $\eta \sim c^{5/4}$ is predicted, similar to semiconcentrated solutions of nonelectrolytes. In aqueous semidiluted polyelectrolyte solutions, it is assumed that the molecules behave like strings of interconnected electrostatic blobs whose specific viscosity increases with the square root of concentration [64]. For charged hydrocolloids this blob chain implies electrostatic stretching by the charges placed along the chains and an additional stiffening of the backbone [83].

4.2.4 Role of filler particles

The viscosity of concentrated dispersions of not interacting solids strongly depends on volume fraction ϕ of the suspended granules and the relative viscosity of the dispersion, simplified for spherical colloids in solution according to *Einstein's equation* [84]:

$$\eta(\phi) = \eta_0(1 + 2.5\phi) \tag{4.22}$$

where $\eta(\phi)$ is the viscosity of the dispersion and η_0 the viscosity of the continuous phase. Consequently, with increasing amount of rigid solids, the viscosity of the dispersion significantly increases. The shape of the colloids only determines numerical factors and equation 4.22 can be also adapted for flexible, nonionic hydrocolloids considering concentration, molecular weight or structure of the dissolved polymers [83].

4.3 Rheology of food gums and gels

Food gums and gels have a much lower flow rate than food fluids and are able to retain and rebuild their former shape after deformation depending on the extent of their elastic part, showing solid-like behavior. Many water soluble hydrocolloids form viscoelastic dispersions or even physical gels, structured by weak interaction. At the molecular level, a gel consists of a continuous network of polymer molecules, in which the stress resisting macroscopic properties are mediated by a framework of polymer chains through the whole gel [18]. Depending on the strength of the three dimensional network, weak and strong gels can be distinguished. Weak gels, such as xanthan gum, are transient in time and can be easily broken by stress application. Strong gels, like agarose, in contrast have a finite energy which maintains the shape by physically crosslinked polymer chains. For both, weak and strong gels, the storage modulus dominates the loss modulus throughout the whole frequency range, but the storage modulus for strong gels stays almost independent of frequency and exceeds the loss modulus significantly. Weak gels rather have a much higher dependence on frequency for storage and loss moduli, suggesting relaxation processes even at short time scales, i.e. high frequencies, and in addition lower values of the storage modulus indicating a worse energy recovery [85].

4.3.1 Model treatment of gels

The elastic response of a gel network can be explained with the help of an ideal rubber. A rubber material can be regarded as a macroscopic three dimensional network of polymer chain strands with both ends as covalent crosslinks. These crosslinks keep the chain strands from flowing away with an applied deformation, enabling rubbers to recover their conformations and shapes once the deformation is released [86]. From an entropic point of view the stretching of the polymer chains during shearing is

inappropriate, that is why the rubber elasticity and the origin of the restoring force arises from the entropy regain after deformation. Thus, only the elastic properties have to be considered during shearing a rubber material. In contrast uncrosslinked polymers only exhibit such elastic response under momentary deformation, while under prolonged molecule chains flow and shape recovery is not possible. Thus, elastic and viscous contributions have to be analyzed. However, the shear modulus for such rubber networks can be simplified as [70]:

$$G = \frac{\rho RT}{M_c} \cong \frac{k_B T}{\xi^3} \tag{4.23}$$

where ρ is the density of the rubber material, RT the product of gas constant and temperature, M_c the mean molecular weight of a chain strand between two adjacent crosslinks and ξ^3 the three dimensional mesh size. Consequently, in an ideal rubber material the shear modulus is directly proportional to the number of crosslinks, behaving reciprocal to M_c. For this simplification, some restrictions have to be taken in account: (1) the network contains N chains per volume and one chain defines the molecule segments between two crosslinks; (2) during deformation the volume stays constant; (3) the mean-square end to end distance of the unstrained chains is equal to that of free chains; and (4) the entropy of the networks results as sum of the entropies of the individual chains [18]. These physical basics for the rubber elasticity are also responsible for the viscoelastic behavior of other polymer networks. In a polymeric liquid with a sufficiently high entanglement density, the entanglements can be treated as transient and impermanent, ”soft” crosslinks, which can be regarded as fixed before deformation is applied and the shear modulus also depends on those numbers. While transferring this conception of rubber elasticity to biopolymer networks, it should be noted that the crosslinks consist of low energy physical interaction and they are not limited to single points but correspond to extended junction zones. In addition, polymer chains can have several degrees of temperature depending rigidity which significantly may influences the shear modulus of the material, too [18]. Nevertheless, adaptions of the network theories for rubber elasticity can be made for soft polymer gels with more or less transient networks, where junction zones are temporary and not permanently, so that by thermal motion existing junctions can continually be destroyed to form new ones [87]. Total agreement cannot be expected, since the actual structure of these networks is more complicated than gels with simple point crosslinks and fully flexible chains, for which the scaling relation in equation 4.23 is derived [83].

4.3.2 Sol–gel transition and structure development

During gelation, a polymer undergoes a transition from a sol with liquid character, $G'' > G'$, to a gel with a solid-like behavior, $G' > G''$. This transition goes along with a loss in entropy and has to be compensated by an enthalpy gain via formation of junction

zones of individual polymer chains. This process of random junction zone formation between different molecules can continue until a three dimensional network results [88]. Near the gel point, where G' crosses G''at a given frequency, the relaxation time of the polymer chains rises sharply and finally diverges to infinity at the gel point. After the gel point when the network has developed, the maximum relaxation time of the network is reached. During network development both moduli G' and G'' increase as a result of the increasing density of junction zones, but G' rises more sharply until it exceeds G''. After the gel point, G' keeps increasing but to a lower extend due to slower formation and nonequilibrium rearrangements of junction zones resulting in shorter elastically active chains [18]. Many biopolymer gels show decreasing viscoelastic properties with increasing temperature. The network stabilizing hydrogen bonds or electrostatic interaction are very heat instable and in addition due to the temperature depending chain rigidity, an increase in surrounding temperature leads to decreasing moduli.

4.3.3 Mixed and filled gels – composite gels

Mixed systems of two or more biopolymers show different mechanical behavior than the individual components and new food structures and textures can be obtained. As already described in chapter 3, different combinations and resulting properties in such multicomponent systems are possible. Segregative interaction, arising from thermodynamic incompatibility either by phase separation or by exclusion effects, usually promotes self–association within a single–phase. Nevertheless, a few systems may show associative gelation of the different polymers into conformational ordered cooperative junction zones [18]. The viscoelastic properties of the mixed gel change considerably compared to that of each component. They may behave synergistic, i.e. the moduli of the composite gel are greater than the sum of the individual gels, they can be additive, when the moduli add up, or antagonistic, i.e. they behave contrariwise, producing lower values of the mixed moduli. However, the resulting viscoelastic profiles of the mixed gels mainly depend on the involved interaction between the polymers, associative or segregative, their proportion in the mixture, ionic conditions, and temperature [18]. Takayanagi and co-workers presented the viscoelastic properties of heterogeneous materials in terms of simple mechanical models comprising elements connected partly in series and partly in parallel [89] (figure 4.8). In the parallel arrangement, the deformation of the weaker component is limited by the modulus of the stronger material and both components are deformed to the same extent. The total stress results as sum of the individuals stresses $\sigma_{total} = \sigma_1 + \sigma_2 + \sigma_3 + \cdots$. In the series arrangement, the strength of the weaker component limits the deformation transmitted to the stronger material and the total strain is $\gamma_{total} = \gamma_1 + \gamma_2 + \gamma_3 + \cdots$ [90].

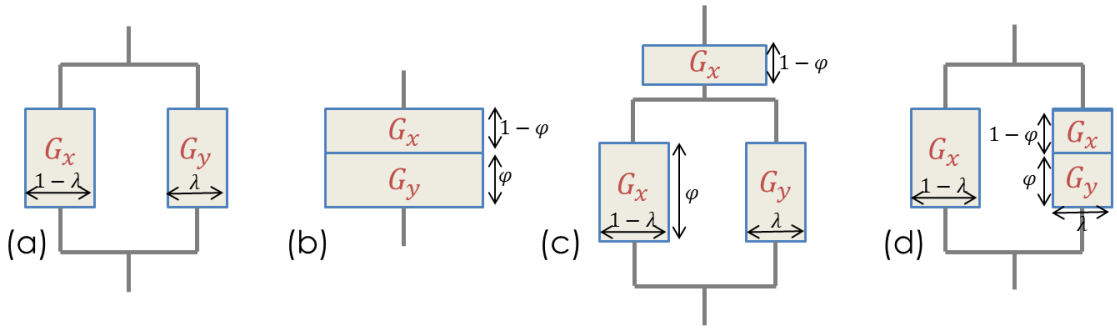

Fig. 4.8 Models for two–phase systems. (a) and (b) present the classical parallel (isostrain) and series (isostress) arrangement; (c) and (d) illustrate the combinations of these two limiting cases. λ and φ denote the according volume fraction. Modified from [90].

Other mixed systems can be described as filler–matrix composites. Filled composites generally have greater elastic moduli compared to unfiled matrix. Various models have been developed to describe this effect, and are comparable to Einstein's equation (4.22) for fluid systems with the general form:

$$G' = G'_0(1 + 2.5\phi) \text{ or } \frac{G'}{G'_0} = \frac{1+AB\phi}{1-B\phi} \tag{4.24}$$

where G'_0 and G' are the unfilled matrix and filled composite moduli, respectively, A is a geometric factor, and B is a function of A and the ratio of the filler and matrix moduli [91]. Consequently, at low concentrations when filler particles do not interact with each other, they mainly contribute by their volume fraction ϕ. A starch gel for example, see chapter 2.2.2, can be understood as a phase separated network of undissolved, elastic granule remnants embedded in a continuous matrix of entangled amylose polymer chains and highly branched amylopectin segments [71]. The modulus of such composite gels depends on the rigidity of the amylose matrix, and the volume fraction and rigidity of the filler particles (granule remnants). Compared to equation 4.24, the dynamic rheological modulus of the composite can be denoted as G', that of the amylose matrix G'_0 and the volume fraction of the granules as ϕ. In general, for noninteracting and randomly distributed filler particles, the shear modulus of the composite yields an elastic reinforcement which is independent of the particle size and increases with increasing volume fraction. Thus, the effects on viscoelastic properties arise from the partial occupancy of volume by the rigid and immobile masses [79].

5 Materials and Methods

The following chapter describes in detail the used methods and performed experiments to characterize the properties of the native tapioca starch TS and the spray dried starch SDTS as well as their mixtures with the different hydrocolloids. The main focus is on a rheological investigation with distinct testing methods to carry out various mechanical parameters for the characterization. Optical analysis, such as confocal laser scanning and light microscopy, supports the results from rheology and helps to gather a model conception of the network structures in the different composite gels. In addition, to understand the structural alteration after the spray drying process of the starch paste, further experiments like dynamic light scattering, differential scanning calorimetry, and various shear experiments are conducted. Before the different methods are presented, the used materials and the preparation process of the spray dried tapioca starch are described.

5.1 Materials

Native tapioca starch (TS) was donated by Cargill B.V. (C*CreamGel 70001, protein 0.4%, ash 0.1%) with an average moisture content of 12.81%. Xanthan gum (XG; E-415, high purity, CAS-No. 11138-66-22, item no. 3557.1) and ι-carrageenan (ιC; high purity, CAS-No. 9062-07-1, item no. 3675.3) are purchased from Carl Roth GmbH & Co. KG; guar gum (GG; CAS-No. 9000-30-0, item no. SLBH5693V) from Sigma–Aldrich Chemie GmbH. Moisture contents of xanthan gum, ι-carrageenan, and guar gum were 12.56%, 9.15%, and 11.78% respectively.

5.2 Preparation of spray dried tapioca starch (SDTS)

In order to produce a cold soluble tapioca starch, an already gelatinized starch paste was spray dried. For this, the dry tapioca starch was suspended in distilled water according to the following equation:

$$m_{dry\,TS} = \frac{3\% \cdot m_{total}}{100\% - MC_{dryTS}} \tag{5.1}$$

During constant stirring (160 rpm) the 3% w/w suspension was heated up to 95 °C in an oil bath, kept there for 10 min and slowly cooled down to room temperature. A 3% per weight solution was chosen, to compromise between the increasing viscosity of the paste at higher concentrations that hampers the spray drying process and the

requirement of sufficient yield of the dry product. The gelatinized starch paste was transferred to a spray dryer on laboratory scale. A *Büchi B-290 Mini Spray Dryer* (Büchi Labortechnik, Switzerland) was used (figure 5.1). The *Mini Spray Dryer B-290* operates according to a co-current flow atomizer principle, i.e. the sprayed product and drying air flow move in the same direction. The spray drying process finally involves the evaporation of water from the atomized starch paste. Therefore, the viscous paste was transported via a peristaltic pump with a pump rate of 10% to a two–fluid nozzle (0.7 mm nozzle tip diameter) and atomized with an inert nitrogen gas flow (flow rate = 1052 L/h). The inlet drying temperature was 200 °C and the aspirator rate was set to 100%. By the use of a high performance glass cyclone, the spray dried tapioca starch was obtained as a dry and white powder with an average yield of 25% and an average moisture content of 8.04%. The outlet temperature ranged between 98 °C and 103 °C and is the result of the combination of inlet temperature, aspirator flow rate, peristaltic pump setting, and sample concentration.

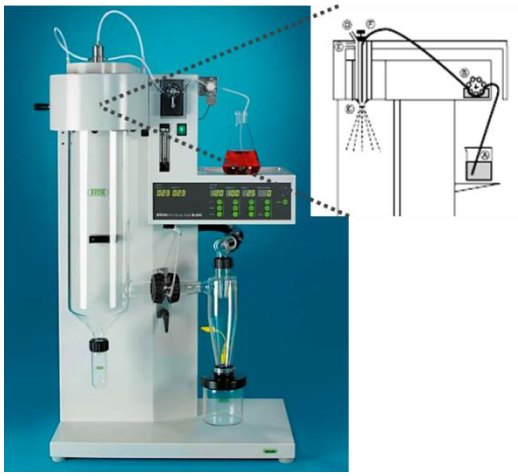

Fig. 5.1 *Büchi B-290 Mini Spray Dryer* used for production of pregelatinized spray dried tapioca starch (SDTS) and schematic diagram of the product flow and spray nozzle. Adapted from Büchi Labortechnik, Switzerland.

The instrument settings, i.e. inlet temperature, feed rate, spray air flow, and aspirator flow, influence the product parameters, such as temperature load, humidity, particle size, and especially yield. Due to subsequent macroscopic analyses of SDTS, the main purpose of optimizing the product parameters was reproducibility and a great yield, and the instrument settings were chosen accordingly. However, the high aspirator speed results in a higher separation in the cyclone; the high spray flow rate tends to yield smaller droplets and increases the drying process (cf. 2.3.2); the low feed rate facilitates a sufficient time for heat and material flow, and the high inlet temperature provides greater drying energy and a lower relative air humidity.

5.3 Mechanical spectroscopy

The viscoelastic properties of the different starch-based systems were measured with a *Gemini 200 Advanced Rheometer* from Bohlin Instruments (Malvern, U.K.). In general, there are two different construction types of rheometers: stress controlled or strain controlled (figure 5.2). The used *Gemini 200 Rheometer* is a stress controlled system, where a shear stress is applied and either the shear strain or shear rate results as measuring size. When a stress is produced, the strain induced in the sample can be measured using a displacement sensor. Additionally, motor and sensor (transducer) are integrated in one device at the upper rotating part of the system. In contrast, motor and torque sensor are separated for the strain controlled rheometer. In this case, the strain or deformation is applied with the motor and the stress (torque) is transmitted as sample response to the transducer [78].

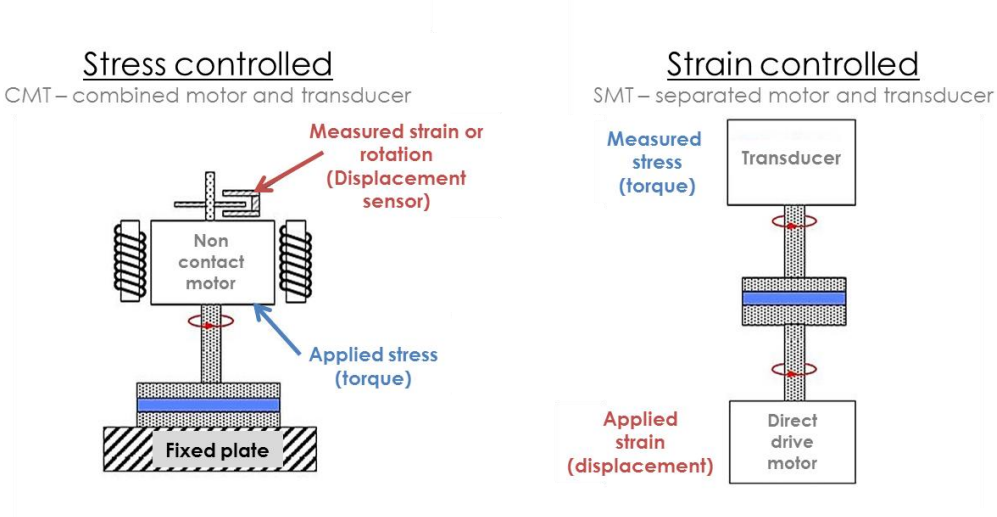

Fig. 5.2 Stress controlled versus strain controlled rheometer set up. Modified according to http://polymerinnovationblog.com/rheology-thermosets-part-2-rheometers/.

The *Gemini 200 Rheometer* used possesses in addition an internal coaxial peltier cylinder system to enable temperature depending measurements. This temperature control system consists of a cylinder system heated by peltier elements and a water/glycol cooling kit to allow the dissipation of heat energy. Thus, a temperature stability of ±1 °C can be realized.

During this study, two different shear methods, i.e. steady and dynamic experiments, were performed yielding different but mutual supporting information. Depending on the nature of the sample and heat application, three different measurement systems were used: cone–plate, plate–plate and vane geometry (figure 5.3).

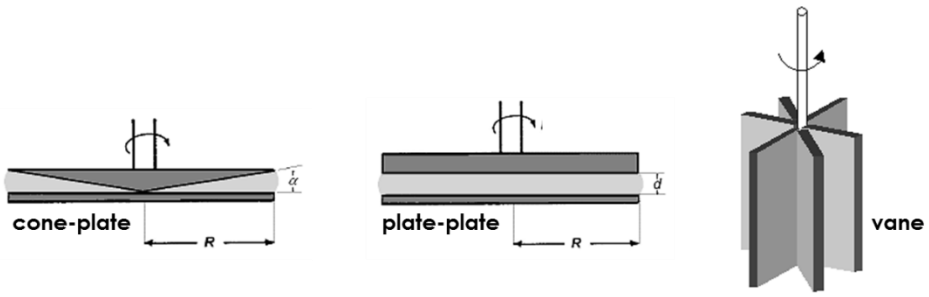

Fig. 5.3 Used measurement systems: cone–plate, plate–plate, and vane.

The cone–plate shear geometry consists of a cone and plate with the cone radius *R* and cone angle α; often the apex is oblate. The advantage of this set-up is a constant shear rate within the whole cone gap. The shear rate, as flow velocity gradient, is defined as the ratio of flow velocity and gap size (cf. 4.1). Due to the angular arrangement, both gap size and velocity increase from cone midpoint to the edge leading to a homogeneous shear deformation:

$$\dot{\gamma} = \frac{v_{max}}{h_{max}} = \frac{\omega R}{R \tan \alpha} = \frac{\omega}{\tan \alpha} \tag{5.2}$$

Consequently, the shear rate or deformation of the plate–plate geometry is radius dependent due to the increasing shear velocity with increasing plate radius *R* and the constant gap size. However, the plate–plate geometry is not as sensitive to gap setting since it is used with a separation between the plates measured in mm. It is ideally suited for testing samples through temperature gradients and due to an automatic gap setting, it qualifies for temperature depending measurements by a constant sample contact during structural transitions. The vane geometry possesses several star-like vane rotors along the rotational axis and is suited very well for shear sensitive structures. In addition, it has a very powerful mixing capability especially for high viscous samples, such as the investigated starch pastes.

As already described in 2.2.2, 3.2.3, or 4.3.2 a starch gel or paste is composed of a continuous amylose matrix filled with swollen starch granules. The rheological data of this material depend on characteristics of the dispersed and the continuous phases, and on their interactions. Especially the conditions during gelatinization and pasting determine the extent of granule swelling and integrity [60]. The degree of heating, heating time, and shear conditions influence the disintegration of the starch granules and amount of released contents, in particular amylose into the continuous phase [92].

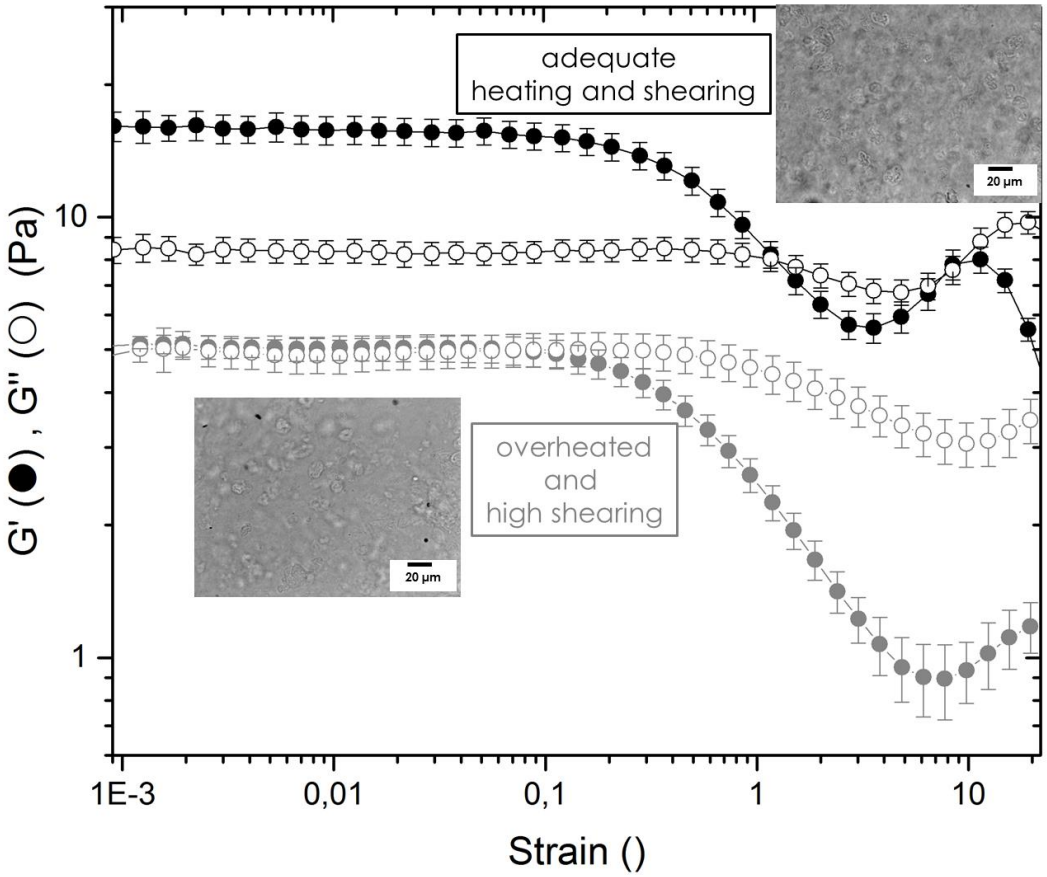

Fig. 5.4 Rheological and microscopic comparison of two differently-prepared tapioca starch pastes. The black curve of the amplitude sweeps represents a starch paste which was gelatinized during adequate heating and shearing conditions; the grey one results after high heating and shearing conditions.

Figure 5.4 shows the influence of shearing and heating conditions during the pasting process for native tapioca starch. Compared are the results of an amplitude sweep test (procedure see 5.3.3) and the corresponding light microscope images for differently-prepared starch pastes. The black curve corresponds to a starch paste gelatinized with the *Gemini 200 Rheometer* by heating to 95 °C and keeping it there with constant stirring at 200 s^{-1} with the vane geometry for 10 min. The grey curve results from a starch paste produced by heating at 95 °C for 45 min during 600 rpm stirring in a glass vessel on a heating plate. The harsh heating and shearing conditions of the latter apparently lead to a higher disintegration of the starch granules and thus to the formation of much weaker network structures, reflected by lower values for G' and G''. Consequently, the knowledge and compliance of the conditions during the pasting process are very important for the evaluation of rheological data and were strictly adhered to the following experiments.

5.3.1 Sample preparations

All following rheological experiments were performed either with the individual polysaccharides, i.e. native tapioca starch (TS), spray dried tapioca starch (SDTS), xanthan gum (XG), ι-carrageenan (ιC), and guar gum (GG), as well as with their mixtures in different composition ratios. Due to the insolubility of native tapioca starch in cold water, no pretreatment was required and the dry TS could be directly dispersed in water at the desired concentration and heated. SDTS, XG, ιC, and GG are soluble in water and to guarantee a complete hydration, they were dispersed in water and stirred at 200 rpm and room temperature for 24 h before each measurement. For all samples the polymer concentration comprises the inherent moisture content of the polysaccharide:

$$m_{polymer} = \frac{wt\%_{polymer} \cdot m_{total}}{100\% - MC_{polymer}} \tag{5.3}$$

Starch-nonstarch mixtures: To obtain the mixtures of TS and SDTS with XG, ιC, and GG, the different polysaccharides were first mixed on dry basis at different mixing rations, water was added and the samples were heated after hydrocolloid hydration (method 1). Two different preparation methods 2 and 3 were tested as well. During method 2, the hydrocolloid was prehydrated in the total water amount and starch was added in dry form, followed by heating. Method 3 included the separate heating of the starch dispersion and hydrocolloid solution and subsequent mixing. Method 2 turned out difficult due to the inhomogeneous distribution of dry starch within the viscous hydrocolloid dispersion. The mixing of the gelatinized starch paste with the hydrated hydrocolloid dispersion in method 3 was due to the high viscosities nonpractical and it was difficult to assure complete mixing. Therefore, method 1 that means, mixing on dry basis, was chosen to prepare the starch–nonstarch mixtures.

For the different mixtures the total polymer concentration was always set to 6% w/w, considering the moisture content of the different components. Four different mixing ratios were analyzed, in which starch was stepwise replaced by the hydrocolloids. The polysaccharide concentration increased from 0.1%, 0.5%, 0.7% to 1.0% and a mixing ratio of starch–hydrocolloid (TS–XG, TS–ιC, TS-GG or SDTS–XG, SDTS–ιC, SDTS-GG) of 59–1, 11–1, 15–2 and 5–1 resulted consequently. Subsequently, water was added, and the mixture was stirred at 200 rpm and room temperature for 24 h to enable a complete hydration of the hydrocolloid, followed by heating.

5.3.2 Data evaluation

All following measurements were repeated at least three times with always a fresh sample for each system. The rheological data were evaluated and plotted via *OriginPro*

9.1G. The results are presented as arithmetic average and the standard deviation was taken as error, but not always shown in plots to maintain the clarity of the graphs.

5.3.3 Viscosity–temperature profile (VTP)

The viscosity–temperature profile allows the determination of the pasting process of native tapioca starch in water or in the corresponding hydrocolloid dispersion. The viscosity η was measured as function of temperature at a constant shear rate of 200 s^{-1}. The temperature increased from 25 °C to 95 °C with a heating rate of 3 K/min; the sample was tempered at 95 °C for 10 min, followed by cooling to 25 °C with a cooling rate of 3 K/min. To avoid water evaporation, the measuring set-up was flushed with moisturized nitrogen. As measuring system a stainless steel vane geometry with four vane rotors and a diameter of 14 mm was used. The dry native tapioca starch was directly prepared as 6% w/w suspension in the cylinder and stirred until the measurement started. The spray dried starch and the starch–hydrocolloid mixtures were prepared as described above; the suspension was transferred to the cylinder of the vane geometry and also stirred until the measurement started. A total of 30 g sample mass was always prepared and during constant rotation the vane stamp was slowly lowered to avoid starch granule settlement.

5.3.4 Viscoelasticity as function of temperature

During this oscillating experiment, both amplitude and frequency are kept constant and only the temperature varies, providing a dynamic thermomechanical analysis of the storage G' and loss G'' moduli. This temperature sweep can be compared to the above presented viscosity–temperature profile but gelatinization is visualized by dynamic measurements, yielding the viscoelasticity in dependence on temperature. Therefore, the temperature ramp was adapted to the upper temperature profile, i.e. the temperature was stepwise increased from 25 °C to 95 °C with a heating rate of 3 K/min, kept there for 10 min and cooled again to 25 °C with a cooling rate of 3 K/min. Deformation was applied with a constant strain of 0.01 and a frequency of 1 Hz. The integration time of each measuring point was 5 s and the delay time between the points was 0.5 s, during 5 applied oscillation periods. As measuring system a stainless steel plate–plate geometry with 40 mm diameter was used. A gap size of 1000 µm was default, but the auto tension was enabled, where a constant force of 0.1 N was applied to assure a constant contact between measuring plate and sample. To avoid water evaporation during the measurement, a thin film of paraffin oil (viscosity η = 25 mPas, Merck KGaA) was used and the nitrogen flushed cover device was wrapped around the loading system. The sample preparation was analogous to the VTP but only a total of 1500 µL of each

suspension was loaded and surplus material was wiped off after lowering the upper plate.

5.3.5 Amplitude sweep

During the amplitude sweep test, an oscillating deformation is applied and the storage G' and loss G'' moduli are measured as response to the deformation. The strain γ ranges from 0.001 to 100 at a constant frequency of 1 Hz and temperature of 25 °C. As default parameters, an integration time of 5 s, a delay time of 0.5 s, and five periods were set. A stainless steel cone–plate geometry with 40 mm in diameter and a 4° cone angle was chosen and a gap size of 150 µm was default. After equilibrating for 4 h, the samples obtained from the viscosity–temperature profile measurements were used for the determination of the viscoelastic properties of the native starch and its mixtures with hydrocolloids. Since the modified starch already formed a paste at room temperature, 6% w/w paste was prepared by stirring for 24 h at room temperature and the corresponding mixtures were prepared as described above. A total of 1500 µL of each sample was loaded in the measuring system and excessive sample material was wiped off. All measurements were repeated after three days to investigate the long-term retrogradation of the starch and the demixing stability of the mixtures.

5.3.6 Frequency sweep

With a frequency sweep experiment under constant shear amplitude and temperature, information about the time dependent deformation behavior of the investigated sample can be obtained. The short time behavior is simulated by fast oscillation, i.e. high frequencies, and the long-term behavior by slow displacements, i.e. low frequencies. The frequency f ranges from 0.01 to 10 Hz at a constant strain γ = 0.01 and temperature of 25 °C. As geometry the cone–plate system (stainless steel, 40 mm diameter, 4° cone angle, and 150 µm gap size) was used as well; the sample preparation and loading was analogous to the procedure of the amplitude sweep test. Due to the time intensive measurement, a thin film of paraffin oil (viscosity η = 25 mPas, Merck KGaA) and the nitrogen flushed cover device were applied to avoid water evaporation.

5.3.7 Steady shear flow measurements

By variation of the rotational shear rate and measurements of the resulting apparent shear viscosity, information about the flow behavior of the different starch pastes and their mixtures is obtained. The shear rate increases stepwise from 0.001 to 1000 s^{-1} followed by a stepwise decrease to the initial shear rate. For each ramp (increasing and decreasing shear rate) 100 points were measured with an integration time of 5 s and a decreasing delay time starting with 30 s. As geometry the cone–plate system (stainless

steel, 40 mm diameter, 4° cone angle, and 150 µm gap size) was used and the sample preparation and loading was analogous to the procedure of the amplitude and frequency sweep test. To evaluate the shear thinning behavior of the different samples, the pseudoplastic index (PPI) was calculated. The PPI helps to examine the extent of shear thinning with the following equation [78]:

$$PPI = \frac{(\log \eta_{low} - \log \eta_{high})}{(\log \dot{\gamma}_{low} - \log \dot{\gamma}_{high})} \tag{5.4}$$

One measuring point at low shear rate (0.01 s^{-1}) and one at high shear rate (1000 s^{-1}) of the up going shear rate ramp were chosen and related to each other using equation (5.4). For an ideal viscous flow $PPI = 0$, for a shear thinning $PPI < 0$ and for a shear thickening behavior $PPI > 0$. It has to be noted that this evaluation method is only qualitative, but helps to compare the different shear thinning behavior of the investigated materials.

5.3.8 Long-term measurements of viscoelasticity

Retrogradation is a long-term process and while measuring the storage G' and loss G'' moduli after gelatinization for several hours at a constant strain ($\gamma = 0.01$) and frequency ($f = 1$ Hz) the extent of retrogradation can be determined. For this, the samples were heated to 95 °C and directly transferred onto the preheated measuring system (plate–plate, 40 mm, stainless steel) of 95 °C and the upper plate was lowered slowly to a gap of 1000 µm. The gelatinized sample was finally cooled down to 25 °C at a rate of 3 K/min and the moduli were measured for further 5 h at 25 °C. To compensate sample shrinkage, the auto tension mode with 0.1 N as well as a paraffin oil film and the nitrogen cover device were used.

5.3.9 Creep experiments

During creep and creep recovery experiments, the viscoelastic behavior is tested during two shear stress jumps. Whereas a constant shear stress is applied during the creep phase, this stress is spontaneously removed during the creep recovery phase and the sample recovers the original shape.

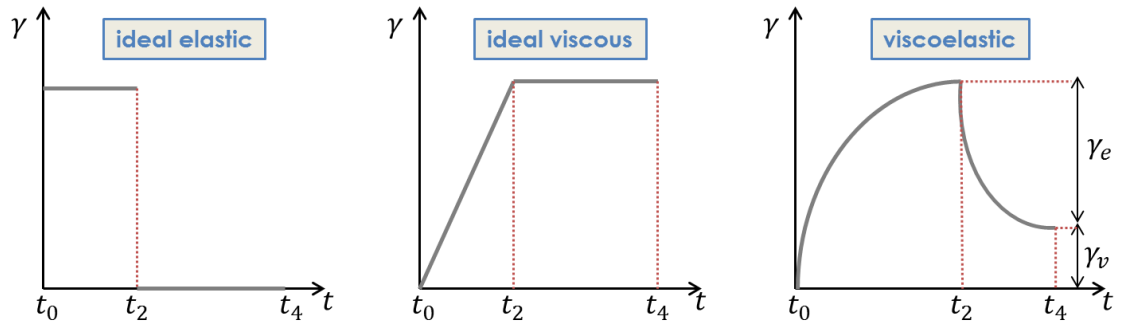

Fig. 5.5 Creep and creep recovery curve for an ideal elastic, viscous, and viscoelastic material. Modified after [78].

An ideal elastic solid shows a spontaneous and abrupt deformation during stress load. After load removal, the deformation recovers completely and spontaneously and the stored deformation energy is used for the resilience. Ideal viscous fluids are constantly deformed during load application and stay completely deformed after load removal, because no deformation energy was stored. Viscoelastic materials show a creeping deformation during load application and due to the viscous contribution a more or less pronounced retarded resilience or unrecoverable residual deformation remains. These creep tests give information about the compliance and amount of residual deformation after a defined stress of the different composite gels. The creep compliance is defined as ratio of resulting deformation with increasing time $\gamma(t)$ and constant applied stress σ_0 and behaves reciprocally to the shear modulus or stiffness of the sample:

$$J(t) = \frac{\gamma(t)}{\sigma_0} = \frac{1}{G} \tag{5.5}$$

The samples obtained after the VTP measurements were loaded onto the cone–plate geometry and during 1000 seconds a stress of 0.15 Pa were applied and after load removal, recovery was measured for further 1000 seconds.

5.4 Optical analyses

5.4.1 Confocal laser scanning microscopy (CLSM)

Confocal laser scanning microscopy is highly suited for structural analysis of biological and food materials. It is possible to label simultaneously two or more components of food with different fluorescence probes and therefore food structures may be described in more detail [93]. In contrast to conventional light microscopy, the light source is replaced by a laser, a scanning unit, and a pinhole in the back focal plane, which improves the limiting depth of focus. The primary advantage of CLSM is the ability to produce optical sections through a three dimensional specimen, which contains information from one focal plane and a stack of optical sections can be produced [94]. To image a sample point by point (scanned), the laser light passing through a pinhole

aperture is reflected by a dichromatic mirror and scanned across the specimen in a defined focal plane. Fluorescence light emitted by this excitation passes back through the dichromatic mirror and is focused as a confocal point at the detector pinhole aperture to eliminate out of focus light [95]. A major limitation of CLSM is that most samples require treatment with a fluorescent dye to get visible, which may result in artefacts and has to be taken into account during image interpretation. Usually, CLSM set-ups have two or more photomultipliers operating at different wavelengths which enable in combination with a set of laser lines of different wavelengths, the simultaneous excitation and detection of different fluorescence probes in the same sample. Thus different probes can be used and individually detected, and interactions or exact location of one polymer can be determined in a mixture of different polymers.

Sample imaging: The network structure of the starch paste and polysaccharide mixtures was analyzed using a commercial confocal laser scanning system *FluoView 300 FV 300* (Olympus, Japan) in combination with an inverted microscope *IX70* (Olympus, Japan). Fluorescence was excited by the 488 nm line of an Ar-laser and the 543 nm line of a He/Ne-laser coupled to the laser scanning unit. Images were taken at different sample depths with a 20× long distance objective (LMPLFL 20×, NA 0.40, WD 12.0 mm, Olympus Japan) on different channels and merged after sequential scanning. The obtained CLSM images were analyzed using the *ImageJ* software package, including the *LOCI* plugin. 500 µl of the each sample were placed inside 8-well chambered borosilicate coverglass systems (*Nunc Lab-Tek*, Thermo Fisher Scientific, USA). As fluorescence probes, fluorescein-5-isothiocyanat (FITC, Sigma–Aldrich Chemie GmbH, CAS-No. 3326-32-7) and rhodamine B (Sigma–Aldrich Chemie GmbH, CAS-No. 81-88-9) were used. The excitation wave lengths are 488 and 568 nm, respectively, and the emission maxima are at 518 and 625 nm, respectively. To achieve the best separation of the different emission lines, BA 510-540 band pass and BA 565IF long pass emission filter were applied.

Sample preparation: Rhodamine B was used for the noncovalent labeling of the starch phase. For this 1% w/w suspension of the native tapioca starch was gelatinized at 95 °C and during cooling 4% v/v (related to the total sample volume) of 0.2% aqueous rhodamine B solution [96] was added. The stained starch paste was allowed to stir (200 rpm) at room temperature for 24 h to warrant a homogenous distribution of the dye. In case of the spray dried tapioca starch, after dissolving the dry powder at room temperature, 4% v/v of the rhodamine B solution was directly added and stirred for further 24 h at room temperature.

Xanthan gum, ι-carrageenan, and guar gum were covalently labeled after a modified procedure of Tromp et al. [97]. The polysaccharide (500 mg) was suspended in 50 mL dimethyl sulfoxide (DMSO) and FITC (70 mg), pyridine (200 µL) and dibutyltin

dilaurate (40 µL) were added and the mixture was heated at 100 °C for 4 h. After cooling, the solution was slowly poured into 200 mL isopropanol; to complete the precipitation, the mixture was stored at 4 °C over night and the yellow powder was extracted by vacuum filtration. To remove unbound dye, the labeled polysaccharide was redissolved twice in 45 mL DMSO for 2 h, precipitated in 200 mL isopropanol and finally dried under vacuum at 40 °C.

To obtain the binary samples, the labeled polysaccharides were mixed with the native or spray dried tapioca starch on dry basis in a mixing ration of starch–polysaccharide 11–1 and a total polymer concentration of 1% w/w. The mixture was stirred at room temperature for 4 h to achieve a homogenous distribution, then 4% v/v of the rhodamine B solution was added and the stirring was continued for further 20 h. In the case of the composite with native starch, the mixture was heated up to 95 °C after the first 4 h of hydration, during cooling 4% v/v rhodamine B solution was added, and stirred at room temperature for 20 h.

5.4.2 Light microscopy (LM)

The gelatinization process of the starch granules was visualized with a light microscope *Axio Scope A1* (Carl Zeiss Microscopy GmbH, Germany) combined with a peltier controlled heating stage *PE120* from Linkam Scientific. The starch granules were dispersed as 6% w/w in pure water or in the appropriated hydrocolloid dispersion with 11–1 mixing ratio. The suspension was placed onto a specimen holder, covered with a cover slid and heated from 25 °C to 95 °C with a heating rate of 3 K/min, kept there for 10 min and cooled down to 25 °C. To enhance the image contrast two drops of a Lugol solution (iodine/potassium iodide solution, diluted 0.33% iodine, AppliChem, Germany, item no. 3U005897) were added. Images were taken with 20×, 40×, and 100× A-plan objectives (A-Plan 20×, 40×, 100×; NA 0.45, 0.65, 0.8; Zeiss Germany) and evaluated with the *ImageJ* software package.

5.5 Further characterization of native and spray dried starch

To get a better understanding of the structural changes which may happen during the spray drying process, native and spray dried starch were additionally compared by further experiments.

5.5.1 Shear/heat experiments and amylase digestion

During the spray drying process, high shear and heat conditions work on the starch paste while being forced through the spray nozzle, atomized, and dried. These influences of high shear and heat application on a starch paste produced by the native

tapioca starch were analyzed in more detail by separate treatments, and the results were compared to a paste obtained by rehydrating spray dried starch. For this, 3% w/w dry tapioca starch was suspended in distilled water and gelatinized as described in section 5.2. This starch paste was finally subjected to four different treatments: (1) the paste was transported through the spray dryer without heat application to isolate the shear conditions; (2) the paste was dried at 200 °C with a halogen moisture analyzer (*HR83*, Mettler Toledo, Germany) and resuspended in distilled water to cull the shear influences; and (3) the paste was treated with an ultra turrax (*T18 basic*, IKA, Germany) at 7000 rpm for 5 min to simulate very high shear conditions. (4) The last treatment included amylose degradation by α-amylase digestion. α-Amylase specifically attacks the α-glycosidic linkage between the glucose units along the amylose chain and offers a controlled hydrolysis of amylose. Due to the tight cluster formation by short side chains, the α-glycosidic linkages along amylopectin molecules are sterically inaccessible for α-amylase. Thus, 2000 µL of the starch paste was mixed with 20 µL of a 0.1% amylase solution (α-amylase bacterial, Fisher Scientific GmbH, CAS-No. 9000-85-5, in MilliQ water), allowed to react for 5, 10, 15, 20, and 30 min and stopped by the addition of three drops 1 N hydrochloric acid. All samples were analyzed by CLSM (cf. 5.4.1; rhodamine B labeling), LM (cf. 5.4.2), and amplitude sweep tests (cf. 5.3.5).

5.5.2 Differential scanning calorimetry (DSC)

To measure the melting temperature T_m of native tapioca starch and spray dried tapioca starch as well as to characterize gelatinization of the native starch in water and in the different hydrocolloid dispersions, DSC measurements were performed with a *DSC 822* from Mettler Toledo, Germany. Differential scanning calorimetry measures differences in change of heat flow rate of the sample and of a reference sample while they are subjected to a controlled temperature program [98]. Therefore, sample and reference are located in an oven and are heated simultaneously with constant heating rate. Structural transitions are accompanied by temperature differences between sample and reference and are directly compensated by an applied heat flow, which is measured in dependence on measuring time. For the starch analysis, DSC provides a microscopic method for observing the starch melting from very small samples, or even from single granules. For the measurement of T_m, the dry powder of TS or SDTS was weighted into 40 µL aluminum pans (~10 mg), sealed, and heated and cooled from 20 °C to 180 °C with 3 K/min; as reference an empty pan was used. Gelatinization was measured in 100 µL pans, following a temperature program of heating and cooling from 20 °C to 95 °C, 3 K/min. Therefore, native TS was suspended in water and with help of an Eppendorf pipette a total of ~87 mg of the dispersions were added, sealed and measured in reference to an empty 100 µL pan. All measurements were repeated at least three times and evaluated with *OriginPro 9.1G*.

5.5.3 Tracer diffusion via dynamic light scattering (DLS)

Dynamic light scattering methods allow the determination of diffusion processes in viscous dispersions or even gels. Here, the diffusion of added nanotracer particles in different concentrated TS and SDTS pastes is measured, which depends according to the *Stokes–Einstein equation* (5.6) on the viscosity and entanglement density of the surrounding medium, i.e. TS or SDTS paste:

$$D_s = \frac{kT}{f} = \frac{kT}{6\pi\eta_0 R_h} \tag{5.6}$$

with the selfdiffusion coefficient D_s of the tracer particles, kT as thermal energy which forces the particles to Brownian motion against friction f, composed of the solution viscosity η_0 and the hydrodynamic radius of the particles R_h [99]. Consequently, the diffusion of the added nanotracer offers valuable information about the network structure and density of the entrapping starch environment. The Brownian motion of the scattering tracers is measured by the mean-square displacement as a function of various lag times τ of the particle's trajectory through the solution [100]:

$$\langle \Delta r^2(\tau) \rangle = \left[\big(r(t+\tau) - r(t) \big)^2 \right] = 6 D_s \tau \tag{5.7}$$

This mean-square displacement can be measured, for example, by the intensity fluctuations of scattered light, which reveal the dynamics of the medium through the decay of the temporal autocorrelation function. In a dynamic light scattering experiment the time correlation function $G(q,\tau)$ of the scattering intensity as function of wave vector q, $|q| = (4\pi/\lambda) \sin\frac{\theta}{2}$, and time t is measured [101]:

$$G_2(q,\tau) = \frac{\langle I(q,t) I(q,t+\tau) \rangle}{\langle I(q,t) \rangle^2} \tag{5.8}$$

$I(q,t)$ is the instantaneous intensity, measured at a given angle θ by the detector at the time t and $I(q,t+\tau)$ is the corresponding one at a later time $t+\tau$. These obtained data can be evaluated via cumulant analysis, which bases on a series expansion and yields the selfdiffusion coefficient on short time scale [99]:

$$\ln G_1(q,\tau) = -\kappa_1 \tau + \frac{1}{2!}\kappa_2 \tau^2 - \frac{1}{3!}\kappa_3 \tau^3 + \cdots \tag{5.9}$$

$$\ln G_1(q,\tau) \approx -\kappa_1 \tau = -\langle D_s \rangle q^2 \tau \tag{5.10}$$

The corresponding measurements were performed in course of a master thesis of Thomas Limbach under supervision of PD Dr. Wolfgang Schärtl at the Johannes Gutenberg University, Mainz. The detailed experimental procedure and the evaluation of the data can be retraced in this thesis from December 2015 [102]. Using water as solvent during these experiments turned out to be very difficult, because highly swollen associated structures remained, resulting in very turbid samples. Accordingly, the scattering experiments were performed in 1/10 water/DMSO as solvent, where all starch

components are completely dissolved. As tracer particles divinylbenzyl polystyrol particles (DVB-PS) with radii of 134 and 378 nm were used and a four–angle scattering apparatus (50°, 70°, 90° and 110°), equipped with a 532 nm laser and 100 mW intensity. It has to be noted that the network structures of starch formed in this water/DMSO differ significantly from the structures built in water. Consequently, to relate the results of the tracer diffusion experiments to all experiments performed in pure water, flow curves (according to 5.3.7) of TS and SDTS dissolved in water/DMSO of various concentrations were also recorded.

6 Native versus spray dried tapioca starch

Before the mixtures of the native and spray dried tapioca starch with the different hydrocolloids, xanthan gum, ι-carrageenan, and guar gum can be examined, the differences of the two starches have to be considered and understood. Spray drying is a very tough process and may provoke serious alterations on molecular level of the spray dried sample. The following chapter first presents the observed functional properties of the native tapioca starch, followed by a demonstration of their changes after the spray drying process and a molecular comparison of the native and spray dried tapioca starch.

6.1 Native tapioca starch – gelatinization, gel structure, and viscoelastic properties

Tapioca starch differs from other starches by its low level of residual materials (lipid, protein, ash), lower amylose content (17%), and high molecular weights of amylose and amylopectin. When heated in excess water starch undergoes an irreversible structural transition and as a result the starch granules lose birefringence and crystallinity. The granules then swell and absorb more water resulting in changes in the rheological properties of the starch–water suspension. The high molecular weights of amylose and amylopectin and its short side chains enable a highly layered (~40 layers with thickness < 0.5 µm per granule) and tight organization within the starch granules [103] rendering tapioca starch more resistant against disintegration and promoting the formation of ghost granules.

6.1.1 Pasting and gelatinization

The granule swelling and molecular solubilization upon gelatinization results in changes of the viscosity and can be monitored by viscosity measurements of a starch suspension depending on temperature (VTP). Therefore, the viscosity is measured continuously under stirring during a programmed heating and cooling cycle and is shown for a 7% w/w tapioca starch suspension in figure 6.1. If starch granules are suspended in excess water and heated progressively to high temperatures, the molecules within the granules start to realign and water is able to diffuse into the granules. The granules start to swell, their volume increases and the viscosity starts to increase, independently of starch concentration (cf. B.1), at $T_{pasting}$ = (66.3 ± 0.2) °C. The swelling continues until the granules reach their maximum size and the dispersion reaches its peak viscosity η_{peak} at T_{peak} = (85.7 ± 0.4) °C. At this temperature the granules cannot swell any further, the outer layers of granules are disrupted, the granules start to break down, and viscosity

decreases rapidly. Amylose and amylopectin partially diffuse into the surrounding environment and disperse in the solution. When this solution is cooled afterwards the released amylose and amylopectin retrograde, and a very viscous paste with weak gel character is formed. The dispersed amylose molecules begin to reassociate and form a three dimensional network [104]. A composite gel of undissolved granule remnants embedded in a continuous matrix of entangled amylose polymer chains and separated highly branched amylopectin molecules is obtained.

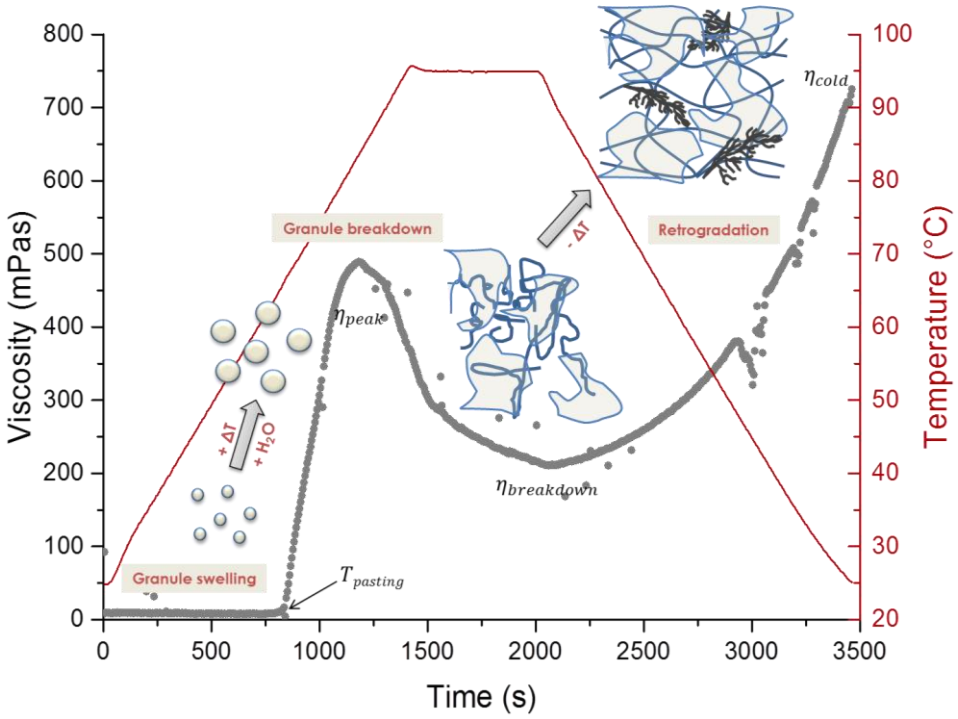

Fig. 6.1 VTP at $\dot{\gamma} = 200\,s^{-1}$ of 7% w/w native tapioca starch suspension with schematic illustration of structural changes during pasting process.

The granule remnants, also denoted as ghosts, are flexible and translucent objects of isotropic shape and lack of their original content [105]. The swollen ghosts are at least twice as large as the original dry granules, no birefringence is visible anymore, and depending on shear they remain partially intact. Atkin et al. [106] found evidences that these starch ghosts predominantly consist of amylopectin. By specific binding between pullulanase gold complexes and granules envelopes, α-1,6 linkages could be visualized indicating densely branched starch molecules. Light microscopy images of gelatinized tapioca starch support this assumption (figure 6.2). The samples were centrifuged at 1000 rpm for 10 min using an *Eppendorf MiniSpin* centrifuge and the precipitate was stained with iodine solution (Lugol).

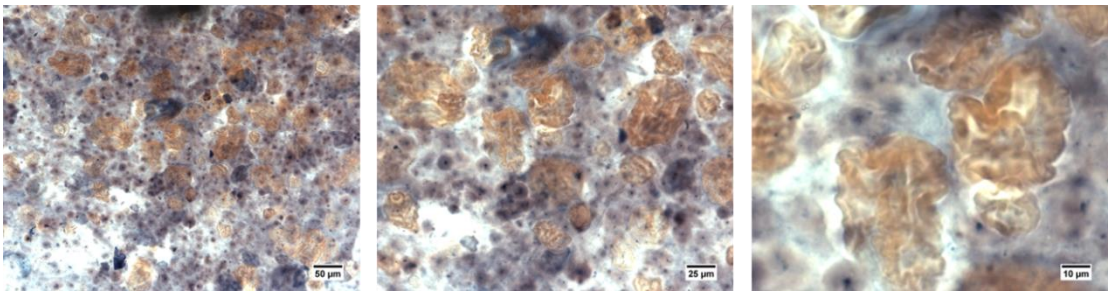

Fig. 6.2 Light microscopy images of 7% tapioca starch paste after centrifugation. Stained with Lugol solution in excess, objective: 20×, 40×, and 100×.

The staining with iodine solution leads to an intense blue color for amylose due to triiodide–amylose complexes while amylopectin in contrast shows only a slight brownish coloration [107]. Figure 6.2 shows the existence of ghosts as folded and winkled bodies, composed, at least primarily, of amylopectin (cf. also with [108]). The structural factors that contribute to ghost integrity are still unclear and not well understood. Starting point for the explanation of ghost granule formation is the existence of gradual changes of amylopectin composition from the center of the granules towards the surface [106b]. As already indicated in figure 2.7 (2.2.1), inner amylopectin is supposed to have longer branching chains resulting in a lower defect structure and a tighter packing possibility. Consequently, the outer amylopectin arrangement should be more flexible and able to form a translucent envelope containing the internal starch components. After swelling the intact amylopectin on the outer surface is thought to form a continuous layer or envelope surrounding the disordered internal starch components. Swelling continues until a critical temperature is reached, and the envelope ruptures at the weakest region releasing large quantities of internal material. The outer envelope undergoes a massive structural collapse and degrades into ghosts or ghost remnants [106b].

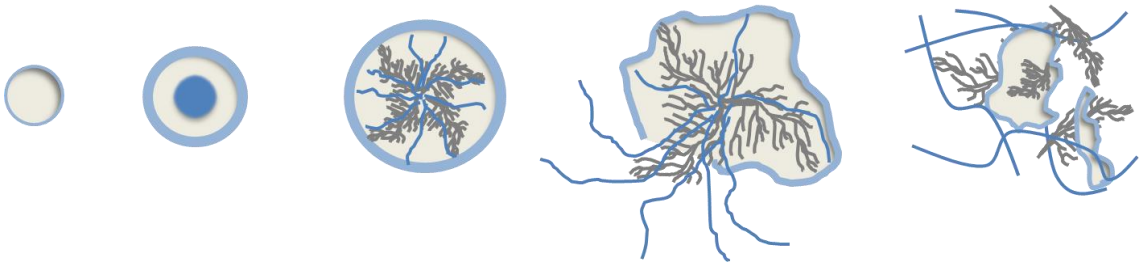

Fig. 6.3 Schematic formation of granule ghost during gelatinization.

The stable ghost structure is assumed to arise by simple entanglements of nonordered polymers mainly amylopectin [109]. Due to the highly branched structure and the high molecular weight of amylopectin, each molecule is expected to be involved in a large number of temporary entanglements and their sum results in the permanent multi micrometer structures of granule ghosts. Only at very high shear and heat conditions or

after dissolving in DMSO, these ghost structures can be destroyed and a starch paste with completely different functional properties remains.

The pasting process including granule swelling and bursting, can be nicely visualized by light microscopy as shown in figure 6.4. Regarding the single granule highlighted by a yellow circle in figure 6.4, first a slight increase in volume, followed by disruption and merging with the environment upon 72 °C can be observed. The corresponding viscosity (figure 6.1) is a result of the macroscopic interaction of all starch granules in the sample; in contrast the microscopic analysis in figure 6.4 enables the examination of single granules and can be compared with the molecular transition within one individual granule, as measured by DSC. During gelatinization tapioca starch is transformed from an ordered, crystalline state to a disordered, amorphous state and by DSC measurements start and end point of this transition can be determined. In excess water one endothermic peak with gelatinization initiation T_{onset}, peak temperature T_{peak}, and end temperature T_{endset} is detectable and the area under the curve measures the energy required for the transition (figure 6.5).

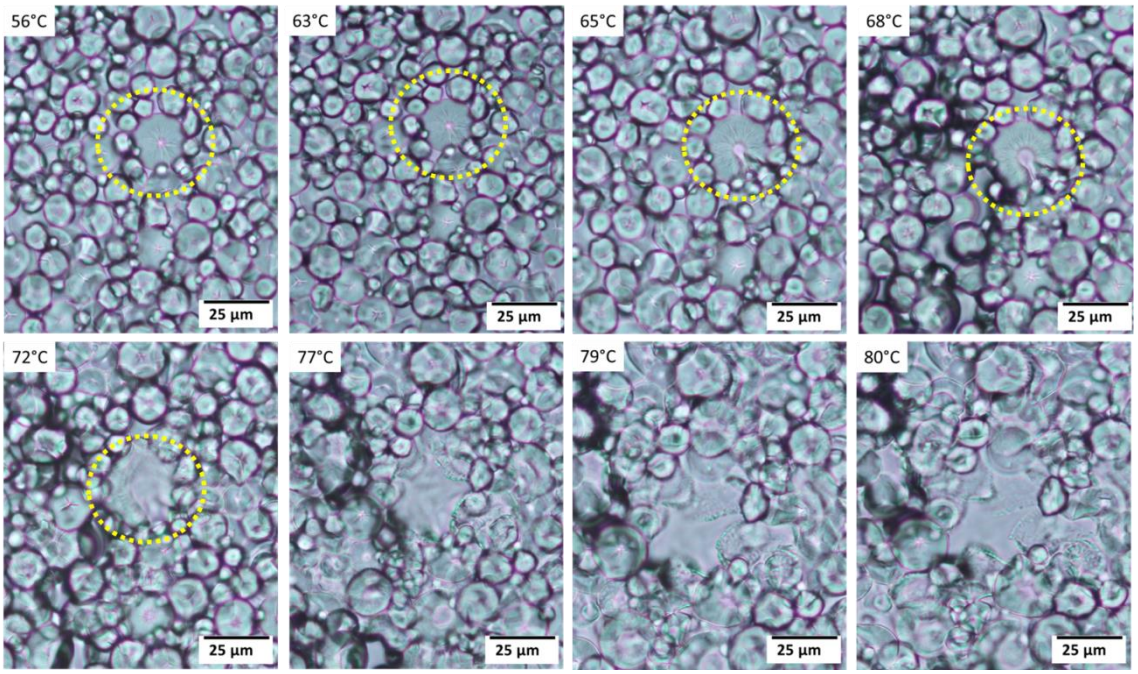

Fig. 6.4 Light microscopy image sections of 7% w/w tapioca starch suspension during heating from 25 to 95 °C, 3 K/min. Objective: 40×.

Basically, gelatinization may be regarded as a nonequilibrium melting process of starch crystallites which requires a previous plasticization (softening) of the amorphous phase [69]. As shown in figure 6.5, in excess water a single endothermic peak can be observed with a peak temperature T_{peak} = (68.4 ± 0.1) °C, initial and final temperature of T_{onset} = (62.6 ± 0.2) °C and T_{endset} = (75.6 ± 0.2) °C, respectively. This endotherm represents the melting transition of crystalline material and depends on the water level. It is suggested that already at ambient temperatures water initially penetrates the amorphous

regions within the granules, followed by the hydration of the intercrystalline amorphous phase as heating proceeds [110]. The level of water in the crystalline lamellae is very low and starts to increase after partial loss of crystallinity by melting, and decreases progressively over the entire order–disorder transition (figure 6.5). Consequently, a cooperative process is supposed to occur where first the amorphous regions absorb water and swell resulting in a facilitated melting of the crystalline regions which promotes further water diffusion and swelling of the entire starch granule [111].

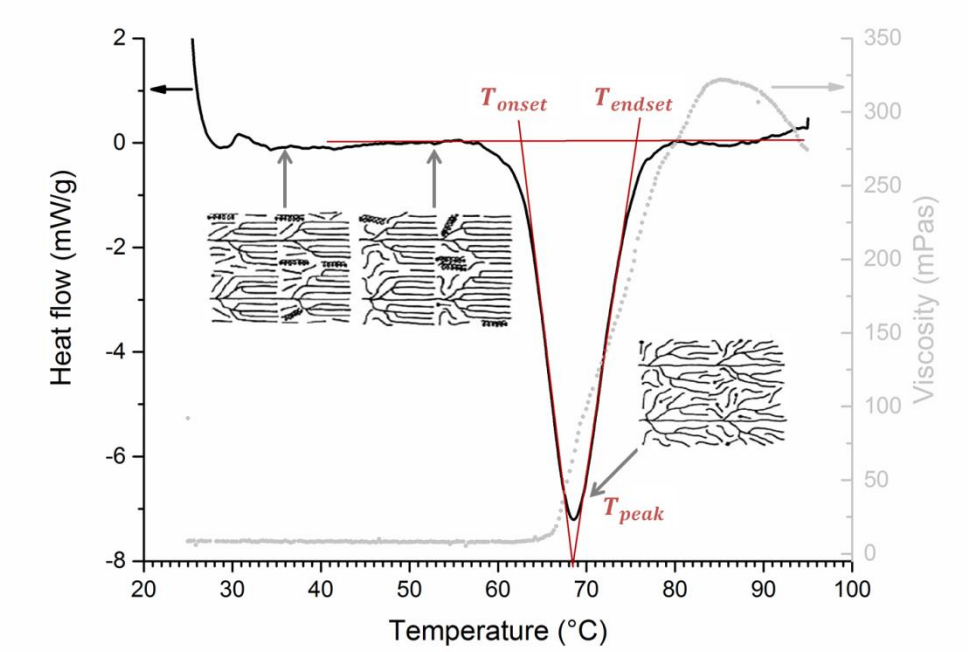

Fig. 6.5 DSC heating curve of 7% w/w tapioca starch suspension, after baseline correction. Scanning rate: 3 K/min, reference: 100 µL empty pan. For comparison the heating curve of figure 6.1 is added on the right side. In addition the molecular order–disorder transition is depicted schematically, according to [69].

Considering the various processes that can take place during gelatinization, i.e. glass transition, partial melting, annealing, crystallization, and final melting, the gelatinization enthalpy does not reflect the original crystallinity [69]. Melting is an endothermic process, whereas hydration and crystallization are exothermic events. It is supposed that the endothermic enthalpy primarily reflects the loss of double helical order rather than the loss of crystalline order, which implies that forces holding the starch granule together, are largely at double helical level [112]. Comparing the microscopic DSC experiment with the macroscopic data of the VTP, the DSC peak temperature T_{peak} = 68.4 °C resulting from the cooperative melting of starch crystallinities in excess water, coincides more or less with the pasting temperature $T_{pasting}$ = 66.3 °C where the viscosity of the dispersion starts to increase. Consequently, amylopectin crystallite melting by double helix dissociation precedes significant water diffusion and macroscopic granule swelling. Only at temperatures

above the gelatinization temperature a considerable increase in swelling and viscosity gets visible and continues well above the onset temperature T_{onset}. It has to be noted that the gelatinization process occurs over a limited temperature range for a single granule (DSC) compared to a wider temperature range for a population of granules (VTP).

6.1.2 Gel structure and viscoelastic properties

The current model of starch paste or gel after gelatinization is a three dimensional matrix of dispersed molecules surrounding the penetrating swollen, collapsed granule ghosts (cf. figure 6.6). According to this model the main elements influencing functional properties are the rigidity and extent of the continuous phase of dispersed molecules, the rigidity of ghosts, the interaction of ghosts with dispersed molecules, and the volume occupied by the ghosts [113]. Ghosts are weak elastic structures and act as soft filler particles which reinforce the surrounding network [114]. The viscoelastic properties of a tapioca starch paste result as an interplay of the three different components: entangled amylose polymer chains, highly branched amylopectin polymers, which cannot interpenetrate each other, and the micrometer-sized ghost granules. They all show different contributions and reactions on different length scales and can be distinguished within an amplitude sweep test.

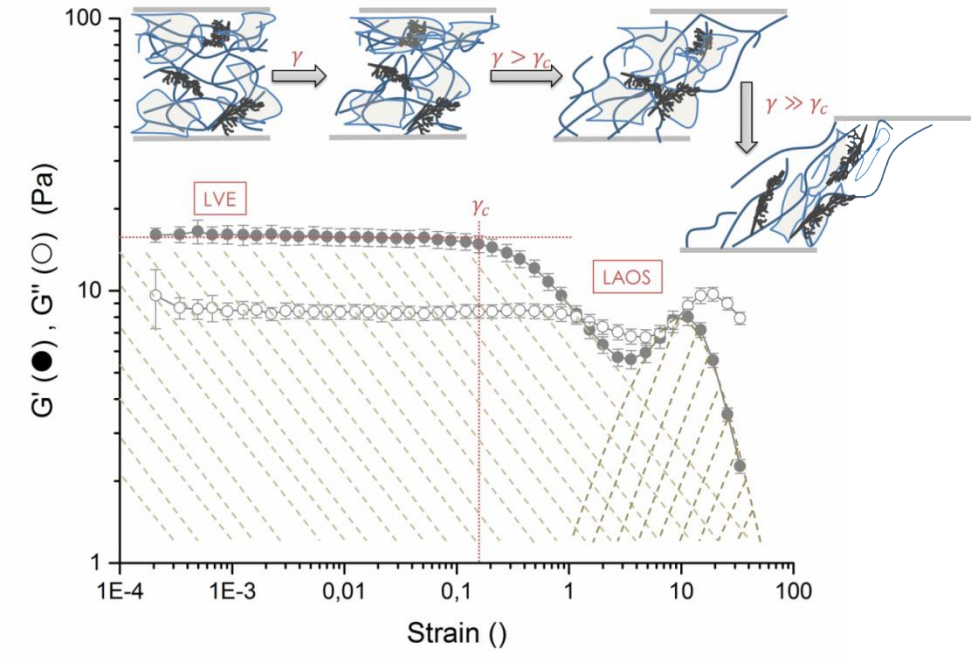

Fig. 6.6 Amplitude sweep test as log-log plot of storage G' and loss G'' modulus as function of strain γ for 6% w/w tapioca starch paste at $f = 1$ Hz and $T = 25$ °C. The molecular rearrangements during deformation are depicted schematically.

Figure 6.6 shows the amplitude depending viscoelastic behavior of 6% w/w gelatinized tapioca starch sample. At relative low amplitudes a linear viscoelastic range (LVE),

where storage and loss modulus are independent of strain, is obtained. Gelatinized tapioca starch shows the typical behavior of a gel-like material with $G' > G''$, $\tan\delta = \frac{G''}{G'} < 1$ and thus a dominantly elastic character. At a critical strain γ_c = 0.2 (20% displacement) the storage modulus starts to decrease more than 10% below the average value along the LVE range, followed by a nonmonotonous strain overshoot and a continuous decrease above γ = 11.2 >> γ_c. The loss modulus follows the same strain dependence with a slight delay corresponding to the viscous deformation response. This observation may be explained as a superposition of different interactions on different length scales in the complex structure of the starch paste. At low applied strain the entire composite system deforms reversibly and the different contributions add up to the zero shear modulus. Similar observation could be made for starch filled gluten networks in wheat dough [115]. At the critical strain the transient network of amylose polymer chains cannot resist any further and the single polymer chains slide along each other. Thus, the bigger and much slower moving obstacles approach, and it is assumed that the local maximum at high deformation, is likely to be caused by trapping interaction between the granule ghosts and jamming of the swollen, highly branched amylopectin molecules. It is suggested that the amylose network in the continuous matrix has a slightly dominating effect on the storage modulus, compared to the other starch components, and the density and stability of its intermolecular junction zones determine the elasticity of the composite gel. Above γ_c it is assumed that the transient network of entangled amylose polymer chains is disrupted, followed by a crossover of G' and G'' and a dominantly viscous behavior. Consequently, no cohesive network exists anymore, and the applied deformation energy dissipates to a higher degree than it is stored. Genovese and Rao [116] also found a moderate higher effect of amylose on elasticity than the other starch components. Finally, the application of very high shear strain led to breakage and destroying effects of the entire systems yielding to the final moduli decay. It has to be noted that the measured moduli at large amplitude oscillatory shear (LAOS) do not have the same physical meaning as those measured under small deformation, but give information about the changing microstructure of a complex fluid [117].

6.2 Viscoelastic properties after spray drying

Comparing the viscoelastic properties of the already discussed starch paste obtained from native tapioca starch with those of a paste made from the rehydrated spray dried starch, significant differences can be observed. Figure 6.7 shows the viscosity–temperature profile of a 6% w/w native TS suspension in comparison to a 6% w/w rehydrated paste of the spray dried TS. SDTS dissolves completely already at room temperature and the paste produces a significant viscosity of

η_{cold}(SDTS) = (140.7 ± 0.3) mPas. TS does not gelatinized without heat application and the viscosity of the ungelatinized TS suspension is almost equal to that of water. With increasing temperature the viscosity of the SDTS paste slightly decreases due to increasing thermal motion, but reinstalls completely after cooling. However, after gelatinization the viscosity of the formed TS paste η_{cold}(TS) = (531.0 ± 3.2) mPas significantly surmounts the cold viscosity of the SDTS paste. The added micrographs do not show significant differences; both starch pastes contain the granule ghosts in a continuous matrix. Consequently, the large discrepancy in viscosity of the two starch pastes is not attributed to structural properties and appearance of the ghosts and seems to arise from molecular, not trivial changes in the continuous phase.

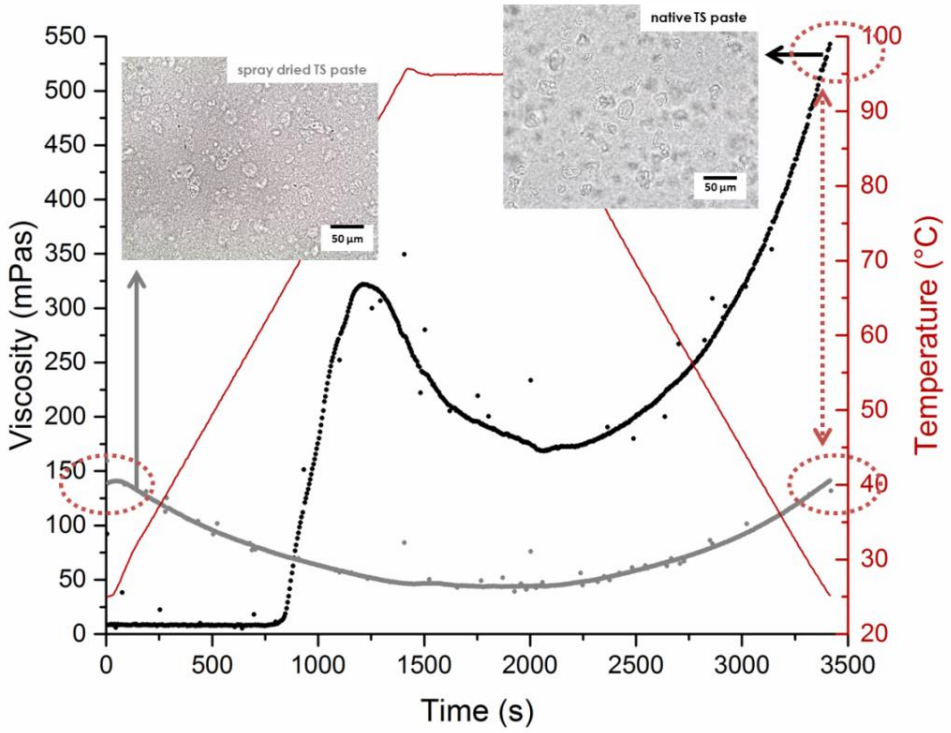

Fig. 6.7 VTP at $\dot{\gamma} = 200\ s^{-1}$ of 6% w/w native tapioca starch suspension (black curve) in comparison to a 6% w/w rehydrated paste of spray dried tapioca starch (grey curve). Light microscopy images of the corresponding pastes at 25 °C are added. Objective: 20×.

Regarding the viscoelastic properties in figure 6.8 remarkable alterations after the spray drying process are notable. The amplitude sweep test, shown in figure 6.8a, yields a significant decrease for G' and G'' for the paste made from SDTS. The decay of G' is more considerable leading to a paste dominated by viscous properties. At a certain strain γ = 0.01 the storage modulus drops about 90% from G'(TS)= (15.74 ± 1.15) Pa to G'(SDTS) = (1.15 ± 0.17) Pa and the loss modulus about 70% from G''(TS)= (8.34 ± 0.49) Pa to G''(SDTS) = (2.40 ± 0.20) Pa.

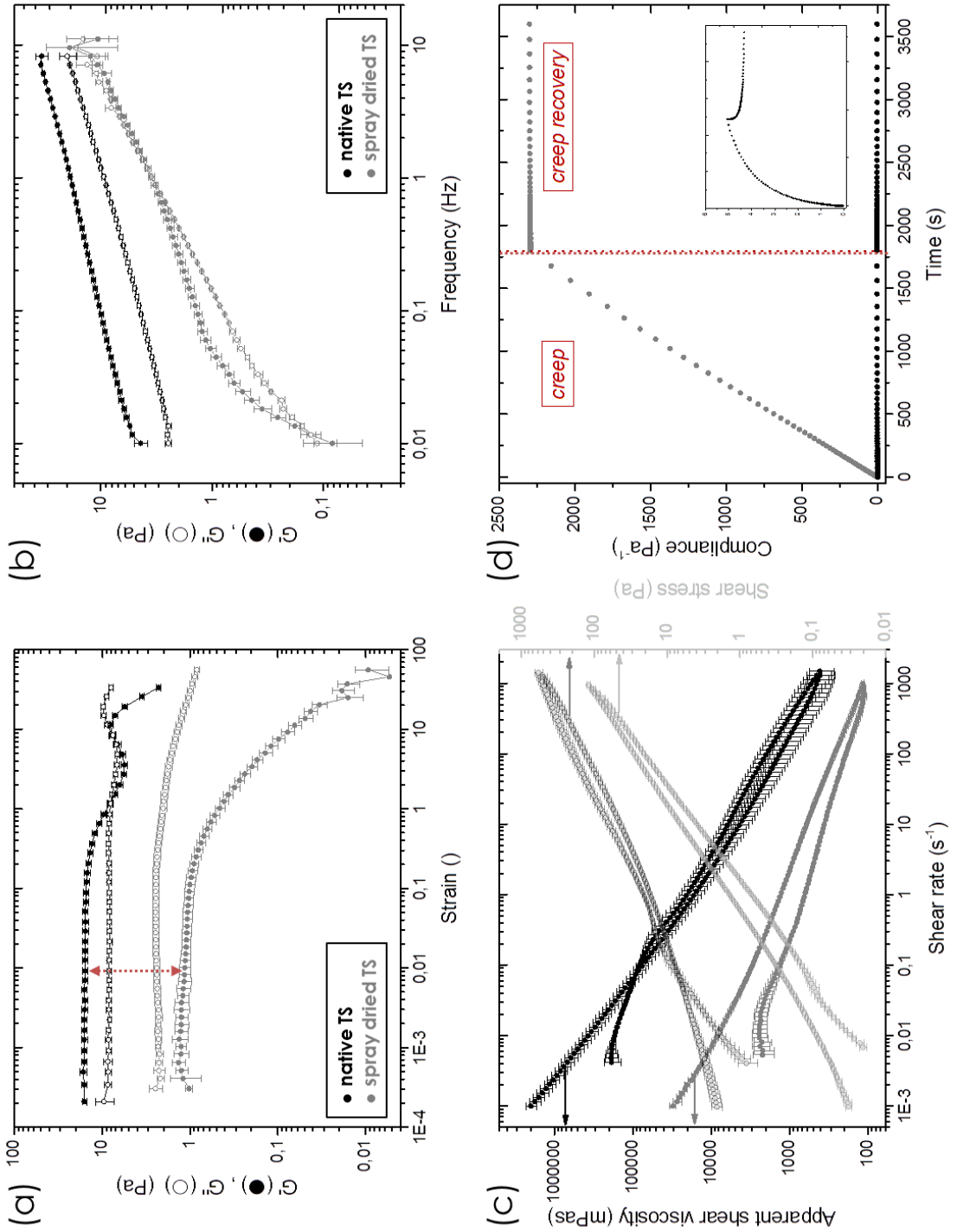

Fig. 6.8 Comparison of viscoelastic properties of 6% w/w native tapioca starch paste and 6% w/w rehydrated spray dried tapioca starch paste. (a) Amplitude sweep test as log-log plot of storage G' and loss G'' modulus as function of strain γ at $f = 1$ Hz and $T = 25$ °C. (b) Frequency sweep test as log-log plot of storage G' and loss G'' modulus as function of frequency f at γ = 0.01 and $T = 25$ °C. (c) Flow curves as log-log plot of apparent shear viscosity (left) and shear stress (right) as function of increasing and decreasing shear rate at $T = 25$ °C. (d) Creep and creep recovery as lin-lin plot of compliance as function of time at constant shear stress σ =0.15 Pa and $T = 25$ °C. Black curves always represent TS and grey curves SDTS.

Due to the presence of granule ghosts in both starch pastes, this decay of shear moduli has to correspond to changes in the continuous matrix of the amylose network. According to pure rubber elastic materials, the shear modulus depends on the number of crosslinks and on the three dimensional mesh sizes (cf. 4.3.1). Thus, increasing mesh sizes, which are determined by the distance between two adjacent crosslinks and the molecular length of the polymer chains, lead to a decrease in shear modulus. Although the physical network of amylose chains is a swollen network without permanent crosslinks, this basic scaling ansatz can be hypothetically applied. Consequently, the hypotheses can be drawn that the amylose network in the continuous matrix has a dominating effect on the composite gel's elasticity and is determined by density and stability of its intermolecular junction zones. In addition to the obvious drop in viscoelasticity, the local minimum in the LAOS range disappears although the micrograph in figure 6.7 still monitors the granule ghosts for the SDTS paste. Over the whole amplitude range the SDTS paste shows fluid character and even under static conditions the sample flows which indicates a lack of a physical, stable matrix enclosing the granule ghost.

The time depending deformation behavior measured during the frequency sweep test, shown in figure 6.8b, supports this assumption. The TS paste follows the typical behavior of dispersions with gel character and physical stability. Even on long term no decomposition is visible. Storage modulus G' dominates loss modulus G'' over the whole frequency range and both curves increase in parallels with weak slopes. SDTS pastes in contrast are strongly frequency dependent and undergo different behaviors along the applied frequency range. In the nonoperating state and at very low frequencies, the SDTS paste behaves like an uncured polymer dispersion with $G'' > G'$ and is prone to decomposition. The granule ghosts are supposed to segregate and a viscoelastic fluid is measured. With increasing frequency the curve of G' crosses the one of G'' and both curves increase steadily. This observation is in accordance to the frequency behavior of a fragile cured polymer with weak structure strength. It is assumed that the increasing movements disperse the granules in the sample, which in turn reinforce the storage modulus of the composite paste with $G' > G''$. During further frequency increase the progression of G' starts to retard whereas G'' increases constantly resulting in a second crossover above 1 Hz. The micrometer-sized granule ghosts cannot react on the high frequency deformation yielding segregation also at high frequencies and short time displacements. Consequently, a rehydrated paste made from SDTS seems to be stable and shows structure strength only under adequate frequency ranges (~0.2 to 2 Hz).

Both TS and SDTS pastes follow a distinct shear thinning behavior, visible in figure 6.8c. After a short transient viscosity "maximum" produced by starting range effects and inhomogeneous distributions of shear rate, both pastes, but SDTS slightly slower,

show constant decreasing steady state viscosity with increasing shear rate. During subsequently decreasing shear rate both pastes possess a yield stress with structure stability in the very low shear range. The shear thinning behavior is generated by the amylose entanglements in the continuous matrix. During shearing the amylose molecules straighten along the shear direction, partially disentangle and minimize the flow resistance. Comparing the flow curves of the two starches significant differences can be observed. At low shear rates the viscosity of the SDTS paste starts at almost two decades lower than the viscosity of the TS paste at the same concentration. Due to lower entanglement density of amylose polymer chains in the paste made from the SDTS, obviously lower values for the viscosity can be produced (cf. figure 6.7). Additionally, regarding the hysteresis loop by increasing and decreasing shear rate the two starches behave differently. The paste of the native starch shows a very narrow loop with a slightly lower viscosity for descending shear rate ramp, which could also be shown by Sikora et al. [118]. During high shear rates the network structure of the native TS is slightly disrupted and needs a certain time to reinstall provoking the viscosity decay along the second ramp. In contrast, the paste of the modified starch has a much broader loop. Here, the viscosity of the second ramp with decreasing shear rate exceeds the viscosity of the upwards ramp, and a slight antithixotropic behavior can be observed. This suggests a structure strengthening under constant shear loading and is in accordance to the former observations made by the frequency sweep tests. The SDTS paste seems to consist of a weak amylose matrix which cannot entrap the granule ghosts and tend to segregation at low shear rates. With increasing shear rate shear thinning by straightening of amylose molecules is reduced since granules are distributed over the whole sample, reinforce the paste structure, and provoke a slower viscosity decay compared to the native TS. Additionally, in the paste made from TS, even at low shear rates the granules are distributed homogenously within the stable and dense amylose matrix resulting in a constant shear thinning behavior. At very high shear rates turbulences disturb the laminar flow of ghosts and amylose molecules in the SDTS paste, and provoke some jamming effects which increase structural interaction and the viscosity.

The different viscoelastic behavior of the two starches becomes even more obvious by evaluating the creep test in figure 6.8d. During stress application and subsequent removal the paste of SDTS exhibits almost ideal fluid behavior. During the creep phase compliance increases directly proportional with proceeding time and after removal no or only very slow recovery occurs. In contrast, typical viscoelastic behavior can be observed for the TS paste in the plot’s magnification. Compliance increases much slower with increasing stress time and even after a sufficient long recovery phase, measurable residual deformation remains indicating a viscoelastic fluid with retarded response on external stress. Creep and creep recovery are irreversible yielding a

permanent deformation of the sample. Extent of deformation recovery is determined by the strength of the physical network in the different starch pastes. No or only very slow healing during the recovery phase reveals a very weak network for SDTS and partial resilience for the TS paste implies elastic components occurring from a strong physical network.

6.3 Specification of degraded starch components

All the results presented in 6.2 suggest a decay of the viscoelastic properties mainly caused by weakening of the amylose matrix structure. During the spray drying process, the strong shear and heat conditions represent a nonequilibrium state and are presumed to have a certain degradation effect on the starch components. The stability and density of amylose polymer chain entanglements is reduced resulting in a weaker transient network structure. Thus, in a paste made from the spray dried starch, shorter amylose polymer chains deplete the intermolecular association and reduce the overall elasticity. Such a degradation effect was also observed by Roger et al. [119] using a microwave dispersion treatment on corn starch solutions.

6.3.1 Optical characterization of gel structures

Confocal laser scanning microscopy was used to investigate this degradation effect in more detail. Figure 6.9 shows CLSM images of pastes made from native and spray dried tapioca starch, both stained with rhodamine B. Both samples were focused bottom-up at two different focal planes in the samples. Consequently, for each sample, one image was taken directly at the bottom of the sample and one at a depth of 100 µm. The images of the spray dried sample show that the granule ghosts were almost completely precipitated to the bottom of the sample volume. In contrast, the paste of the native starch shows these ghosts in deeper regions of 100 µm. This suggests that in the spray dried starch paste the viscosity is too low, and no stable and dense matrix structure is formed to enclose and keep the granule ghosts resulting in a segregation of the granule ghosts to the bottom of the sample.

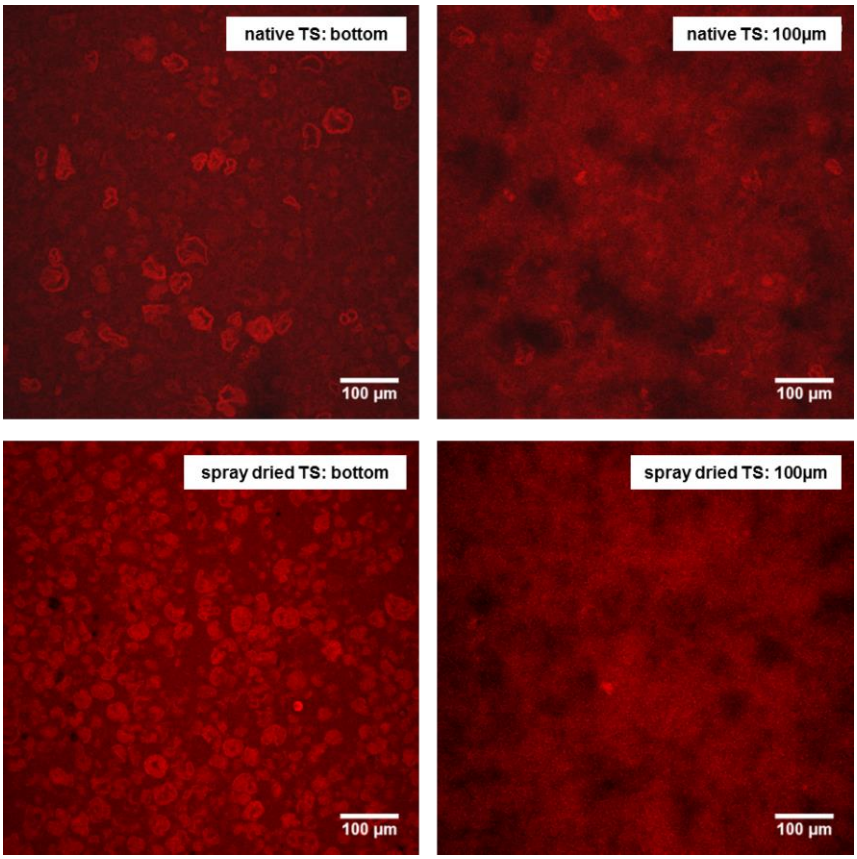

Fig. 6.9 Confocal laser scanning microscopy images of 1% w/w TS and SDTS paste stained with rhodamine B. Both samples were imaged at two different focal planes. Objective: 20×, image size: 707.11×707.11 µm^2, electronic zoom: 0.

Light microscopy images, shown in figure 6.10, support these observations. The different starch pastes were centrifuged at 1000 rpm for 10 min and stained with one drop of Lugol solution. During centrifugation the continuous amylose matrix is supposed to be more or less destroyed, and the granule ghosts settle as residue.

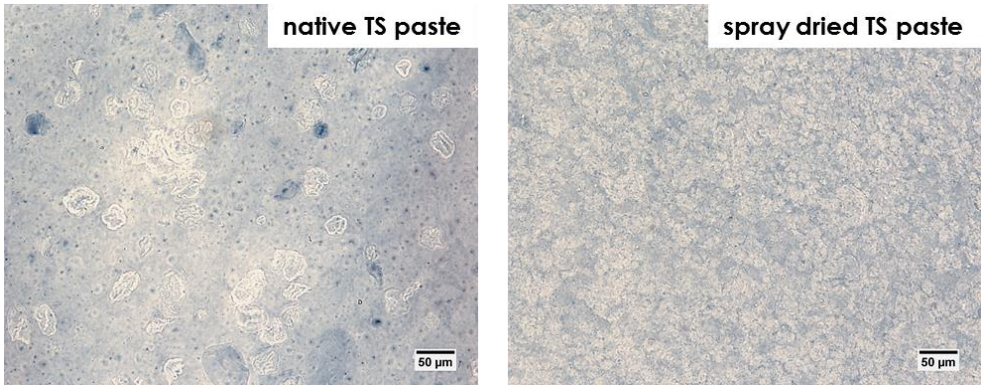

Fig. 6.10 Light microscopy of 3% w/w TS and SDTS paste after centrifugation. Stained with Lugol solution, objective: 20×

These residues, presented in figure 6.10, differ significantly for the two starches. Native TS shows only a few granule ghosts whereas the micrograph of SDTS is crowded with overlapping ghosts. The weak amylose matrix of SDTS cannot withstand the high shear

forces during centrifugation yielding a complete settlement of the granule ghosts. The physical network of TS seems to be more stable and partially endure centrifugation.

6.3.2 Shear/heat experiments and amylase digestion

To evaluate the high shear and heat influences on network structures during spray drying, different treatments of a native TS paste were performed. Figure 6.11 shows the results of the amplitude sweep test of the different pastes after corresponding treatments as described in 5.5.1. Drying without shear application (purple curve) do not have drastic influences on the viscoelastic properties and their strain depending behavior is only slightly shifted to lower values compared to the native TS paste (black curve). On the other hand, spray drying without heat application (dark yellow curve) but harsh shear conditions during transportation through the spray nozzle seem to have already structure changing power. The treatment with the ultra turrax (blue curve) and the amylase digestion (green curve) have destructive effects; no stable networks remain, and approach the behavior of the 3% w/w SDTS paste (grey curve). Even at small amplitude oscillatory shear, no linear viscoelastic range is apparent, and the storage modulus constantly decreases for all three pastes.

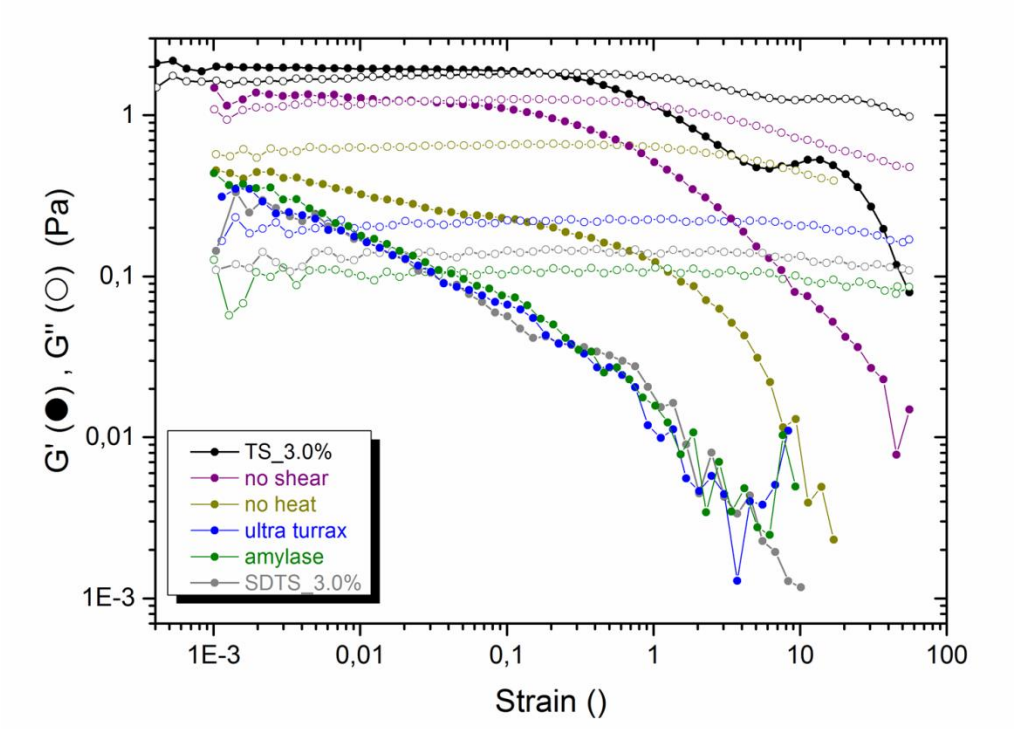

Fig. 6.11 Amplitude sweep test as log-log plot of storage G' and loss G'' modulus as function of strain γ at $f = 1\,\mathrm{Hz}$ and $T = 25\,°\mathrm{C}$ for 3% w/w native TS paste and SDTS paste in comparison with the pastes after four different treatments. Averages of threefold determination, standard deviation not shown.

It has to be noted that figure 6.11 presents the results of 3% w/w TS and SDTS paste where SDTS, in particular, has not passed its critical concentration for structure

stabilizing entanglements (detailed discussion follows in 6.3.3), and thus they are not directly comparable with the viscoelastic properties shown in figure 6.8a. Additionally, by evaluating the micrographs of the corresponding pastes in figure 6.12, the network structures can be correlated to the viscoelastic properties. Paste structures after different treatments are compared: a) 3% w/w native TS paste with granule ghosts embedded in a continuous matrix; b) resuspended paste of a dry powder obtained by drying paste (a) at 200 °C without any shear application in a halogen dryer; the visible structure resembles the starting material. (c) Paste (a) after transportation through the spray nozzle without heat application; the granule ghosts are still visible but slightly disrupted. The micrographs shown in d) demonstrate the native TS paste after amylase digestion for 10 min. The LM image clearly shows the granule ghosts but no continuous matrix can be distinguished, which is confirmed by the CLSM images where all ghosts are settled to the sample bottom. Amylase digests specifically the amylose network yielding a complete breakdown of the composite network structure; due to the branched cluster structure of short side chains, amylopectin is only susceptible to α-amylolysis to a limited degree. The native TS paste treated with the ultra turrax with 7000 rpm for 5 min can be observed in e). The very high shear conditions destroy the entire system and neither granule ghost nor embedding matrix are evident. Finally, in f) a 3% w/w rehydrated SDTS paste, where shear and heat application are combined, is presented.

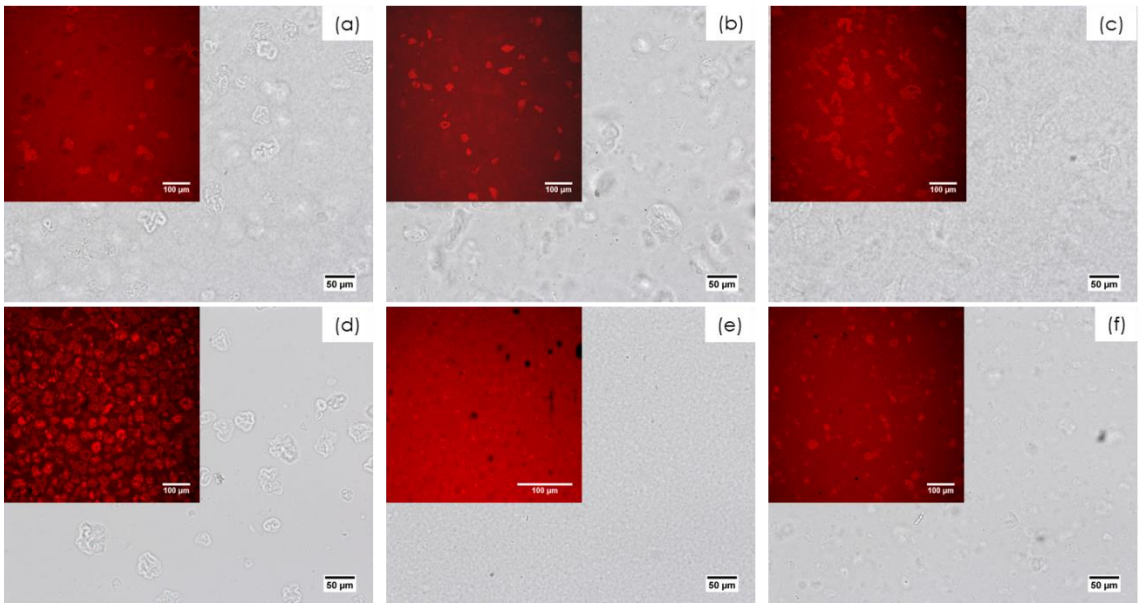

Fig. 6.12 Light microscopy images of 3% w/w a) native TS paste, b) resuspended dried powder without shear application, c) TS paste after spray drying without heat application, d) TS paste after amylase treatment for 10 min, e) TS paste after ultra turrax treatment, and f) rehydrated SDTS paste; objective: 20×. For a better visualization of granule ghosts, CLSM images of the corresponding pastes, stained with rhodamine B, are added; objective: 20×, image size: 707.11×707.11 µm^2, electronic zoom: 0.

It can be concluded that the heat addition during spray drying does not provoke the huge structural decay. However, the high shear conditions during atomization into small droplets have the most structure influencing effect. Drying by heat application only and without shearing does not change the network structure significantly, and the viscoelastic properties hardly deviate. Shearing a starch paste leads to destructive effects; the shear forces during spray drying provokes a slight disruption of granule ghosts, but due to the significant decay of storage modulus, as seen in figure 6.11, a more relevant disruption of the amylose matrix is assumed. The treatment with the ultra turrax destroys all network components; however, when comparing these viscoelastic properties with those of a paste after amylase digestion no significant differences are observed. In the latter one, only the matrix structure of amylose is destroyed, and the viscoelastic properties of the resulting material approach those of the SDTS paste. Thus, the destruction of the amylose matrix has to be the main reason for the viscoelastic decay. This becomes more obvious by a stepwise increase in the extent of amylase digestion, presented in figure 6.13: a 6% w/w native TS paste was mixed with 20 µL of a 0.1% amylase solution and the reaction was stopped after 5, 10, 15, 20, or 30 minutes to simulate a stepwise degradation of the amylose network. With proceeding amylase digestion the storage modulus of the respective starch pastes decreases noticeably and approaches gradually the elastic part of the rehydrated SDTS paste.

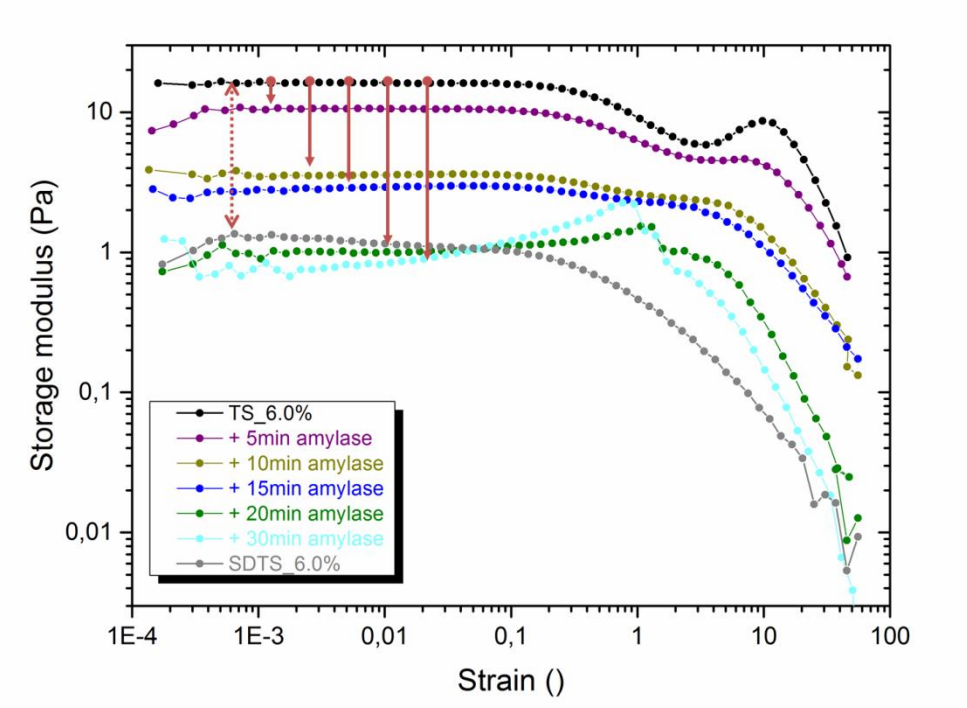

Fig. 6.13 Log-log plot of storage modulus G' in dependence on strain γ at $f = 1$ Hz and $T = 25$ °C for 6% w/w native TS paste, the same paste digested for 5, 10, 15, 20, and 30 min by amylase and compared with 6% w/w rehydrated SDTS paste. Averages of threefold determination, standard deviation not shown.

Amylase does not attack amylopectin or the granule ghosts, which is supported by figure 6.12d, and thus the decrease of G' is mainly due to the degradation the amylose network. In addition, regarding the LAOS range, the strain overshoot at high amplitudes, which is supposed to stem from trapping interactions and jamming of the granule ghosts, diminishes and relocates progressively to lower amplitudes and finally disappears completely for SDTS. Consequently, with increasing amylose degradation the enclosing stable network disappears and granule ghosts already approach at lower amplitudes. Thus, the different interactions on different length scales of the different starch components cannot be separated as distinctive as in the native TS paste. The sudden spike along the curve of amylase pastes digested for 20 and 30 min can be contributed to inhomogeneity and already occurring retrogradation processes during the measurement.

6.3.3 Tracer diffusion and determination of critical concentration

Tracer diffusion via dynamic light scattering allows the determination of structural properties of polymer networks by observing the selfdiffusion of added tracer particles. The diffusion of DVB-PS particles is measured in different concentrated TS and SDTS pastes, which depends according to the *Stokes–Einstein equation* (5.6) on the viscosity and entanglement density of the surrounding medium, i.e. TS or SDTS paste. Initially, the different starch pastes were analyzed without tracer particle addition. As described in 5.5.3, the measurements were performed in 1/10 water/DMSO mixtures to prevent interferences of multiple scattering by turbidity. DMSO is a better solvent than water for starch samples and enables a complete dissolution of all starch components, even granule ghosts. It has to be noted that all presented measuring points result from single experiments and their validity cannot be guaranteed. The left diagram in figure 6.14 shows the evaluated hydrodynamic radius on short-term diffusion in dependence on starch concentration for TS and SDTS. Both starch types show a significant decrease of R_h with increasing concentration, although the curve for TS has a slightly steeper slope and lies above the one of SDTS up to 8% w/w. Above 8% w/w both starch pastes seem to converge to a limiting value for R_h. On the right side of figure 6.14, the apparent hydrodynamic radius of the added tracer particles are presented as function of concentration of the surrounding starch medium. For both starch pastes, R_h of the particles follows a logarithmical increase with a limiting value above 12% w/w. Up to a starch concentration of 4% no significant difference can be distinguished; upon this critical concentration the increase of R_h in the SDTS environment deviates and decelerates. In both diagrams the apparent hydrodynamic radius was evaluated by cumulant analysis. Therefore, the diffusion coefficient, which describes the initial decay of correlation function, is calculated and only the selfdiffusion of smaller particles on short time are considered.

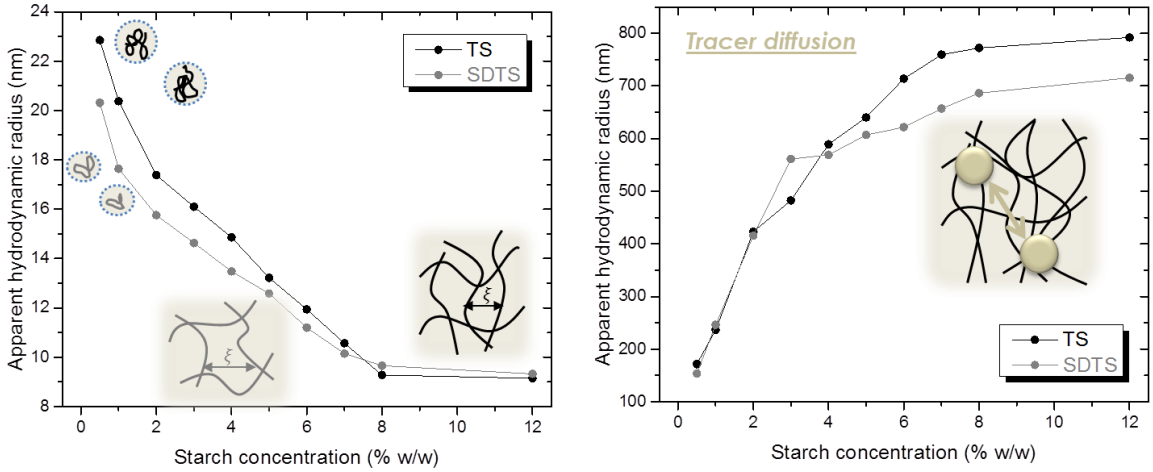

Fig. 6.14 Apparent hydrodynamic radius as function of starch concentration; left: measurement in pure starch paste and right: measurement after addition of 134 nm DVB-PS tracer particles. Evaluation of hydrodynamic radii via cumulant analysis at a scattering angle of 90°.

However, the results of the scattering experiments of the pure starch solutions suggest that the evaluated radii are due to the diffusion of mainly amylose molecules. The high molecular weight amylopectin molecules should have slower relaxation times compared to amylose. Because measurements on polymer concentration dependence are performed, a separation between solution and gel has to be considered. In a solution, polymer molecules are able to diffuse throughout the sample. In contrast, in a gel consisting of a polymer network (transient or crosslinked), the polymer segments are restricted to particular regions of the sample and are only able to perform limited Brownian motions around fixed averaged positions [120]. At very low starch concentration, amylose polymer coils can be observed separately, and significant differences between amylose of SDTS and TS can be detected. For the TS solution bigger radii are measured, which indicates more extended polymer coils formed by slightly longer chain lengths than in the SDTS solution. At higher concentrations the polymer coils start to overlap creating a more or less stable transient network of entanglements, and the sample transforms from a polymer solution to a soft gel. According to DeGennes [70], the diffusional behavior in semidiluted solutions is determined by cooperative diffusion processes of a transient network of random coil polymers, where $c \geq c*$ and anisotropic aggregates dominate the solution behavior. Consequently, a hydrodynamic correlation length ξ_h can be interpreted as the mean distance between two points of entanglements and defines the diffusion:

$$D_c = \frac{kT}{6\pi\eta_0\xi_h} \tag{6.1}$$

$$\xi_h = R_h \left(\frac{c}{c^*}\right)^{-\frac{3}{4}} \tag{6.2}$$

These cooperative diffusion processes are apparently measured in figure 6.14 on the left side. The coil radii, measured at the very beginning of the scattering experiment, transform to a network whose correlation length depends on starch concentration. At high concentrations the hydrodynamic correlation length for TS is slightly smaller than for SDTS. This is due to the longer amylose polymer chains forming a tighter network structure with higher entanglement density. This observation is supported by the results of the measured selfdiffusion of the tracer particles in figure 6.14 on the right side. At low concentrations no stable network is formed and the tracer diffusion is more or less independent from the different starch molecules and only slightly retarded by the increased viscosity. Upon a critical concentration the network of entangled amylose polymer chains is formed for TS as well as for SDTS. However, due to longer polymer chains, the critical concentration, upon which the entanglement density starts to influence the diffusion of the tracer particles significantly, is reached for TS at an earlier state and hampers their further motion more drastically.

The analysis of the viscosity–concentration relationship for TS and SDTS in water/DMSO strengthens the previously obtained observations of the differences in entanglement density and critical concentration. Figure 6.15 presents the relative viscosity at $\dot{\gamma}$ = 200 s^{-1} with increasing starch concentration. All systems show shear thinning behavior with increasing shear rate (cf. integrated flow curves). To calculate η_{rel}, as ratio of solution viscosity and solvent viscosity η_0 (equation 4.21), the apparent shear viscosity was chosen at a shear rate of 200 s^{-1} where the solvent water/DMSO shows a stable laminar flow. Water and DMSO are miscible and behave Newtonian in all ratios. At 25 °C a viscosity of η_0 = 2.70 mPas was measured for a 1/10 mixture [121]. Figure 6.15 demonstrates that above 2% w/w the viscosity–concentration behavior of the two starches diverges. Native TS shows a significantly faster increase of viscosity with increasing concentration. The critical concentration, where $\eta_{rel} = \frac{\eta}{\eta_0} \geq$ 100 mPas, is reached slightly above 4% w/w and η_{rel} increases continuously, almost proportional with rising concentration. For spray dried TS this critical value is reached just above 6% w/w, and the following linear increase is significantly slower indicating a higher critical concentration for the formation of a tight entanglement density and a stable physical network.

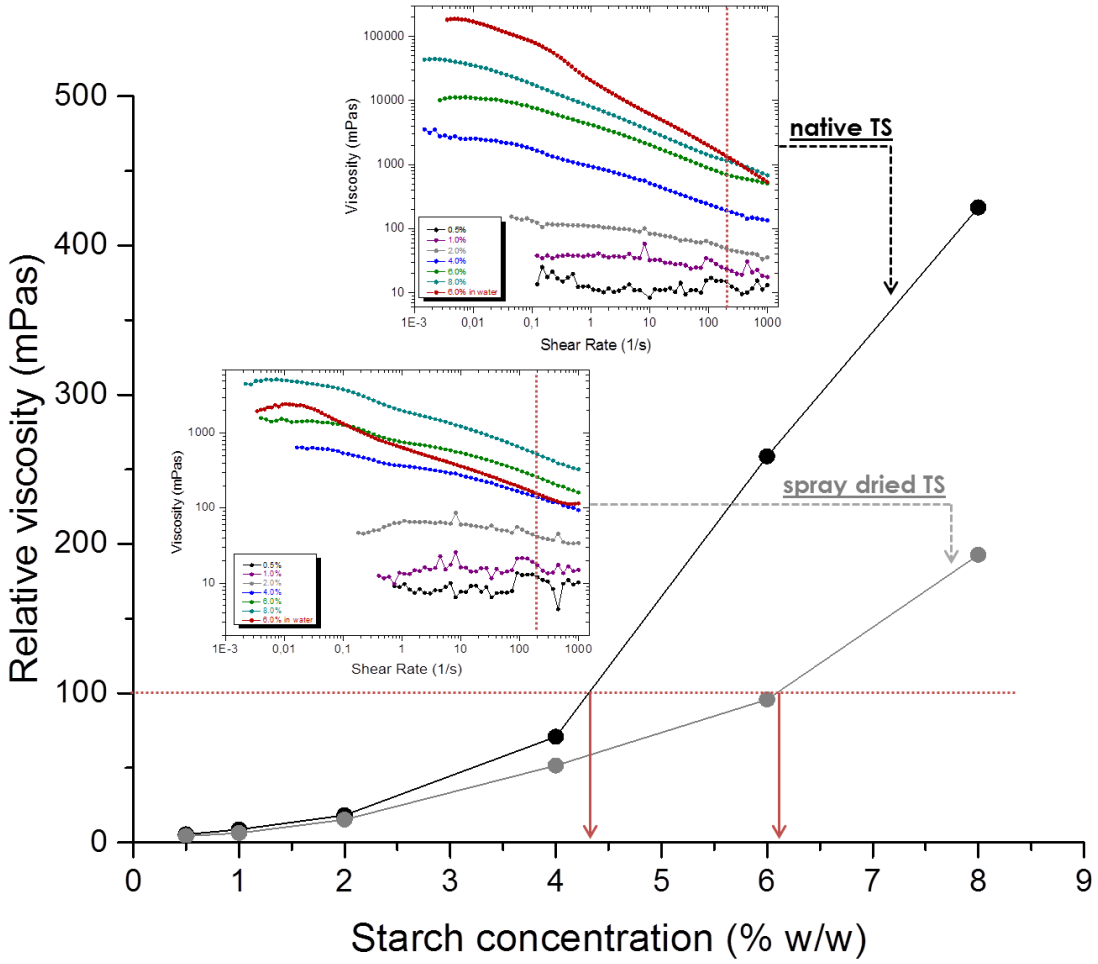

Fig. 6.15 Relative viscosity at $\dot{\gamma}$ = 200 s^{-1} and T = 25 °C as function of starch concentration for native TS (black curve) and spray dried SDTS (grey curve) in 1/10 water/DMSO solvent. The flow curves for all corresponding systems are added in separate graphs to clarify the evaluation of η_{rel}, additionally the red curves present the corresponding systems as 6% w/w solution in water.

6.3.4 Melting behavior of dry TS and SDTS powder

Tapioca starch exhibits only a weak glass transition as a consequence of the nature of the amorphous phase, which is mainly located between crystallites and act as physical crosslinks, restricting the segmental motion of the intercrystalline amorphous phase. Thus, in contrast to synthetic polymers, a glass transition is not readily detectable by DSC, and figure 6.16 shows only the DSC heating curve and the melting behavior of the dry powders. Comparing the melting behavior of the two dry starch powders, no significant differences can be observed. The heating curve of SDTS is slightly shifted to higher temperatures, although for both powders a very narrow endotherm for crystal structure melting can be determined.

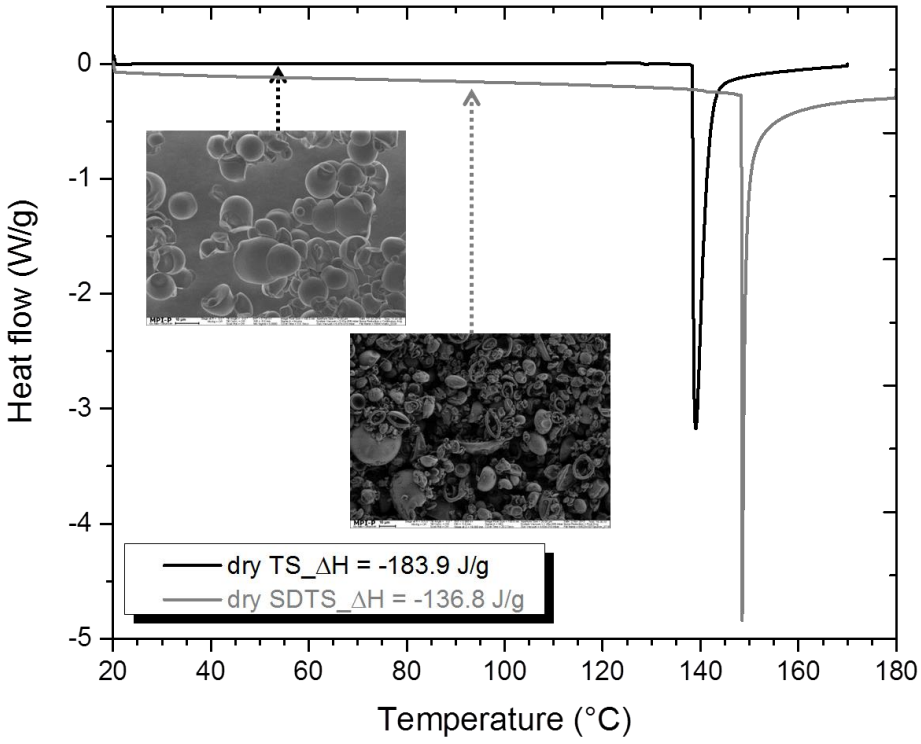

Fig. 6.16 DSC heating curve of dry native TS and spray dried TS powder, after baseline correction. Scanning rate: 3 K/min, reference: 40 µL empty pan. The added SEM pictures of the powders display their dry granular structure.

Such narrow melting endotherms suggest a uniform crystallinity within the single starch granules. Already low defect concentrations in the regular chemical structure of the polymer chains, e.g., branching or entanglements, result in a drastic broadening of the melting ranges. Melting of amylopectin crystallites is dependent on the crystalline polymorphs, its degree of perfection, and the amount of water present [26]. Water is the plasticizer of starch granules and amorphous regions are plasticized by water into a rubbery state even at ambient temperatures. For TS melting starts at T_{onset} = (138.2 ± 0.5) °C and reaches its peak temperature already at T_{peak} = (138.9 ± 0.7) °C; for SDTS the peak is shifted around 10 K with T_{onset} = (147.2 ± 0.2) °C and T_{peak} = (147.5 ± 0.5) °C. This shift can be attributed to the different moisture content of the examined sample. For native TS an intrinsic moisture content of 12.81% and for the powder after spray drying an average moisture content of 8.04% can be found. Water has a plasticizing effect on the amorphous phase of starch. Due to an interconnection of amorphous and crystalline domains in native starch, plasticization of the nonordered regions has also an influence on the melting of starch crystallites [69]. Garcia et al. [110] showed the influences of various water content on the endothermic transition of cassava starch, which reflects the melting of amylopectin, by a significant shift of melting temperatures to higher temperatures by lowering the water content. Similar DSC curves were also obtained by other authors for various starches [111] [122]. With

decreasing water content the availability of water is reduced and increases the thermal stability of the remaining starch crystals. During starch gelatinization water is supposed to initially penetrates the amorphous phase followed by hydration of the intercrystalline amorphous regions as heating proceeds; the water level in the crystalline lamellae is very low and only starts to increase after partial loss of crystallinity by melting [123], which supports the formation of granule ghost by insufficient heat application. For cassava starch the melting of starch crystallites approaches 250 °C with decreasing water content or in the absence of a diluent; however starch would decompose prior to the melting [110]. The SEM images for TS show smooth and intact spherical starch granules; after spray drying fractured and dished lenticular particles remain. This deformation can be attributed to atomization into small droplets by high applied pressure and following drying. In figure 6.16 also a significant decrease of transition enthalpy during amylopectin crystallite melting after spray drying is visible. Consequently, the amount of crystalline structures or the cohesion within these structures is supposed to degrade while gelatinizing and subsequent spray drying, which can be supported by structural determination via X-ray diffraction.

In general for semicrystalline polymers a two–phase structure (amorphous and crystalline areas) clearly appears in the X-ray diffraction diagram. In the fully amorphous state the diffuse halo, characteristic for liquid structures, is observed. It is caused by short range ordered states which also exist in unordered systems between neighboring molecules or chain segments, wherein the maximum represents the most probable distance. At increasing crystallinity this halo is superposed by sharp reflexes which are caused by the crystalline areas.

X-ray patterns of the native TS in figure 6.17 depict broadened diffraction lines and an underlying band of amorphous (noncrystalline) scattering. These features reflect both the partial crystallinity of granules and diffraction from small or imperfectly organized crystallinities [124]. Defined diffraction peaks at 2θ = 15.1°, 17.1°, 17.9°, and 23.1° can be determined. After spray drying the single diffraction patterns disappear completely indicating a conversion into a less crystalline state with a broad, featureless peak, typically for more amorphous spectra.

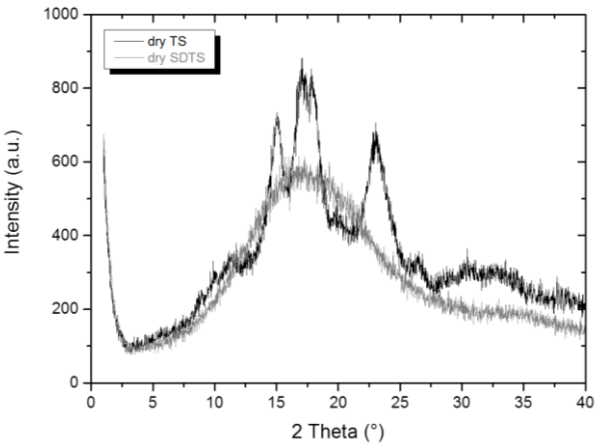

Fig. 6.17 X-ray diffraction of the dry powders; Philips PW1810 instrument with Cu-Kα radiation 1.5418, 40 kV, 30 mA.

The crystallinity does not disappear completely for the SDTS powder, but the single patterns blur and are overlapped by a huge unresolvable halo due to a higher defect structure. Gelatinization destroys the granular structure and the containing radial crystalline arrangement. This pregelatinized paste is basis for spray drying and during the drying process the time to recrystallize is insufficient and the amount of molecular chain ends as defect structures, which cannot incorporate the crystal structure, increases enhancing the defect concentration and decreasing the degree of crystallization. Similar alteration was also observed for tapioca starch after mechanical activation via ball mill grinding by Huang et al. [125]. After intensive grinding for 3h, the crystallinity of tapioca starch entirely vanished. DSC heating curves, SEM images and X-ray patterns reveal a significant alteration and degradation in crystal structure and granular morphology of tapioca starch by gelatinization and spray drying.

6.4 Summarized comparison of TS and SDTS

Spray drying is a very harsh process and provokes serious alterations on molecular level of tapioca starch. All the presented results in 6.2 suggest a decay of the viscoelastic properties of the rehydrated paste made from the spray dried starch, mainly caused by weakening of the amylose matrix structure and is supported by the results of the experiments in 6.3. Optical investigations indicate that the main differences in gel structures are caused by molecular, not trivial changes in the continuous phase and are not attributed to the structural properties and appearance of the granule ghosts. During the spray drying process the strong shear and heat conditions represent a nonequilibrium state and are assumed to have a certain degradation effect on starch’s amylose structure. The stability and density of amylose polymer chain entanglements would be reduced which in turn forms a weaker transient network structure. Thus, in a paste produced by the spray dried starch, shorter amylose polymer chains deplete the intermolecular associations resulting in a decay of the overall elasticity. These assumptions are additionally supported by measurements of the molecular weight distribution of native TS and spray dried TS dissolved in DMSO as well as by measurements of the electrophoretic mobility of gold nanoparticles in different concentrated TS and SDTS paste, shown in the appendix A.2 and A.3, respectively.

7 Starch–hydrocolloid mixtures

The functional properties of starch can be modified by the incorporation of nonstarch polysaccharides, with the major practical advantages being enhancement of viscosity [126], modified flow behavior [127], reduced setting time [58] and tendency to syneresis, and better freeze–thaw stability [128]. The mechanical properties of the resulting starch–hydrocolloid mixtures strongly depend on the physicochemical properties of the added polymers. Hydrocolloids have a variety of different structures including different branching, flexibility, molecular weight ranges, and ionic charge, all of which influences their behavior and the rheology of their solution. Therefore, three hydrocolloids with distinctly different flexibility and polarity have been chosen to study the limiting cases of mixtures with very stiff or very flexible polymer chains. Xanthan gum represents highly charged polysaccharide molecules with a very rigid polymer backbone. In solution xanthan molecules behave as charged and rigid rods, which undergo a nonequilibrium jamming transition above a critical concentration. In a mixture with other polysaccharides, the rigid and randomly oriented xanthan gum molecules reduce the mobility and diffusion of the co-solute. In addition, ι-carrageenan, which is a highly charged linear polyelectrolyte but with a sufficiently flexible backbone, is chosen. Consequently, in aqueous solution carrageenan molecules are distributed as random coils with intrinsic chain flexibility and are expanded by polyelectrolyte effects. Guar gum is a neutral polysaccharide which forms an open, flexible nonordered random coil conformation after dissolution. Above a critical concentration the polymer chains will come into contact resulting in mutual entanglements and an exponential increase in viscosity.

Xanthan gum, ι-carrageenan, and guar gum were thus added systematically in different concentrations to native and spray dried tapioca starch to study their effect on the mechanical properties of the resulting final pastes. Focus was set on the effect of their different physical properties, such as chain conformation and stiffness and the resulting interaction with native and modified tapioca starch. The different interactions result in different gel structures and determine the mechanical properties of the binary starch-based systems. Thus, the main purpose is to study the different interactions and effects of a highly charged, but very stiff hydrocolloid, i.e. xanthan gum, in comparison to one with a charged and very flexible molecular structure, i.e. ι-carrageenan, and a neutral and flexible polymer chain, i.e. guar gum, in a composite gel with the different types of tapioca starch. The addition of hydrocolloids to a starch paste or gel further increases the complexity of the system. Starch–hydrocolloid mixtures can be summarized as systems of swollen starch granules suspended in mixed polymer solutions or polymer

networks of varying rheological properties. The contribution of the dispersed and continuous phase to the properties of the overall system vary with relative concentration of starch and hydrocolloid, preparation conditions, and interaction or compatibilities between the various polymer molecules present [4].

7.1 Pasting behavior of tapioca starch in different hydrocolloid surroundings

Native starch in excess water shows pasting under continuous heating and shearing. During pasting considerable granule swelling and leaching of starch polymers, primarily amylose molecules, occurs. A peak viscosity resulting from swollen granules, is reached and during holding at 95 °C, the fragile swollen granules disintegrate and the viscosity decreases (breakdown). During cooling retrogradation as nonequilibrium, polymer crystallization process occurs. On short-term retrogradation, a network of entanglements and/or junction zones between amylose molecules forms producing an elastic gel. Granule ghosts and remnants are embedded within the network filling the network with dispersed particles. This pasting behavior of native starch alters significantly when the surrounding water environment is exchanged by hydrocolloid dispersions. Different hydrocolloids have different effects on the pasting and paste properties of a given starch. Chemical structure, ionic charge, and stiffness/flexibility determine viscosity and degree of interaction and associations with other molecules, especially with water molecules. Figure 7.1 demonstrates the different pasting profiles of tapioca starch in different mixtures with a) xanthan gum, b) ι-carrageenan, and c) guar gum. Therefore, the appropriate amount of tapioca starch and hydrocolloid were mixed on dry basis, water was added, and the mixture was stirred at 200 rpm and room temperature for 24 h to enable a complete hydration of the hydrocolloid. Subsequently, the sample was loaded in the measuring system and the viscosity η was measured as function of temperature at a constant shear rate of 200 s^{-1}. The temperature increased from 25 °C to 95 °C with a heating rate of 3 K/min, the sample was tempered at 95 °C for 10 min, and cooled to 25 °C with a cooling rate of 3 K/min.

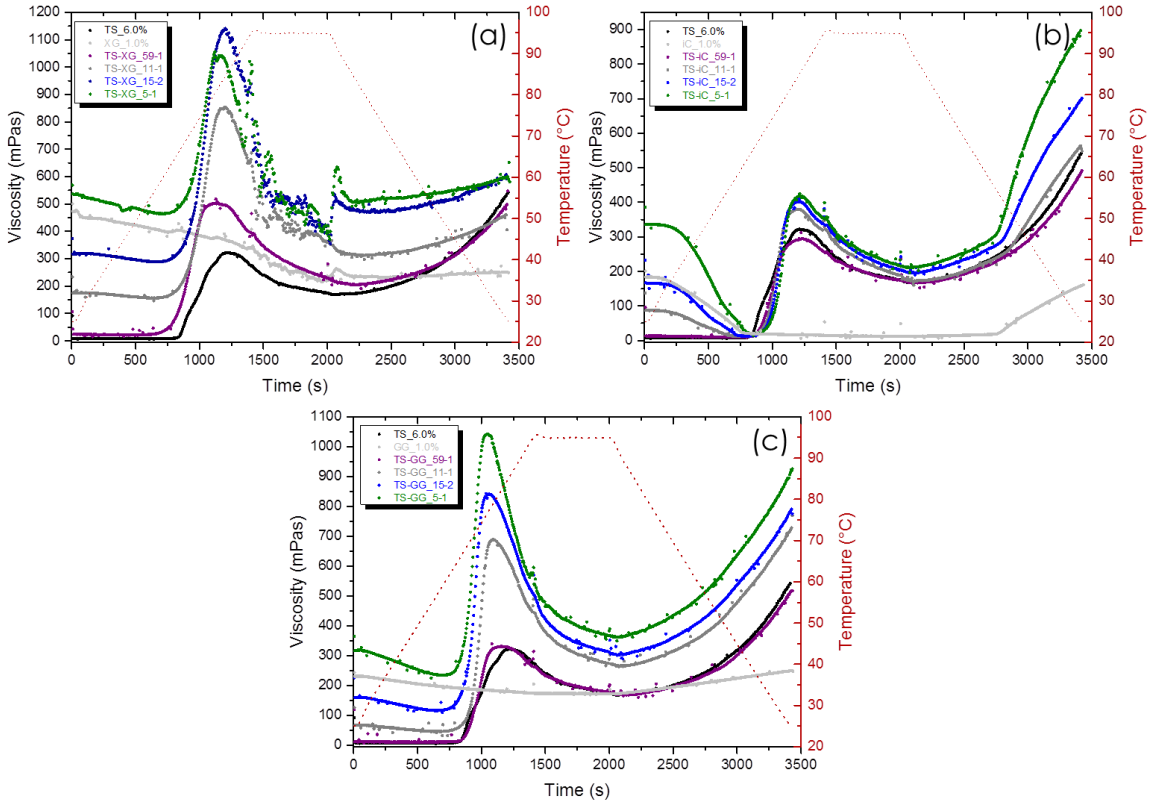

Fig. 7.1 VTP at $\dot{\gamma} = 200\ s^{-1}$ of native TS in mixtures with a) xanthan gum, b) ι-carrageenan, and c) guar gum of different compositions 59–1, 11–1, 15–2, and 5–1. For a better comparison native TS in 6% w/w (black curve) and the corresponding hydrocolloid in 1% w/w (light grey curve) are added. Averages of threefold determination, standard deviation not shown.

Table 7.1 summarizes parameters to evaluate the pasting properties of the different mixtures. There, the breakdown viscosity $\eta_{breakdown}$ describes the viscosity after the tempering stage and where the cooling phase initiates.

The setback viscosity $\eta_{setback}$ defines the difference between cold paste viscosity η_{cold} at the end of the measurement and $\eta_{breakdown}$, and thus compares the transition from a more viscous hot paste to the resulting cooled solid gel. In all mixtures an increase of the initial early stage viscosity with increasing hydrocolloid content can be observed. The measurements were performed after the complete hydration of the hydrocolloids, which provokes a stepwise increase of the suspension's viscosity by a successive increased hydrocolloid concentration.

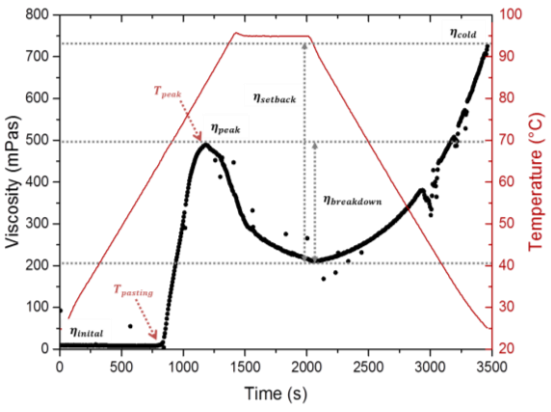

Fig. 7.2 VTP at $\dot{\gamma} = 200\ s^{-1}$ of native TS to indicate the evaluated parameters.

Comparing the initial viscosity of the individual hydrocolloid components, i.e. 1% xanthan gum, ι-carrageenan or guar gum paste, with the mixtures a significant increase is apparent.

Tab. 7.1 Pasting properties of 6% w/w TS–XG, TS–ιC, and TS–GG mixtures in different compositions and viscosities of 1% w/w hydrocolloid solution before and after temperature treatment.

	$T_{pasting}$ (°C)	T_{peak} (°C)	$\eta_{initial}$ (mPas)	η_{peak} (mPas)	η_{cold} (mPas)	$\eta_{breakdown}$ (mPas)	$\eta_{setback}$ (mPas)
TS	66.3±0.2	85.7±0.4	8.6±0.4	321.7±4.9	531.0±3.2	173.7±2.2	357.3±3.9
TS–XG 59–1	64.5±1.6	82.0±1.5	24.1±7.8	500.9±72.3	498.6±56.9	228.4±31.4	270.2±64.9
TS–XG 11–1	67.8±2.2	84.3±2.6	174.0±14.3	853.3±238.5	460.2±98.8	354.4±91.5	105.8±134.7
TS–XG 15–2	70.0±2.8	84.9±2.4	318.6±23.1	1140.7±59.6	601.6±17.8	-	-
TS–XG 5–1	69.3±2.6	82.7±1.6	536.4±25.9	1040.3±347.8	595.2±22.8	-	-
XG	-	-	451.6±12.3	-	251.4±2.5	-	-
TS–ιC 59–1	69.7±0.4	84.9±0.3	13.4±0.3	294.6±11.4	492.1±15.7	166.9±8.3	325.2±17.8
TS–ιC 11–1	71.0±0.8	84.2±0.1	87.4±2.9	379.7±18.2	563.8±18.9	176.0±11.5	387.8±22.1
TS–ιC 15–2	72.0±0.5	84.7±0.1	165.9±3.9	409.9±19.9	695.0±3.7	206.1±5.2	488.9±6.4
TS–ιC 5–1	74.8±0.3	84.9±0.2	336.2±19.8	417.6±19.8	887.5±28.2	214.8±6.5	672.7±28.9
ιC	-	-	183.4±6.7	-	160.2±66.8	-	-
TS–GG 59–1	68.2±0.2	82.4±0.2	11.8±0.3	334.6±4.4	515.2±13.9	175.8±2.1	336.4±14.1
TS–GG 11–1	69.0±1.1	79.0±1.0	67.5±14.8	688.8±64.6	724.0±37.9	276.2±16.8	447.8±41.5
TS–GG 15–2	67.3±0.5	77.2±0.2	160.5±4.3	840.4±53.0	790.8±31.7	304.4±14.0	486.4±34.7
TS–GG 5–1	66.7±0.8	76.9±0.3	317.3±50.1	1042.5±161.6	922.5±68.7	390.3±33.8	532.2±76.6
GG	-	-	231.1±3.1	-	249.5±17.9		

Before gelatinization the aqueous ungelatinized starch suspension reaches only a viscosity of 8.6 mPas while 1% xanthan gum, ι-carrageenan, and guar gum solutions have a viscosity of 451.6 mPas, 183.4 mPas, and 231.4 mPas respectively. The 5–1 mixture for example with xanthan gum enhances synergistically the early stage viscosity to 536.4 mPas, with ι-carrageenan to 336.2 mPas, and with guar gum to 317.3 mPas. Shi and BeMiller [129] already showed the pasting of tapioca starch in a xanthan gum environment and also reported an increasing early stage viscosity. These authors pointed out that the initial viscosity is strongly dependent on the ionic character of the added hydrocolloid and on the botanical source of the starch. At the beginning of the temperature profile the starch granules are still completely intact and the initial viscosity of the mixtures can be interpreted as the corresponding hydrocolloid viscosity, enhanced by rigid spherical filler particles, i.e. starch granules (cf. 4.2.4). The starch–hydrocolloid dispersion can be regarded as discontinuous systems of intact starch granules, surrounded by a continuous water phase containing the dissolved hydrocolloids. Additionally, the locally increased effective concentration of hydrocolloids, caused by the volume occupancy of starch granules, influences the initial viscosity of the mixtures. However, Heyman et al. [130] already showed that the increasing initial viscosity bases on both, increasing effective hydrocolloid concentration and filler effects by the starch granules. Consequently, $\eta_{initial}$ strongly depends on the hydrocolloid's viscosity at the corresponding concentration (figure 7.3, left). Compared to the other hydrocolloids, the mixtures with xanthan gum as well as the pure xanthan solutions, show in all concentrations the highest values for $\eta_{initial}$. Xanthan gum consists of highly charged polymer chains with molecular weights around 2 500 000 g/mol. Already at 0.5% w/w the nonequilibrium jammed molecular arrangement of charged and rigid rods in xanthan gum leads to viscosities twice as high than that of guar gum and ι-carrageenan at the same concentration. Guar gum and ι-carrageenan are both made up of long-chain and flexible polymer molecules, which interpenetrate and entangle above a critical concentration. The dissociated sulphate groups along the polymer chains of ι-carrageenan provoke slight repulsions, hinder chain overlapping, and at high concentrations (1% w/w) slightly lower viscosity compared to guar gum are achieved. In semidiluted solutions of guar gum the polymer chains adopt flexible disordered conformations with entanglements giving the thickening effect with classical flow behavior [131]. In the mixture with starch, these different strong viscosity developments are adapted, but shifted to higher values, produced by the filler effect of the added starch granules according to Einstein's equation (4.22).

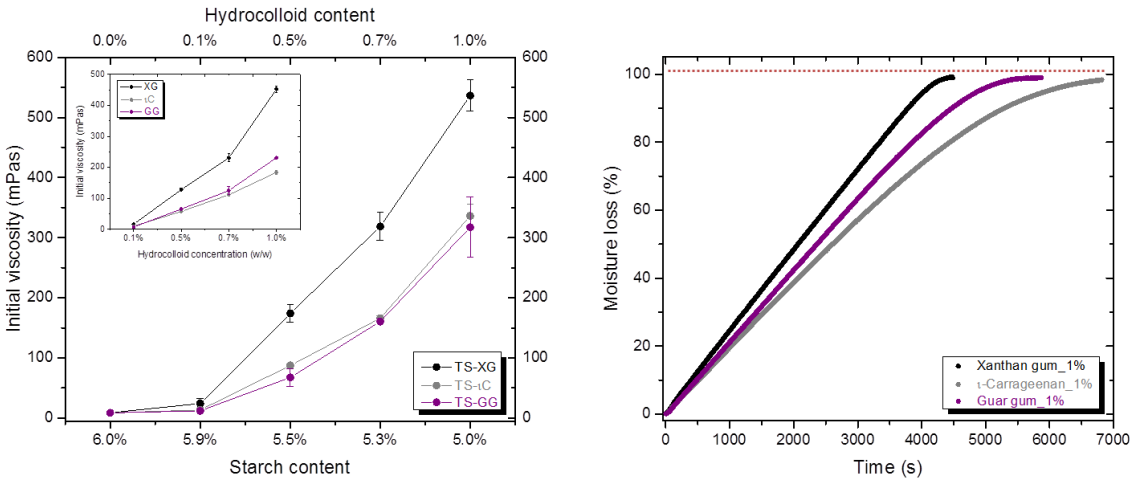

Fig. 7.3 Initial viscosity in dependence on mixture composition for TS–XG, TS–ιC, and TS–GG and for the single hydrocolloid solutions (left). Moisture loss for 1% w/w XG, ιC, and GG solutions while drying at 40 °C with halogen moisture content analyzer (right).

The influence of the different molecular architectures of the hydrocolloids is also reflected in the water holding capacity. Hydrogels are susceptible to syneresis and tend to release water spontaneously or upon energy addition. Heat exposition forces the bound water molecules to transfer into the gaseous state by migrating to the surface, and leaving the gels or dispersions while drying out. The ability to retard this effect of syneresis depends on the water holding capacity of the different hydrocolloids. To study this, the moisture content as a function of time was measured while drying at 40 °C with a halogen moisture analyzer. The diffusion of water molecules to the surface is a transport property and depends on the mobility and velocity of the molecules. The slope of the presented curves in figure 7.3 on the right side describes the velocity of water evaporation at start of heat exposition, i.e. at short time scale. It can thus be associated with the free water, which evaporates already at short times [51]. The faster 100% moisture loss is reached the worse is the water holding capacity of the hydrocolloid system. Therefore, the water holding capacity for 1% hydrocolloid solutions increases in the order from XG < GG < ιC. The formation of hydrogen bonds between hydrocolloids and water molecules is always accompanied by a loss of entropy. Regarding the stiff and rigid xanthan molecules, the positions of the hydroxyl groups are fixed due to the ordered structure in the system. The orientation of hydrogen bonds is strongly forced into the given direction of the xanthan molecules in the jammed configuration which demands a larger entropy loss. The water binding with flexible, uncharged guaran molecules is comparably more favored and results in a better water holding ability of guar gum. Here, the hydroxyl groups are randomly distributed along the chain and the water molecules are not forced into a certain orientation. ι-Carrageenan has slightly charged polymer chains which provokes chain elongation and enables extended orientation of water molecules around the hydrocolloid, and significantly better water holding capacity. Figure 7.4 shows the CLSM images of the

tapioca starch granules in aqueous suspension (above) as well as in ι-carrageenan (left), guar gum (middle) and in xanthan gum solution (right), before gelatinization. The microscopy images of the aqueous TS suspension and the ι-carrageenan and guar gum mixture, respectively, reveal no distinctive differences. The granules are homogenously distributed in an even environment. In contrast, the appearance of the mixture with xanthan gum differs significantly. Here, the high viscosity of the surrounding xanthan gum solution causes a separation of the starch granules in the dispersion and a hampered settling to the bottom of the sample, so that only the bigger and heavier granules are visible at the presented focal plane.

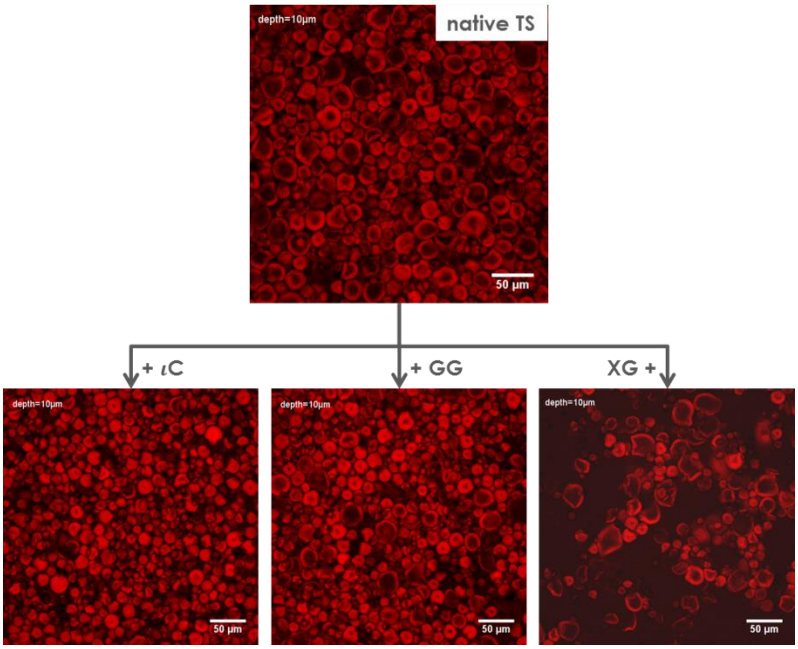

Fig. 7.4 Confocal laser scanning microscopy images of ungelatinized 1% w/w TS, TS–ιC, TS–GG, and TS–XG (11–1) suspensions, stained with rhodamine B. All samples were imaged at 10 µm focal depth plane. Objective: 20×, image size: 707.11×707.11 µm^2, electronic zoom: 2.

Previous studies [132] proposed an adsorption of xanthan gum on the granules surface and a stabilizing effect of the granular shape, but these are still under debate. However, these CLSM images show the increased early stage viscosity and in addition a significant heterogeneity in the mixtures with xanthan gum in comparison to the mixtures with guar gum or ι-carrageenan.

Regarding the viscosity–temperature dependence of the pure hydrocolloid solutions in figure 7.1 significant differences can be observed. ι-Carrageenan shows in comparison to xanthan gum and guar gum a much stronger temperature dependence. Xanthan gum and guar gum have weak temperature dependence whereas ι-carrageenan exhibits an approximately linear decreasing viscosity with increasing temperature. This behavior is also visible in the mixtures with tapioca starch and leads in all mixtures to an initial viscosity decay. Thus, independent of the ι-carrageenan concentration, all mixtures have

the same starting viscosity before pasting. All three hydrocolloids follow the Arrhenius relationship and with increasing temperature the energy of the whole system increases. Consequently, more and more energy is available to move molecules and to overcome the energy barrier for the elementary flow, which leads according to equation 4.17 to a decreasing viscosity. For ι-carrageenan it has to be noted, that there occurs also a temperature induced disorder–order transition during cooling from random coil to double–helix conformation. Consequently, with increasing ιC content retrogradation of the mixtures with starch is also accompanied by this gelling process. This is visible in figure 7.1b by the abrupt, almost linear viscosity increase during cooling, and is gradually pronounced with increasing ιC content.

Neither in the mixture with xanthan gum nor with guar gum a significant change of the pasting temperature compared to the pure starch suspension can be found. In all mixtures the onset temperature of the pasting process is around 67.7 °C ± 1.7 °C and almost independent of the type of added hydrocolloid and its concentration, which shows that the hydrocolloids do not interact energetically with the starch granules. The addition of ι-carrageenan slightly increases $T_{pasting}$ to higher values and even to 74.8 °C in the 5–1 mixture; this was also already observed by [58]. This may be attributed to the strong viscosity–temperature dependence of ιC. In addition no significant effects on T_{peak}, i.e. the temperature where the highest peak viscosity is measured, are visible for XG and ιC. Slight variations from the value for pure TS suspensions may be attributed to reduced heat transfers by more viscous systems [133]. GG in contrast shows slightly lower peak temperature with increasing hydrocolloid content and for the 5–1 mixture even about 8.8 K. The increased shear forces exerted to the swollen granules in the highly viscous dispersion may accelerate granular breakdown. Funami et al. [134] suggest in addition interaction between high molecular guaran molecules and starch granules, by which they become less resistant to heat and mechanical shear, and which might provoke the granular bursting already at lower temperatures.

Regarding the peak viscosity, all hydrocolloids, albeit xanthan gum and guar gum more distinctive than ι-carrageenan, provoke a significant increase with increasing polysaccharide concentration (figure 7.5). Strong inhomogeneity in the 5–1 mixture with xanthan gum leads to a drop of the peak viscosity and to the spiky setback pattern in the mixtures containing xanthan gum in high concentrations. However, the mixtures with ι-carrageenan and guar gum produce a more homogenous pasting profile. The pure 6% starch suspension reaches a peak viscosity of 321.7 mPas while with increasing hydrocolloid concentration a continuous increase is found.

Thereby, for xanthan gum again the biggest influence can be monitored, followed by guar gum and ι-carrageenan. This trend is in consistency with the development of the initial viscosity in figure 7.3 and indicates as well a predominant effect of the hydrocolloid when the granules are still intact. At this stage of the temperature profile, the starch granules have absorbed the highest possible amount of water resulting in highly swollen and voluminous, but still solid filler particles.

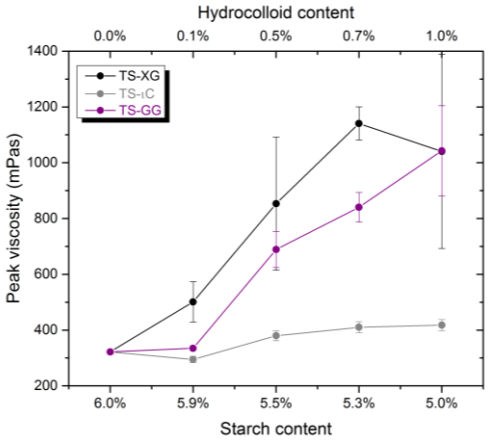

Fig. 7.5 Peak viscosity in dependence on mixture composition for TS–XG, TS–ιC, and TS–GG.

In addition, due to this water absorption of the starch granules, the effective concentration of the hydrocolloids in the continuous phase raises and may also produce the apparent viscosity increase [130]. During heating, the hydrocolloids, mainly found in the continuous phase, are in the soluble phase and swelling of starch granules yields a reduction in volume fraction of the continuous phase, and thus an increase in hydrocolloid concentration. The viscosity increase is not assumed to be the result of specific interaction between starch granules and hydrocolloids, but rather the result of the larger amount of work needed to move the swollen granules past each other in the increasing viscous media [135].

During cooling the mixtures with guar gum and with ι-carrageenan additionally show a much steeper viscosity increase than the pure starch paste or the mixtures with xanthan gum. This can be mainly attributed to the strong temperature dependence and slight gelling ability of ιC. In general, the addition of the different hydrocolloid provokes a significant increase of cold paste viscosity η_{cold}, which will be discussed in more detail in section 7.4. It has to be noted that the measurements for the highly concentrated TS–XG mixtures after starch gelatinization were strongly influenced by increasing rod climbing effects within the used vane geometry, and due to the high viscosity, mixing of the xanthan containing system was not as thoroughly as for the pure starch dispersion or the other mixtures [57].

7.2 Viscoelastic properties during gelatinization and retrogradation

The visualization of the pasting process can also be performed while detecting the viscoelastic properties in dependence on temperature. Consequently, the ungelatinized starch suspension and their mixtures with the corresponding hydrocolloid were poured onto the measuring system, heated to 95 °C, and subsequently cooled to 25 °C while detecting storage and loss moduli. Figure 7.6 presents the results for the 5–1 mixtures with a) xanthan gum, b) ι-carrageenan, and c) guar gum as well as the temperature behavior of the corresponding hydrocolloid dispersions; the other compositions can be found in appendix B.2. G' and G'' of the TS suspension stay almost constant up to 66.8 °C ± 0.4 °C; however, the sensitivity of the rheometer was not sufficient to determine G' in the sol state accurately due to the low viscosity of ungelatinized starch suspensions in the sol state. Thus, G' is overestimated due to inertia effects and much lower results were expected.

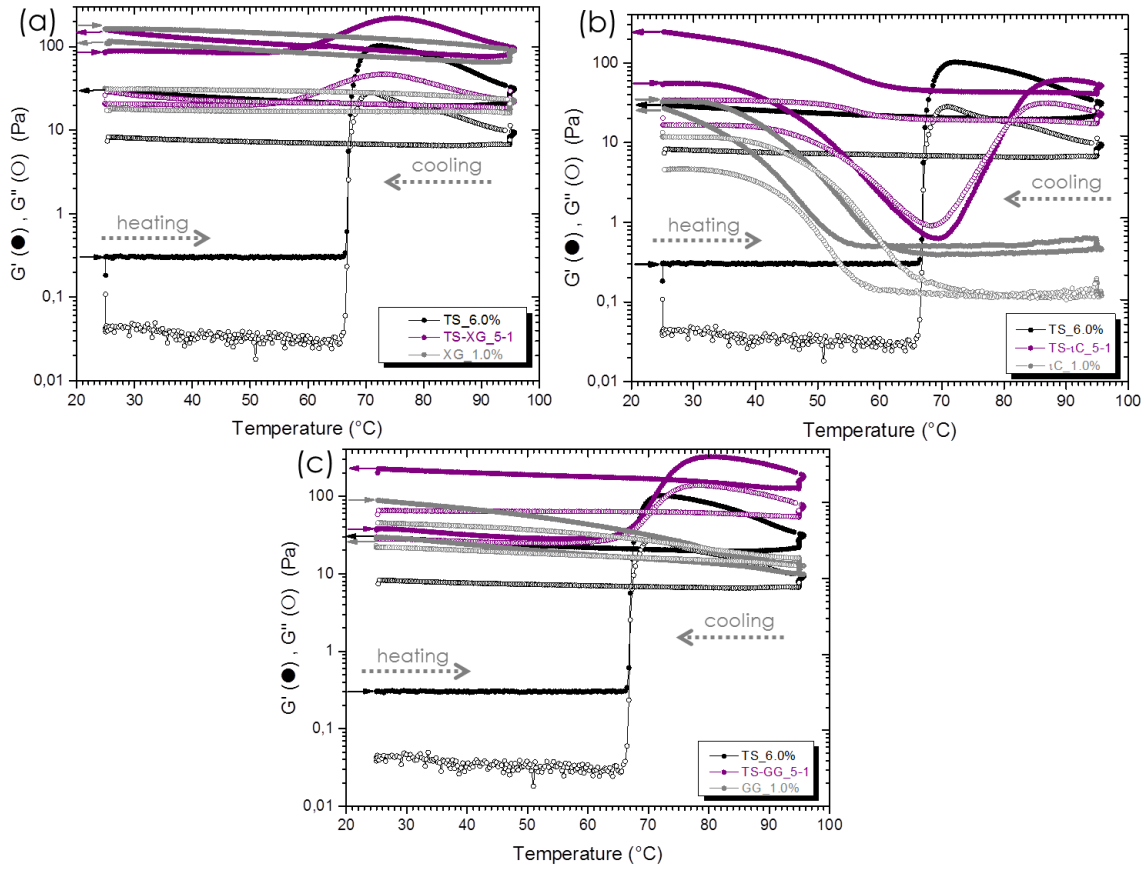

Fig. 7.6 Log-lin plot of G' and G'' as function of temperature during heating and cooling at constant γ = 0.01 and f = 1 Hz of 6% w/w native TS suspension, 5–1 mixture with a) xanthan gum, b) ι-carrageenan, and c) guar gum as well as the pure 1% w/w hydrocolloid dispersions. The small arrows indicate the direction of the curves. Averages of threefold determination, standard deviation not shown.

However, above (66.8 ± 0.4) °C G' and G'' sharply increase and reach their maxima at (72.5 ± 0.4) °C and (71.0 ± 0.3) °C, respectively. The starting point of this abrupt rise coincides with $T_{pasting}$ of the VTP measurements, and indicates the beginning of water absorption and granule swelling producing a viscoelastic response on deformation. After passing their maxima, G' and G'' start to decrease up to 95 °C and finally increase steadily during cooling reaching their endpoint at (29.5 ± 1.1) Pa and (8.3 ± 1.2) Pa, respectively. The hysteresis loop following the maxima of G' and G'' results from starch granules bursting and is followed by leaching out of starch components. During cooling the three dimensional network of reassociated amylose molecules is formed and reinforced by swollen starch granules. Comparing T_{peak} of the TS suspension in figure 7.1 with the temperature where G' and G'' reach their maxima, a difference of about 10 K can be observed. T_{peak} of the VTP represents the temperature where the viscosity of the whole system reaches its maximum during pasting, i.e. where the internal friction of the system is highest due to strong interactions between the still intact granules. The measurement of G' and G'' shows already the reduction in elasticity of the granules by the plasticizing effects of the absorbed water. In consequences, the decay of G' and G'' during further heating corresponds to the superposition of granule softening, bursting, and finally starch component leaching. Nevertheless, the direct comparison of results of the VTP and the presented viscoelastic properties is difficult due to different measuring geometries.

The temperature behavior of G' and G'' of the different hydrocolloids strongly influences the viscoelastic properties of the starch–hydrocolloid mixtures. In particular, the mixture with ι-carrageenan is strongly determined by the temperature induced disorder–order transition of ιC. For pure 1% w/w ιC dispersions G' significantly dominates G''; at 25 °C both start to decrease and finally at 49.7 °C they cross each other and G'' dominates G'. This intersection indicates the gel–sol transition and the gelling point T_{gel}, where $\tan\delta = \frac{G''}{G'} = 1$ [136] [137]. Above T_{gel} G'' should continue to dominate G', until the coil–helix transition occurs again during cooling. Nevertheless, the measurement in figure 7.6b shows that the low viscosity of ιC in the sol state also provokes an overestimation of G' and masks the crossover during cooling. In the mixture with TS granules, this transition is shifted to 56.2 °C due to the occupied volume by the starch granules which increase the effective concentration of ιC. This is more obvious by looking at the isothermal transition from sol to gel; the aggregation of ιC polymer chains in solution is facilitated by locally increased number of molecules.

Comparing the slope of the initial increase in viscoelasticity induced by granule swelling, significant differences for starch suspended in water or in the different hydrocolloid dispersion are apparent.

This more or less steep increase is mainly thought to arise from starch granule swelling and therefore from water absorption. This water absorption depends on the capability of water molecules to diffuse into the starch granules and, consequently, on the free moving space of water in the granules' surrounding media. Due to the high water holding capacity of the added hydrocolloids in the starch–hydrocolloid mixtures, this water diffusion into the starch granules should be retarded and impeded.

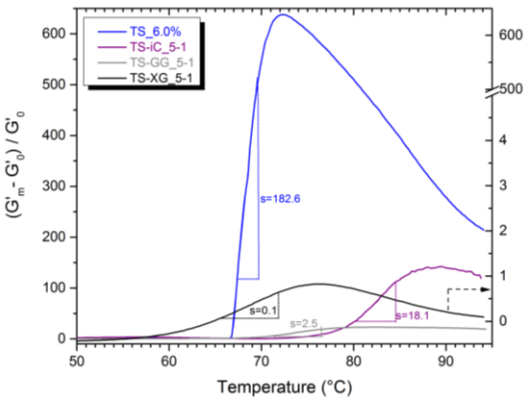

Fig. 7.7 Lin-lin plot of systematized storage modulus as function of temperature for the different TS–hydrocolloid systems.

Figure 7.7 clarifies this observation by magnifying the results of figure 7.6, plotted in a lin-lin diagram. Only the granule swelling in the different surrounding media, i.e. water for the pure starch suspension, 1% xanthan gum, ι-carrageenan, and guar gum dispersions in the TS–XG, TS–ιC, and TS–GG mixtures, respectively, are shown. Thus, the relative effect of hydrocolloids on the starch granule swelling by influencing the water diffusion can be evaluated. Therefore, the storage moduli G'_m measured in figure 7.6 for native TS and the corresponding hydrocolloid mixtures are substituted and divided by the contribution of the surrounding media G'_0: $(G'_m - G'_0)/G'_0$. For the aqueous starch suspension, a constant value of G'_0 = 0.16 Pa was used for water [138], and the values of the pure 1% hydrocolloid dispersions, measured during the temperature profile was used for the hydrocolloid mixtures. Subsequently a linear function was fitted to the transition and the slope for the different systems was determined: TS >> TS–ιC >> TS–GG > TS–XG. The different scaling for the TS–XG mixture has to be noted. This slope determines the velocity of starch granule swelling within the corresponding surrounding media. Without added hydrocolloid, diffusion of water molecules into the starch granules is not influenced, and the aqueous starch suspension exhibits the fastest and greatest increase in figure 7.7. Xanthan gum and guar gum have a significant retarding effect on starch granular swelling. Due to the water binding ability of the hydrocolloids, the water molecules are immobilized, and the amount of water available for the starch granules is reduced, and the granular swelling is impeded [139]. For ιC this effect is much less pronounced, due to the high temperature dependence of the viscosity of ιC dispersions and subsequently low viscosity at high temperatures. Figure 7.1b has already demonstrated that above 60 °C the viscosity of 1% carrageenan dispersion almost equals that of water and the diffusion of water molecules is hardly influenced.

To study the influences of the hydrocolloids on long-term retrogradation, hot gelatinized samples were placed on preheated plates, subsequently cooled to 25 °C, and kept there for 5 h while measuring G' and G'' at constant strain. Figure 7.8 shows the development of storage modulus as function of time, during cooling and tempering, for 6% w/w TS paste, 1% w/w XG, ιC, and GG dispersion as well as their 5–1 mixtures. Here, gelatinization has already occurred and the development of G' during cooling and the gel formation can be observed. Upon cooling association of aligned amylose molecules by entanglements or even hydrogen bonding takes place, and a three dimensional network structure is formed. After network formation, only relatively slow structural alterations remain effective, in which junction zones are expanded and reinforced [58]. For all systems, G' first rises during cooling before adopting a plateau-like behavior with increasing time. During the first cooling step no significant differences in elasticity development is monitored for the different systems; however, the mixture with ιC is again strongly governed by its gel formation process. The storage modulus for TS, XG, TS–XG, GG, and TS–GG pastes increases during cooling from 95 to 25 °C with the same velocity, for pure GG slightly faster, and differ only by the absolute value of G'.

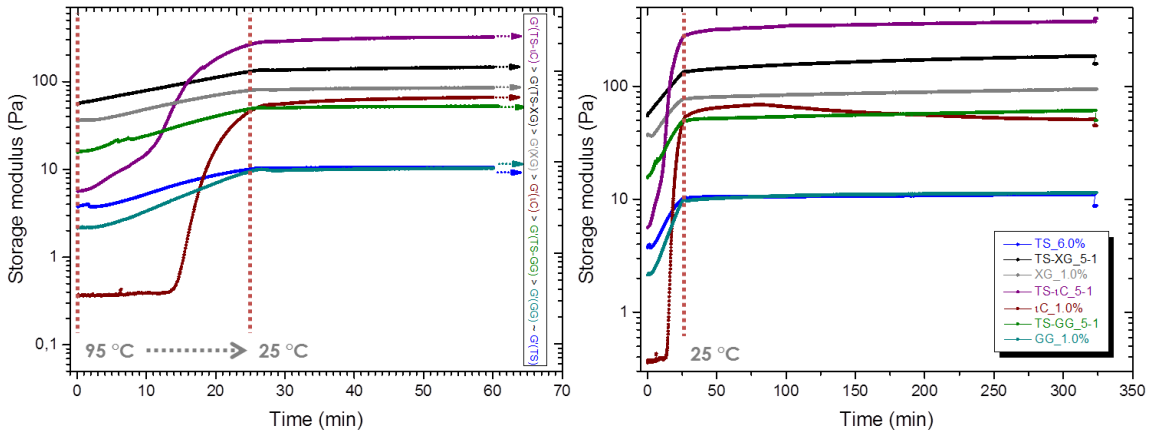

Fig. 7.8 Long-term measurements of storage modulus during cooling from 95 °C to 25 °C for the individual components and the 5–1 mixtures at constant γ = 0.01. The graph on the left side represents a magnification of the initial 60 minutes. Averages of threefold determination, standard deviation not shown.

Consequently, XG and GG do not influence the short-time retrogradation of starch molecules during cooling, i.e. association of amylose molecules and formation of the three dimensional network structures. In contrast, the short-time retrogradation within the mixture with ιC is strongly influenced by the hydrocolloid, expressed by a two–stage increasing storage modulus, which combines the amylose molecule association as well as the coil–double helix transition of ιC polymer chains. During long-term retrogradation during along 5 h, no changes of G' are detected, indicating a quasi–equilibrium state in all systems. Regarding the end values of elasticity for the different

mixtures, the substitution of 1% starch content by hydrocolloids provokes higher values of storage moduli: TS–ιC > TS–XG > TS–GG > TS and is discussed in more detail within the following section.

7.3 Viscoelastic properties of TS/SDTS–hydrocolloid mixtures

To reduce the huge alteration of the mechanical properties imparted to the native tapioca starch by spray drying, and to recover the viscoelastic properties of the paste, the modified tapioca starch was mixed with three different cold soluble thickening agents: xanthan gum, ι-carrageenan, and guar gum. The viscoelastic properties of such a composite gel depend on the volume fraction occupied by the dispersed phase, the deformability of the granule ghosts, the rheological properties of the gelled continuous phase, and on possible interaction between these two phases.

7.3.1 Amplitude dependent deformation behavior

Figure 7.9 presents the results of the amplitude sweep tests for 6% w/w tapioca starch paste in its native and modified form, and the development of viscoelastic properties by substituting the starch content by different amounts of a) xanthan gum, b) ι-carrageenan, and c) guar gum. For a better comparison the storage moduli G' of the native TS (black curve), spray dried TS (purple curve), hydrocolloid in 1% w/w concentration (grey curve) as well as their corresponding 5–1 mixtures (green and blue curves) are magnified at the left side and the absolute values of G' at γ = 0.01 are summarized in table 7.2 for the different systems.

Tab. 7.2 Storage modulus at γ = 0.01 for the different systems presented in figure 7.9 on the left side.

	SDTS	**TS**	**XG**	**TS–XG**	**SDTS–XG**
G' **(Pa)**	1.2±0.2	15.8±1.2	54.6±5.8	107.7±6.2	193.9±11.1
	SDTS	**TS**	**ιC**	**SDTS–ιC**	**TS–ιC**
G' **(Pa)**	1.2±0.2	15.8±1.2	36.2±5.7	112.3±17.4	160.8±18.7
	SDTS	**SDTS–GG**	**TS**	**GG**	**TS–GG**
G' **(Pa)**	1.2±0.2	9.2±0.9	15.8±1.2	25.9±4.4	54.6±4.2

Regarding the mixtures of the spray dried starch with xanthan gum and ι-carrageenan, a significant increase of the storage modulus compared to the pure starch paste is observed. Compared to the single components both mixtures show synergistic effects. For example at a strain of γ = 0.01, the modulus rises in the mixture with xanthan gum from 1.2 Pa for the pure SDTS paste to 193.9 Pa and in the mixture with ι-carrageenan

to 112.3 Pa. Thus, an enhancement of elasticity of almost 200 times with xanthan gum and about 100 times with ι-carrageenan can be achieved. The stronger increase of G' for the addition of xanthan gum can be attributed to the different thickening power of the two hydrocolloids. At the same concentration the storage modulus of a xanthan gum paste is a factor of 1.5 higher than that of the ι-carrageenan paste. Also in the mixtures between the native starch and the hydrocolloids a distinct increase of the storage modulus can be observed, though compared to the pure TS paste, the enhancement is not as strong as for the spray dried one. In addition notable is the reverse order of G' for the different mixtures: G'(SDTS–XG) > G'(TS–XG) whereas G'(TS–ιC) > G'(SDTS–ιC). It is assumed that the mixture with xanthan gum and starch results in a mutual exclusion and phase separation. The formation of the three dimensional structure of jammed rigid xanthan molecules, which is responsible for the viscoelastic properties of xanthan gum, is less hindered in the weak and defective network structure of SDTS than in the crowded gel structure of TS with the tight amylose matrix. Consequently, the strength of the weaker starch component limits the deformation transmitted to the stronger xanthan phase; how it was proposed by Takayanagi for in series arranged components (cf. 4.3.3). ι-Carrageenan is supposed to form a well-mixed phase with starch and to interact synergistically with the amylose network which is more favored in the mixture with native TS than in SDTS. Both components are arranged in parallel manner and deformed to the same extend, and the deformation of the starchy phase is limited by the shear modulus of the stronger ιC network.

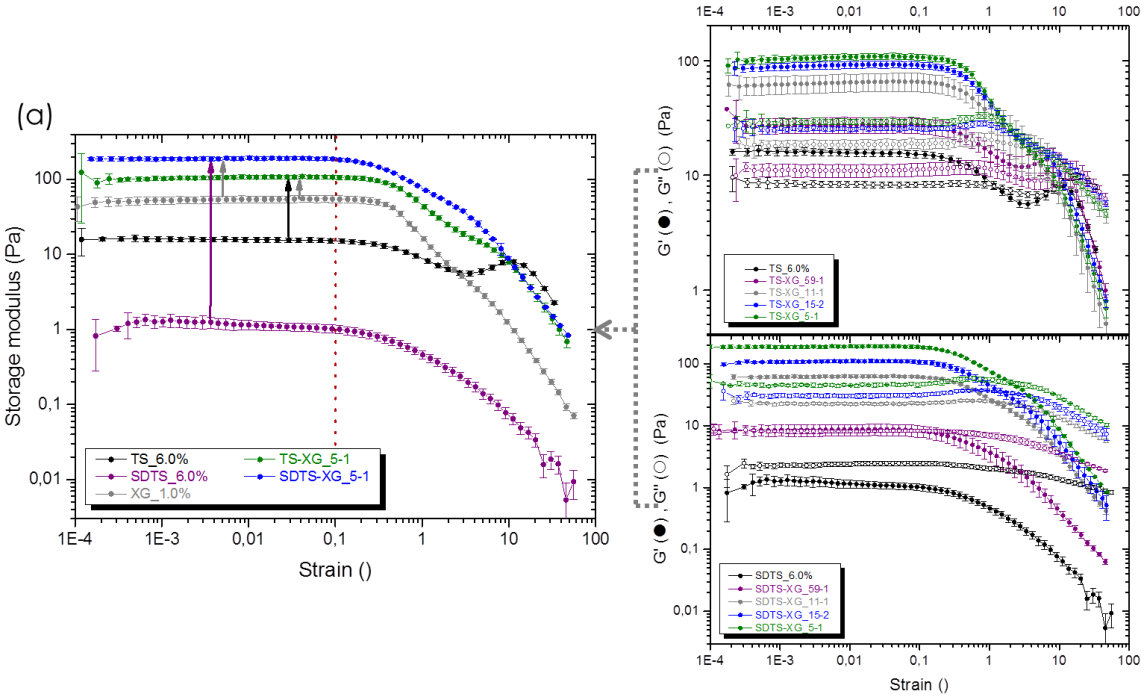

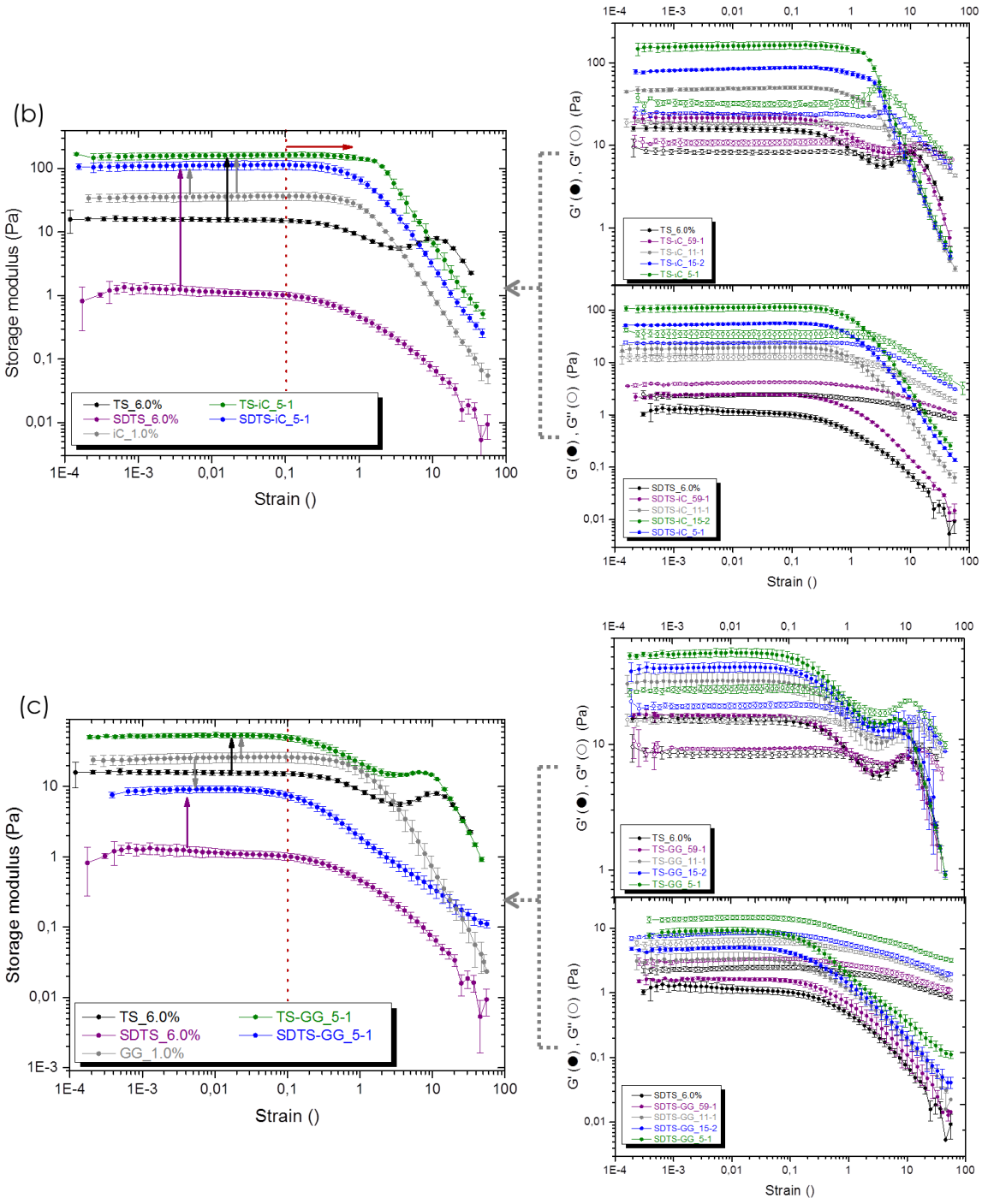

Fig. 7.9 Log-log plot of G' and G'' as function of strain γ at constant f = 1Hz and T = 25 °C for the mixtures of native TS and spray dried TS with a) xanthan gum, b) ι-carrageenan, and c) guar gum in mixing ratios of 59–1, 11–1, 15–2, and 5–1. For a better comparison the functions of storage modulus for the individual components and the 5–1 mixtures are magnified on the left side.

The substitution of starch by guar gum does not provoke such drastic changes of the viscoelastic properties. For the 5–1TS–GG mixture the storage modulus behaves only slightly additive, and for the SDTS–GG mixture compared to the pure GG dispersion, even antagonistic effects install. A 1% w/w paste of guar gum has, compared to the other hydrocolloids, weaker viscoelastic properties with only slightly dominantly elastic

part. The mixture between starch and guar gum is also assumed to form a phase separation, where deformations of the slightly weaker TS phase determines the deformation of the entrapped guar phase. The mutual entanglements of guaran polymer chains are assumed to be impeded by the added spray dried starch, yielding the decay of G'. With regard to the changes compared to pure starch, for both starches in contrast the substitution by guar gum stabilizes the starch network structure and provokes increasing viscoelastic properties. These different phase behaviors of starch and hydrocolloids will be discussed in detail in chapter 8.

Furthermore, the range of the linear viscoelastic (LVE) region is significantly altered, in particular apparent by the addition of ι-carrageenan. Comparing the black and green curves in figure 7.9b on the left side, the TS–ιC mixture is able to resist much higher deformation amplitudes, and the storage modulus starts to deviate more than 10% from the average value along the LVE range at a critical strain γ_c = 1 (100% displacement), whereas the pure native TS paste already at a critical strain γ_c = 0.2. The network of flexible ι-carrageenan polymer chains maintains very high deformations (grey curve); consequently within the composite gel, the network of starch components and hydrocolloids respond together and increase the deformability of the whole mixture. For the mixture with xanthan gum only slight extension of the LVE range can be obtained, due to the increasing yield stress among the jammed xanthan molecules. The addition of guar gum in contrast provokes minor shortening of the linear regime, and the storage modulus of the TS–GG mixture already starts to decrease at γ_c = 0.1. Here, the composite system is likely to decompose and is destabilized already at weak deformations (cf. chapter 8). For the corresponding mixtures with spray dried starch, the development of the LVE range follows the same trend when adding the respective hydrocolloids, but due to the weak starch network not that significantly. Additionally, regarding the curve progression of the native starch paste in the large amplitude oscillatory shear (LAOS) region, the appearance of the local minimum of G' (cf. 6.1.2) significantly changes for the different hydrocolloids. This local minimum of G' is expected to be the result of the complex structure of the composite starch gel, which consists of three components with different molecular architectures and resulting properties: the entangled amylose polymer chains, the highly branched amylopectin polymers, which cannot interpenetrate each other, and the huge granule remnants. They all show different contributions and reactions on different length scales on the imposed strain, and it is assumed that the local maximum is likely to be caused by trapping interaction between the granule remnants and jamming of the swollen, highly branched amylopectin molecules. However, this local minimum of G' disappears or diminishes gradually by adding ι-carrageenan and xanthan gum, respectively; guar gum has no or only very slight influences. The added xanthan molecules move on much shorter time scales than the high molecular weight amylopectin molecules or even than the granule

remnants and act as a lubricant by preventing the local approach of the starch components. In the mixture with ιC, the additional network of carrageenan polymer chains stabilizes the composite gel and even when the amylose network is destroyed and the other starch components should provoke the local maximum, the still intact ιC network prevents their approach.

Figure 7.10 demonstrates the development of the viscoelastic properties with changing mixture composition for the different starch–hydrocolloid blends. Therefore, tan δ at a constant strain of γ = 0.01 is monitored for the different mixture compositions. Starting with a pure starch paste made of the native or the spray dried starch, the starch content decreases whereas the hydrocolloid content stepwise increases. In the mixture with the spray dried starch a stronger influence of the hydrocolloids is observed; for xanthan gum and ι-carrageenan even an inversion of the viscoelastic properties can be induced. The more viscous dominated behavior of the starch paste evolves successively into a more elastic dominated paste by the addition of the different hydrocolloids.

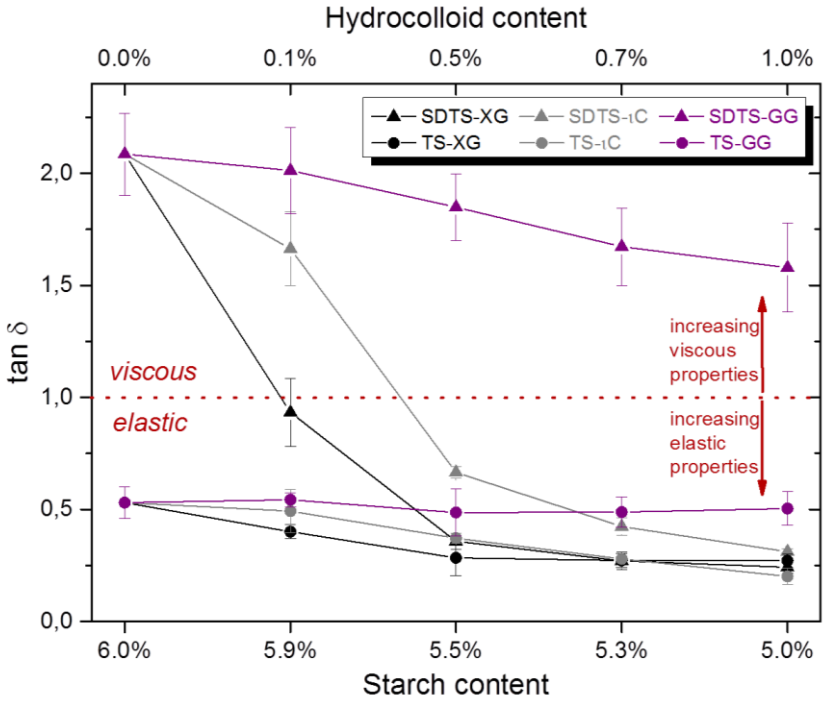

Fig. 7.10 tan δ at γ = 0.01 as function of composition for the different starch–hydrocolloid mixtures. The triangles illustrate the mixtures with the spray dried TS and the circles the mixtures with native TS, respectively.

The replacement of as little as 0.7% spray dried starch by ι-carrageenan suffices to approach the viscoelastic behavior of the native starch; for xanthan gum even 0.5% are more than enough to regain the former mechanical properties. With guar gum even the substitution of 1% does not modify the viscoelastic properties of spray dried starch in such extent and to approach those of the native starch. Compared to the SDTS paste, tan δ of the native TS paste is only marginally influenced by the hydrocolloids and

slightly gains elasticity or stays almost constant. This more pronounced influence of the hydrocolloid addition on the viscoelastic properties of the mixture with the modified starch can be explained by the much weaker network structure formed by the degraded amylose. From a steric point of view, the hydrocolloid molecules are less hindered and are capable to form their own structures more easily, whether in a separated phase (xanthan gum and guar gum) [140] or in a well-mixed phase (ι-carrageenan) [141]. In consequences, the viscoelastic properties of the spray dried starch can be tuned and adjusted stepwise by the substitution of starch by hydrocolloids and the extent can be adapted by the choice of hydrocolloid. With increasing hydrocolloid concentration, a decrease in $\tan\delta$ and the formation of a more rigid and solid-like material, have been also reported for different starch–hydrocolloid mixtures, e.g. for tapioca starch, xanthan gum, and guar gum [56, 142], corn starch and ι-carrageenan [143], rice starch and xanthan gum [144], or for different composites between starches and red algal polysaccharides [145]. All results take together that different paste and gel characteristics are obtained with different specific starch–hydrocolloid combinations and significantly depend on methods of gel preparation and conditions during measurements.

7.3.2 Time dependent deformation behavior

The various strong influences of the hydrocolloids in the different composite pastes with the native or the modified starch become more apparent by regarding the time dependent deformation behavior. Figure 7.11 shows the results of frequency sweep experiments for hydrocolloid mixtures in different composition ratios with native TS on the left side and with spray dried TS on the right side. In addition, figure 7.12 presents the ratio of loss G'' and storage G' modulus as $\tan\delta$ in dependence of frequency for 6% w/w native TS paste (black curve) and a rehydrated 6% w/w paste of the modified starch (purple curve) as well as the 5–1 mixtures with a) xanthan gum (green for TS–XG and blue for SDTS–XG) and b) ι-carrageenan (green for TS–ιC and blue for SDTS–ιC), and c) guar gum (green for TS–GG and blue for SDTS–GG). For a better comparison the frequency behaviors of XG paste, ιC paste, and GG paste (grey curves) in 1% w/w concentration are also shown.

The pastes produced by the native starch as well as its mixtures with the hydrocolloids exhibit typical behavior of stable dispersions and gels. During the whole frequency range the storage modulus dominates the loss modulus ($G' > G''$) and $\tan\delta$ is smaller than 1; $\tan\delta$ stays almost constant with slowly increasing values as the frequency rises. Both, storage G' and loss modulus G'' proceed parallel to each other with a constant slope during the whole frequency range. All three added hydrocolloids shift storage and loss modulus along the y axis to higher values and do not significantly influence their slope in dependence to the frequency. In a hydrocolloid concentration manner, G' seems

to be more influenced than G'', hence the distance between the two curves increases and the slope of $\tan\delta$ for the corresponding 5–1 mixtures, presented in figure 7.12, slightly decreases compared to the pure TS paste. Consequently, the addition of hydrocolloids to the native TS significantly makes the material more rigid and solid than influencing the fluid nature of the composite. Compared to xanthan gum and ι-carrageenan, the addition of guar gum produces the weakest effect which is in accordance to the observations of 7.3.1.

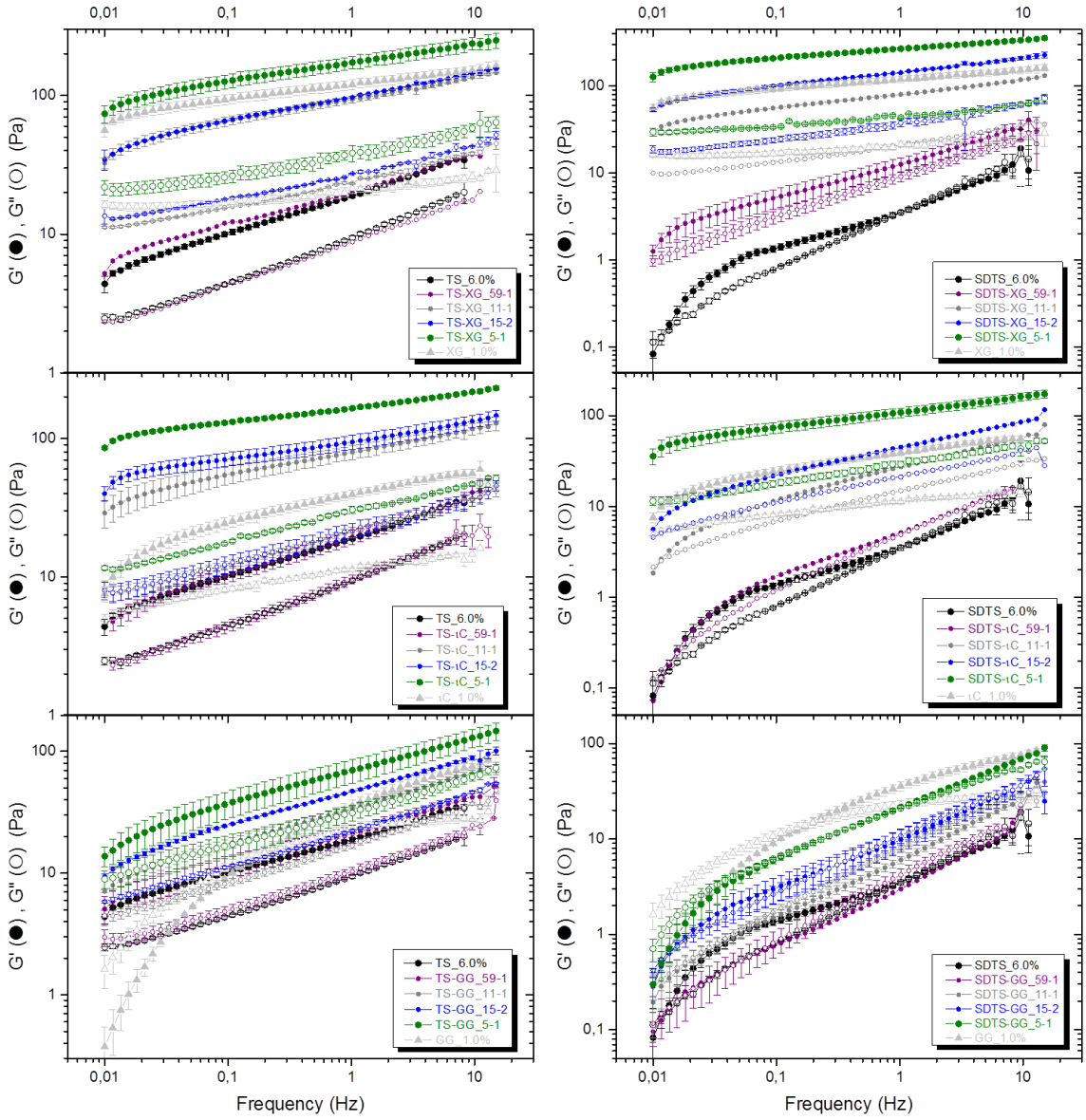

Fig. 7.11 Log-log plot of G' and G'' as function of f at constant γ = 0.01 and T = 25 °C for native and spray dried TS in different mixtures with xanthan gum (above), with ι-carrageenan (middle), and guar gum (below).

The rehydrated paste of the spray dried starch possesses strong frequency dependence and behaves like an uncured polymer dispersion in the nonoperating state and like a fragile cured polymer with weak structure strength in a moderate frequency range (cf. 6.2). With increasing frequency G' and G'' increase constantly, whereas the progression

of G' is slightly slower resulting in a crossover above f = 1 Hz. At low frequencies, i.e. at long-term displacements, tan δ decreases with increasing frequency, followed by a short plateau and a continuous increase. At high frequencies, i.e. at short-term deformations, even an inversion of the viscoelastic behavior can be induced, where G'' equals or dominates G'. By adding the different hydrocolloids the behavior of the pure hydrocolloids is stepwise adapted and even surmounted. For XG and ιC a strong and elastic gel or paste with two parallel running curves for G' and G'' is gradually achieved, similar to those produced by the mixture with the native TS. Notable is the coincidence of the curve for SDTS–XG and the pure xanthan paste over the whole frequency range, shown in figure 7.12. The viscoelastic properties even exceed those of the TS–XG mixture, although the behaviors of the pure starch pastes are strongly divergent. This observation confirms the results of the amplitude sweep test.

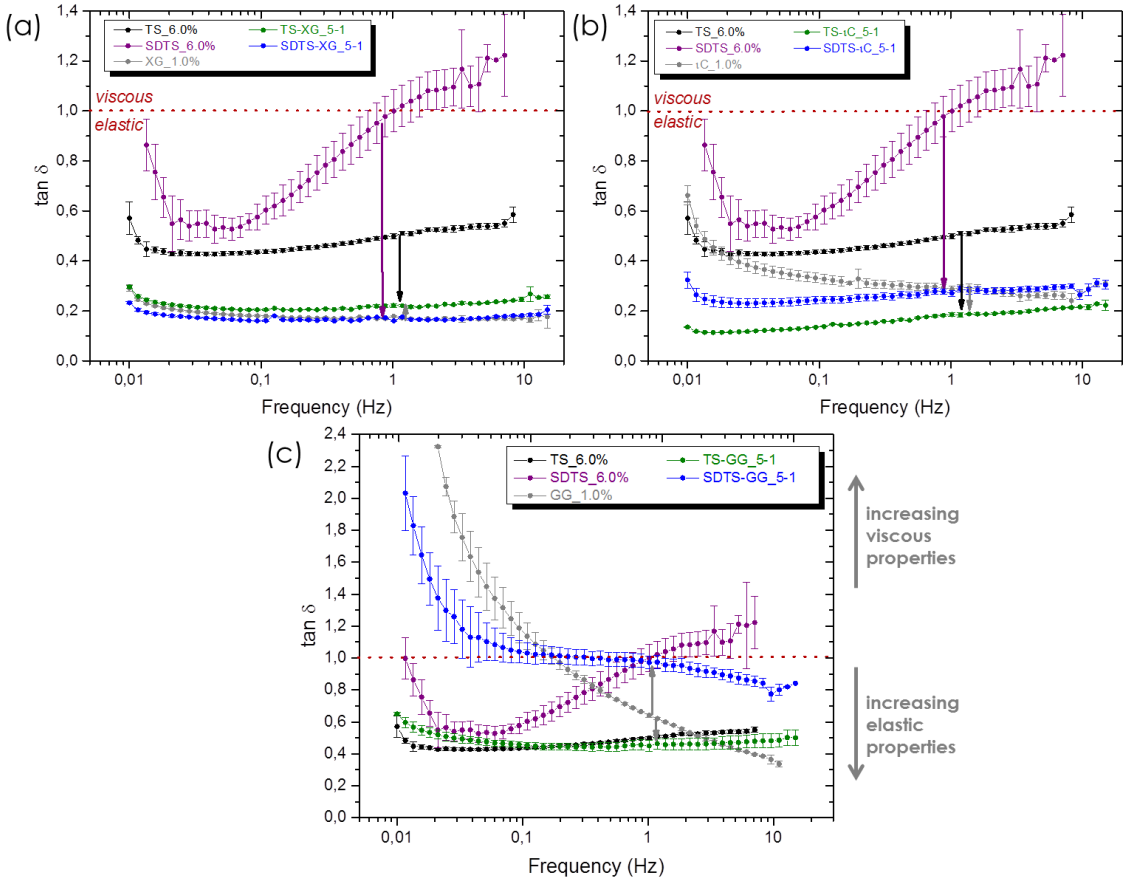

Fig. 7.12 Lin-log plot of tan δ as function of f at constant at constant γ = 0.01 and T = 25 °C for 6% w/w native and spray dried TS as well as their 5-1 mixtures with a) xanthan gum, b) ι-carrageenan, and c) guar gum.

The addition of xanthan gum has a more pronounced influence on the viscoelastic properties in the mixture with the spray dried starch than in the mixture with the native one (cf. table 7.2). The frequency dependent performance of the SDTS–XG mixture adapts significantly the behavior of the pure xanthan gum paste, whereas the mixture TS–XG is more dominated by the behavior of the native starch. The addition of ι-

carrageenan also induces an increase in the elastic properties of the mixtures with the spray dried starch, but to a lower extent. Although the frequency depending behavior of the pure ιC paste and the pure SDTS paste significantly differ from that of the native TS, the behavior of SDTS–ιC follows a similar trend to that of TS–ιC only shifted to more viscous dominated properties. As already mentioned in the previous section, the addition of guar gum to SDTS is not sufficient to reach the viscoelastic properties of the mixture with the native TS. Guar gum consists of uncured polymer molecules which overlap and entangle above a critical concentration. Besides mechanical interaction, like friction and chain entanglement elasticity, neither permanent chemical bounds nor physical crosslinks form the three dimensional structure. Due to missing intermolecular attractions, the guaran polymer chains slip off from each other and disentangle already at low shear forces where G'' dominates G'. With increasing frequency the long relaxation time of the polymers provokes a temporary entanglement network leading to a crossover of G'' and G' and a more elastic dominated behavior. This performance of G' and G'' is gradually transformed to the mixtures with SDTS and maintains the strong frequency dependence of the pure SDTS paste. However, all starch–hydrocolloid mixtures represent constant structure stability during the whole frequency range, and no decomposition effects during the measurement are noticeable.

7.4 Flow behavior of TS/SDTS–hydrocolloid mixtures

To evaluate the flow behavior of a paste produced by the native tapioca starch and the spray dried starch as well as their mixtures with the different hydrocolloids, the steady shear viscosity was measured in dependence on shear rate. The specific adjustment of the flow behavior of starch gels is of significance in order to regulate production processes and to optimize applicability, stability, and sensory properties of end products [141]. Figure 7.13 presents the apparent shear viscosity for native and spray dried starch in different compositions with a) xanthan gum, b) ι-carrageenan, and c) guar gum while increasing the shear rate and subsequently decreasing rate. On the left side the corresponding 5–1 mixtures are compared again with the single components. The rheological flow behavior of TS pastes strongly depends on its composite structure of swollen granule remnants embedded in the continuous amylose network. Rao et al. [146] investigated the influences of granule size on the rheological properties of gelatinized tapioca starch dispersions in terms of different empirical models and found consistency with the simple power law (cf. equation 4.14) and the more complex Casson–Quemada model [147], considering the yield stress of gelatinized starch dispersions. After gelatinization and complete disintegration of starch granules, the starch dispersions behaved shear thinning, whereas after inadequate heating and still intact granules shear thickening behavior could be observed. Other authors [148] [149] compared intensively different models (power law, Bingham, Herschel–Bulkley,

Casson) regarding starch concentration, temperature, pH, or cooking time and also reported adequate description by power law; prediction of yield stress via Herschel-Bulkley or Bingham was not suitable. Figure 7.13 obviously shows non-Newtonian behavior for the native TS paste, the rehydrated SDTS paste as well as their mixtures with the three different hydrocolloids. In general, the viscosity of a liquid is a function of intermolecular forces that restrict molecular motion.

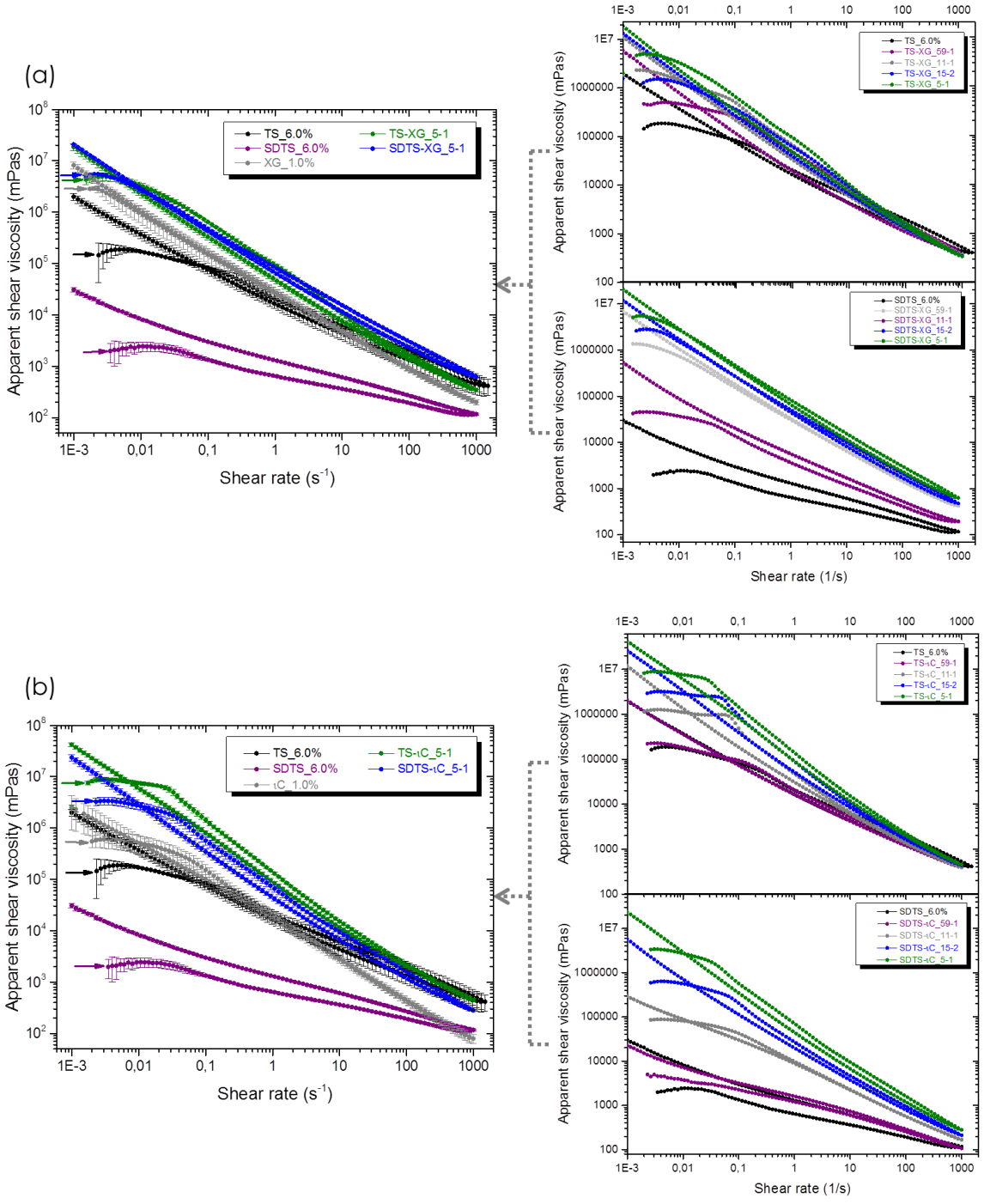

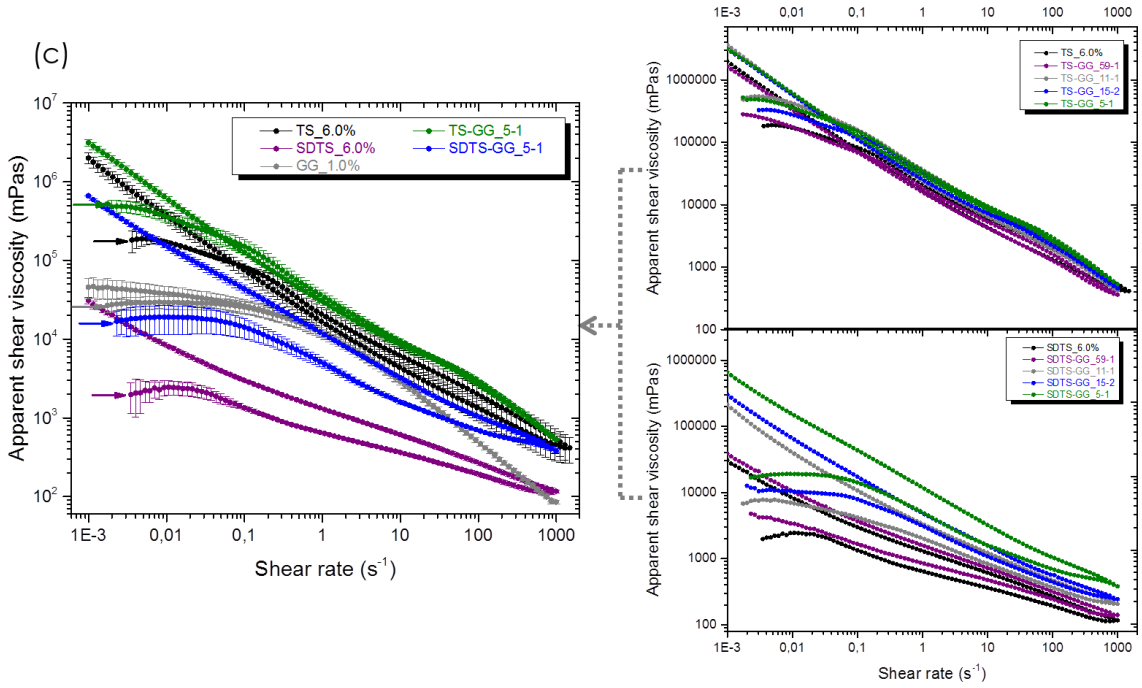

Fig. 7.13 Log-log plot of apparent shear viscosity as function of shear rate $\dot{\gamma}$ at constant T = 25 °C for the mixtures of native TS and spray dried TS with a) xanthan gum, b) ι-carrageenan, and c) guar gum in mixing ratios of 59–1, 11–1, 15–2, and 5–1. For a better comparison the functions for the individual components and the 5–1 mixtures are magnified on the left side; the small arrows indicate the beginning of measurement.

With increasing shear rate, disentanglement of long-chain starch molecules (amylose) occurs, they get oriented in shear direction and the viscosity, i.e. resistance to flow, is reduced. Furthermore, the highly swollen starch granules might be progressively sheared away with increasing shear rate causing a reduction in effective size and hence a reduction in apparent viscosity [150]. Regarding the second cycle of the measurements during decreasing shear rate, all systems also show a yield stress for the shear rate approaching zero. All systems show significant shear thinning behavior with increasing shear rate and comparing the shear viscosity at very low shear rates for both starches, the values are increased by the addition of hydrocolloids. Table 7.3 summarizes theses values and the same trend as for the storage modulus in table 7.2 can be observed for each composite gel. Viscosity increase might be due to the increased work required to move starch components past each other in a more viscous hydrocolloid rich surrounding media. In addition, due to exclusion effects, the effective concentration of hydrocolloid and starch molecules in the continuous phase increases causing enhanced intermolecular friction. Especially with ι-carrageenan a significant increase can be observed. Here in addition, regarding the initial state of measurement, a certain plateau with apparent zero shear viscosity and an almost two–stage decay of viscosity with increasing shear rate can be determined. Since this plateau is becoming more pronounced by increasing ιC concentration, it is assumed to arise from mutual

enforcing three dimensional networks of starch components and ιC polymer chains filling the whole sample volume.

Tab. 7.3 Apparent viscosity at very low shear rate for the different systems presented in figure 7.13 on the left side.

	SDTS	**TS**	**XG**	**TS–XG**	**SDTS–XG**
η_{app} **(Pas)**	30.9±2.7	1 992±318	8 200±1 275	18 552±2 793	20 972±362
	SDTS	**TS**	**ιC**	**SDTS–ιC**	**TS–ιC**
η_{app} **(Pas)**	30.9±2.7	1 992±318	2 594±167	23 558±3 145	42 410±3 482
	SDTS	**GG**	**SDTS–GG**	**TS**	**TS–GG**
η_{app} **(Pas)**	30.9±2.7	45.6±13.3	660±5.6	1 992±318	3 128±327

The addition of guar gum does not provoke such viscosity increasing effects, and especially in the mixture with spray dried starch, the slight antithixotropic behavior during descending order of shear rate, is preserved. The shear thinning behavior of all mixtures is increased, which can be attributed to the strong shear thinning behavior of the hydrocolloids. This observation is clarified by regarding figure 7.14, which illustrates the alteration of pseudoplastic index (equation 5.4) by stepwise replacement of starch by hydrocolloids. The pseudoplastic index is a parameter to evaluate the extent of shear thinning and calculates the slope of the flow curve during increasing shear rate. A pure resuspended paste of spray dried starch exhibits a much lower pseudoplastic index, i.e. weaker shear thinning behavior than the paste produced by the native starch. For both starches this behavior is enhanced by a successive replacement by xanthan gum, ι-carrageenan, or guar gum. Even 0.5% substitution of spray dried starch by XG and ιC suffice to convergence the pseudoplastic index of the native tapioca starch paste; GG only slightly increases the shear thinning behavior of the SDTD paste. Regarding the shear thinning power of the single hydrocolloids, ι-carrageenan (PPI = –0.77) and xanthan gum (PPI = –0.73) have a higher shear thinning power than guar gum (PPI = –0.51), and is also adapted in the starch mixtures. The three dimensional network of associated double helices within the ιC gel and the rigid, log jammed conformation of xanthan molecules are more responsive to shear than the flexible entangled coil conformation of guaran polymer chains [43]. Especially, xanthan solutions show, due to the jamming of rod-like molecules, already at low concentrations a significant shear thinning behavior with yield stress. During shearing above the yield stress the xanthan molecules become oriented in shear direction and the logjam is released which facilitates their sliding along each other.

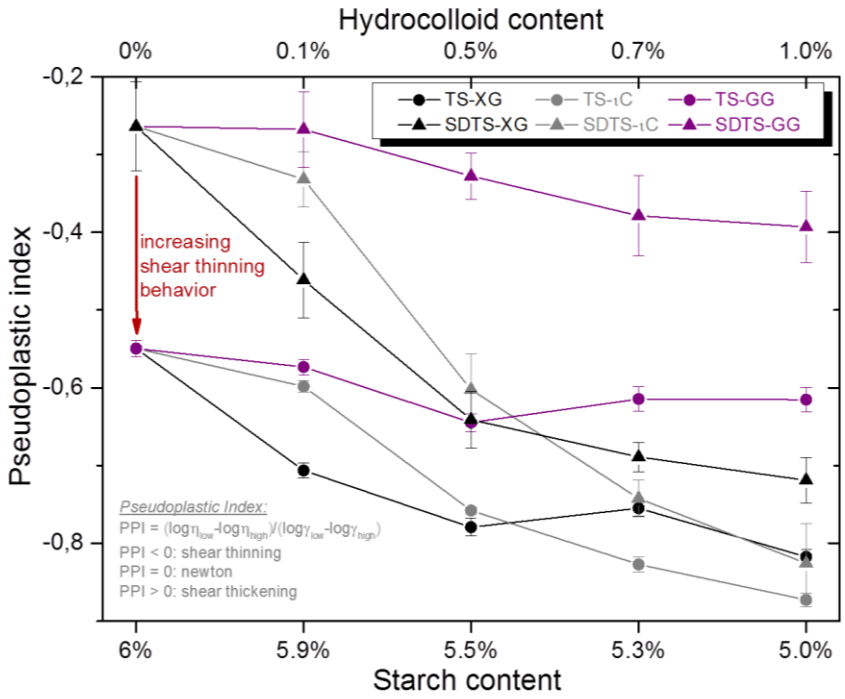

Fig. 7.14 Pseudoplastic index as function of composition for the different starch–hydrocolloid mixtures. The triangles illustrate the mixtures with the spray dried TS and the circles the mixtures with native TS, respectively.

8 Phase behavior of starch-based hydrocolloid mixtures

The existence of a thermodynamic incompatibility between starch polysaccharides and several hydrocolloids has been suggested [58] [141] [57] [151] [140]. Besides the exclusion effect of swollen starch granule ghosts, which induces an enrichment of the nonstarch polysaccharide in the continuous phase, other interactions between starch and nonstarch polysaccharides may be involved [58] [145a]. Exclusion effects may occur in binary mixtures, where interaction between chain segments of the same type is favored energetically in comparison with interaction between different species. Same polymer molecules arrange themselves in layers next to one another in a type of phase separation so that their concentration increases in local domains [58]. Alteration of viscoelastic properties is essentially due to thermodynamic incompatibility leading to mutual exclusion of polymers, although exceptions of specific intermolecular interaction are found for starch–ι-carrageenan mixtures. Eidam et al. [58] even assumed intermolecular binding between carrageenan and amylose molecules, and thus the formation of a coupled network due to energetically favored intermolecular interaction in which junction zones exist between both, like and unlike molecular species. In the most common situation, the dissimilar polymers exclude each other from their polymer domains, so that the effective concentration of each polymer is raised, which in turn results in an exponential viscosity increase. This is especially the case when the starch granules are not completely disintegrated, and the nonstarch polysaccharide is concentrated in the continuous phase. If there is intermolecular interaction, hydrocolloids interact with amylose, the gelling fraction of starch, and may influence its gelation. Crystallization of amylopectin does not seem to be influenced by the admixture of hydrocolloids, as it was seen for starch–xanthan gum mixtures [57]. These authors also reported higher viscoelastic properties of starch–xanthan gum mixtures which were prepared by heating both components together than compared to the pure additive properties by simple mixing, and suggest some kind of synergistic interaction. Based on rheological measurements, they concluded that incompatibility exists between starch and xanthan gum, which probably promotes formation of microphase separated systems, where amylopectin, amylose, and xanthan molecules are mutually excluded. Synergistic effects between starch and xanthan gum are more likely caused by phase separation, rather than due to intermolecular association [152]. Excluded volume effects of the different polymers increases the local concentration in the continuous phase and phase separation of xanthan molecules and amylose polymers are supposed to be promoted [59]. Such thermodynamic incompatibility was also assumed between starch

polysaccharides and galactomannans, i.e. guar gum [151]. It is suggested that based on phase volume ratio after bulk phase separation, the continuous phase is starch based and the dispersed phase galactomannan based. Consequently, enhanced structural strength of blends was caused by volume exclusion effects rather than by true synergistic interaction between starch and galactomannans. Both nonionic, galactomannans, and ionic polymers, xanthan, are supposed to exhibit mutual exclusion in starch-based composite gels by thermodynamic incompatibilities. Savary et al. [60] investigated the influences of ι-carrageenan and presumed a composite gel, obtained after cooling, where swollen starch granules are embedded in a network containing the gelling nonstarch polysaccharide. The viscoelastic properties of such a composite gel depend on the volume fraction occupied by the dispersed phase, the deformability of the swollen starch granules, the rheological properties of the gelled continuous phase and on the possible interaction between these two phases. Besides the exclusion effect of swollen starch granules, which induces an enrichment of the nonstarch polysaccharide in the continuous phase, other interactions between starch and nonstarch polysaccharides may be involved. Indeed incompatibility between starch and nonstarch polysaccharide molecules coexisting in the same phase would result in the phase separation of the two polysaccharides.

The alteration of the viscoelastic properties of the tapioca starch pastes by the addition of the hydrocolloids can be explained with a simple phenomenological model of the network structures describing the molecular interaction in starch–hydrocolloid mixtures resulting from different chain flexibilities of the hydrocolloids (figure 8.1). A pure starch gel or paste can be understood as a phase separated network of undissolved granule remnants embedded in a matrix of entangled amylose polymer chains and separated branched amylopectin molecules. The addition of ι-carrageenan is assumed to form a well-mixed phase with intermolecular, transient crosslinks. Both, ι-carrageenan and amylose consist of linear and flexible polymer chains, and due to the electrostatic elongation of carrageenan molecules, the stereochemical approach of the two different polymers is facilitated and enables intermolecular physical interaction. After heating a permanent and stable network of amylose and ι-carrageenan chains is obtained, and strengthens and reinforces the matrix structure of the mixed paste. Due to the presence of the carrageenan polymer chains the number of crosslinks in the three dimensional gel network is increased, resulting in an increasing overall elasticity for the whole composite.

On the other hand the addition of guar and xanthan gum causes phase separation where the guaran and xanthan molecules separate into local domains and thus interaction of the two species are impossible. In contrast to ι-carrageenan, the nonionic guaran molecules favor a flexible nonordered random coil conformation in aqueous solution, and separate as dispersed phase within the amylose containing continuous phase. The

main difference between xanthan gum and guar gum or ι-carrageenan is their chain flexure; xanthan gum is very stiff and has a rod-like character, in contrast guaran molecules and ι-carrageenan are dominated by flexible structures. From a steric point of view, the stiff and large xanthan gum molecules are not able to diffuse into the starch network and vice versa. Thus, for entropic reasons a local separation in domains is favored for the whole system. The viscoelastic properties of the mixed systems are thus dominated by both components which lead to synergistic or additive effects for the moduli.

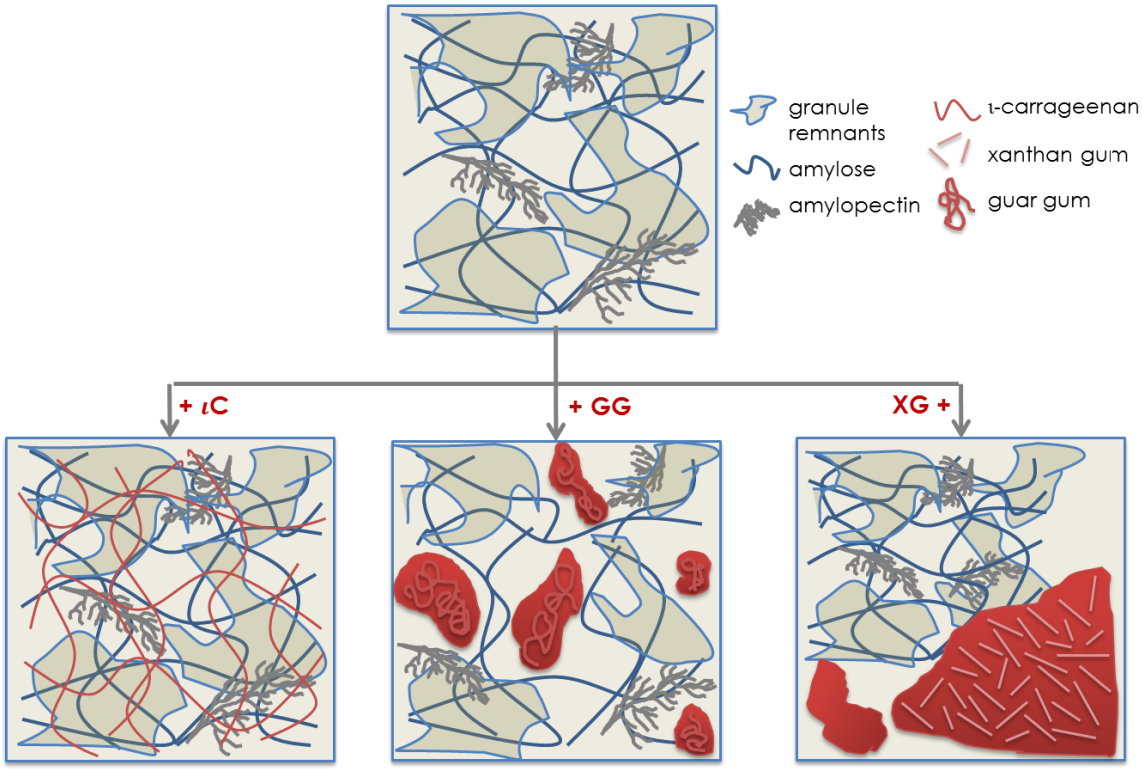

Fig. 8.1 Schematic illustration of the network structure in a pure tapioca starch paste (above) and in addition of ι-carrageenan (left), guar gum (middle), and xanthan gum (right). The red structures represent ι-carrageenan polymer chains (left), guaran polymer coils (middle) and xanthan gum domains (right). The tapioca starch paste can be viewed as a phase separated network of swollen starch granule remnants embedded in a continuous phase of amylose. The addition of ι-carrageenan results in the formation of a well-mixed phase, whereas the addition of guar gum and xanthan gum leads to mutual exclusion.

The addition of the different hydrocolloids leads to changes in gel and network structures which can be monitored by confocal scanning microscopy. CLSM observations help to characterize the continuous and dispersed phases of the composite gels. By covalent labelling of the hydrocolloids it was possible to visualize the hydrocolloid rich zones in the mixture. Starch was stained by adding the fluorescent dye rhodamine B, which adsorbs due to local accessibility and affinity to the starch molecules.

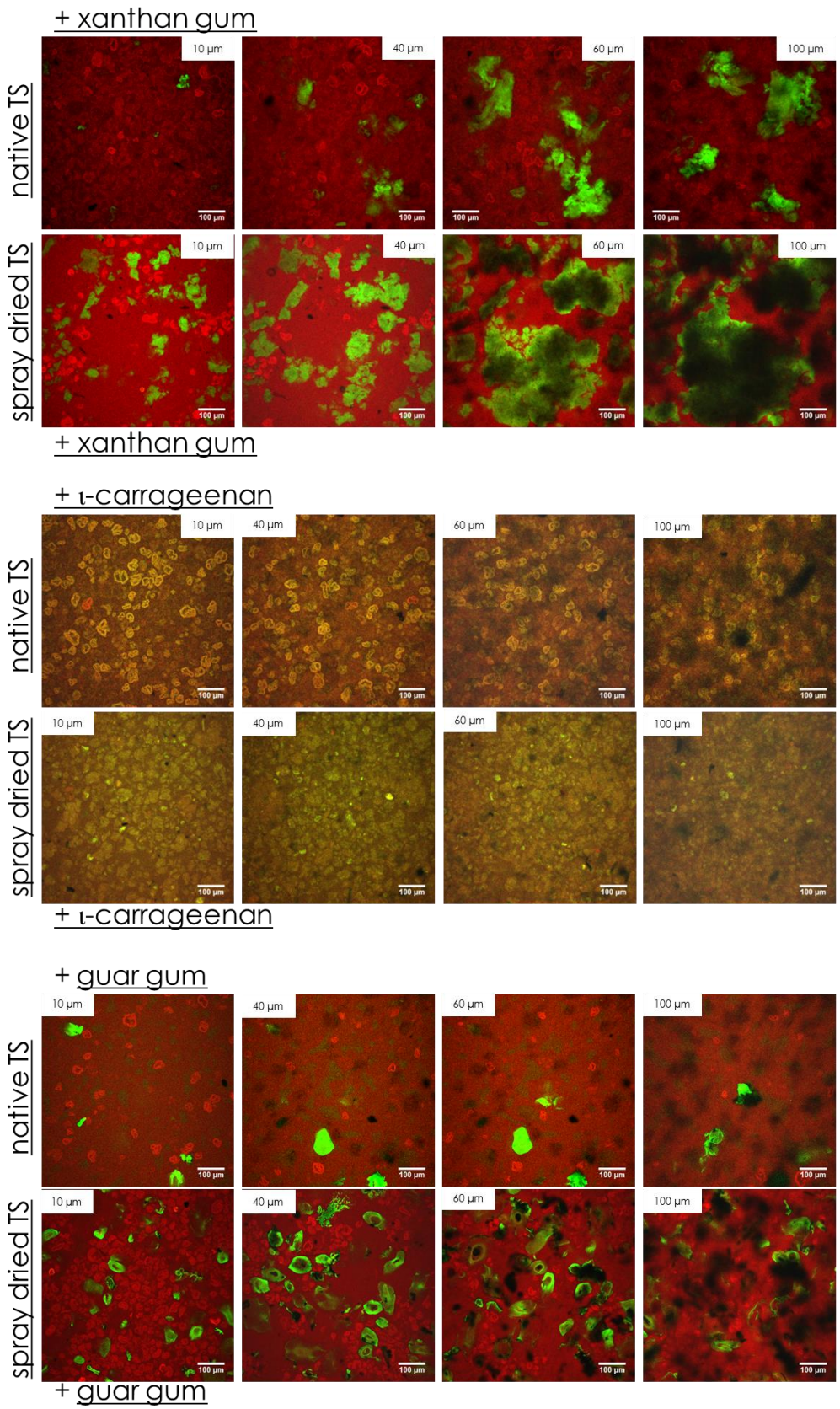

Fig. 8.2 CLSM images of different 1% w/w starch–hydrocolloid mixtures in 11–1 ratio at four different focal planes (10, 40, 60, and 100 µm). The starchy phase was stained with rhodamine B and the hydrocolloids were covalently labeled with FITC. Objective: 20×, image size: 707.11×707.11 µm^2, electronic zoom: 0.

Figure 8.2 summarizes the CLSM images of native TS and spray dried TS in 11–1 mixtures with xanthan gum, ι-carrageenan, and guar gum along the sample height from the bottom to 100 µm sample depth. The formation of the local domains of xanthan gum is clearly visualized by CLSM in figure 8.2. Xanthan gum was labeled covalently with FITC to distinguish in detail the location of the hydrocolloid in the mixture. Apparently, xanthan gum does not fill the entire sample volume and appears as large lumps of undefined shapes. The z-stack shows the three dimensional structure of the xanthan domains. While at 10 µm only protruding parts of the large domains are visible, their maximum size and real dimension are revealed only at deeper focal planes. Carrageenan was also covalently labeled with FITC and the starchy phase with rhodamine B. An overall yellowish coloration can be monitored in the mixture. The appearance of the mixtures with ι-carrageenan is independent of the z-stage; as expected the hydrocolloid is distributed homogenously in the whole sample. This observation can be interpreted as a homogenous distribution of the two dyes and thus of the different components in the whole sample. In the mixtures with covalently labeled guar gum, the formation of local hydrocolloid rich domains is also significantly apparent and along the z-axis no alteration of their shape is visible. Though compared to the xanthan separated phase, these domains are less expanded and more homogenously distributed within the sample volume. Due to high chain flexibility, the galactomannan is supposed to separate as dispersed phase entrapped by the continuous starch-based phase, whereas xanthan even tends to the formation of a bulk phase separation.

Comparing the mixtures of the native starch with the mixtures of the spray dried one, slight differences can be observed. In the mixture SDTS–XG and SDTS–GG the local domains of xanthan gum have a bigger dimension than in TS–XG or TS–GG and in the SDTS–ιC mixture the network seems to be tighter than in TS–ιC. This observation is consistent with the results of the rheological experiments. Here, the addition of the hydrocolloids exerts a more pronounced influence on the mechanical properties of the modified starch paste than on the native one. Due to the weaker network structure in the starch paste produced by the spray dried tapioca, the mobility and diffusion of the xanthan, guaran, and ι-carrageenan molecules are enhanced leading to a facilitated separation into the local domains or formation of a physical network, respectively. In addition, for SDTS–GG, the appearance of guar gum enclosures seems to be more pronounced in the lower focal planes due to sedimentation effects. This is more obvious by looking at the long-term stability of the different composite gels. Figure 8.3 compares the storage modulus in dependence on applied strain of native TS, spray dried TS, and their 5–1 mixtures with XG, ιC, and GG measured 4 h after preparation and after storage at room temperature for 3 days. For the pure TS paste, TS–XG, and TS–GG mixtures, a significant increase of G' is visible after 3 days, whereas for TS–ιC no changes are detected. It is assumed that the increase of storage modulus for TS, TS–XG,

and TS–GG is based on an increased development of phase separation as well as on continuous progression of amylopectin retrogradation, which also promotes the increasing separation of amylose and amylopectin. Figure 8.4 presents pictures of the corresponding paste after 4 h and after 7 days (better visualization of long-term stability). In all systems increasing turbidity, attributed to the amylopectin retrogradation, is discovered. Additionally, for the pure TS paste a more turbid upper phase separates which is supposed to consist of aggregated amylose chains. Kalichevsky and Ring [71] described that by mixing solutions of amylose and amylopectin bulk phase separation occurred yielding in an upper amylose rich and a lower amylopectin rich phase. It is presumed that this phase separation is promoted by an asymmetry in affinity of the two polymers to the solvent water, and as a consequence of mutual exclusion, amylose as polymer fraction with less favorable interactions with water, tend to be driven out of solution [153]. In the mixtures with added xanthan gum and guar gum the separation between starch and nonstarch phase dominates, indicated by the turbid enclosures of macroscopic aggregated hydrocolloids and as expected more distinctive for the admixture of xanthan gum.

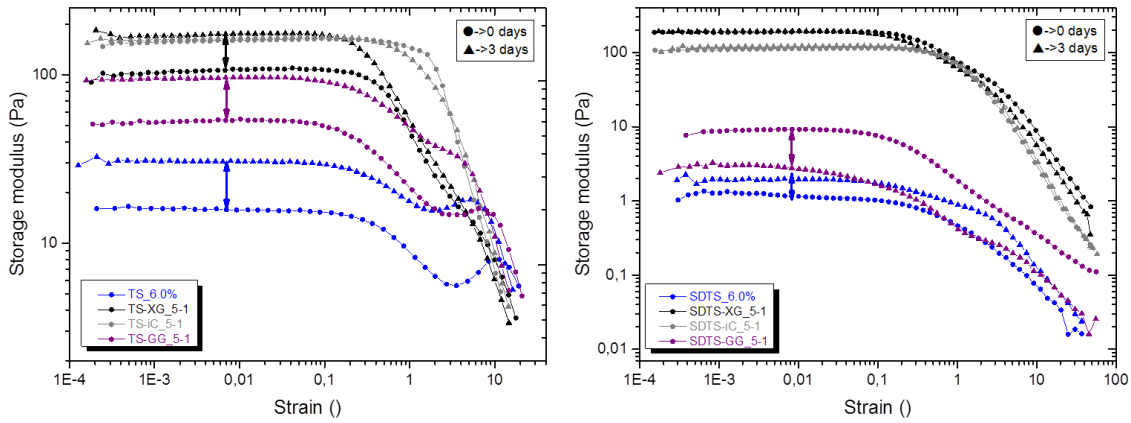

Fig. 8.3 Storage modulus as function of strain γ for 6% TS (left) and SDTS (right) paste and their 5–1 mixtures with XG, ιC and GG 4h after preparation (circles) and after storing at room temperature (triangles) for 3 days.

The mixture of TS and ιC is not affected during long time storage supporting the presumption of a well-mixed composite with a stable and homogenous network structure. Even the retrogradation of amylopectin and the resulting phase separation of starch components seem to be suppressed due to the additive carrageenan network which additionally spans the whole sample. In the SDTS-based systems, no changes of G' can be observed for SDTS–XG and SDTS–ιC after 3 days. The rheological measurements as well as the CLSM images have indicated a hydrocolloid dominated composite paste even directly after preparation. Consequently, no structural alteration is provoked by time induced effects for the mixtures with SDTS.

The xanthan gum domains have reached their full extent, and the ιC network was completely formed after 4 h.

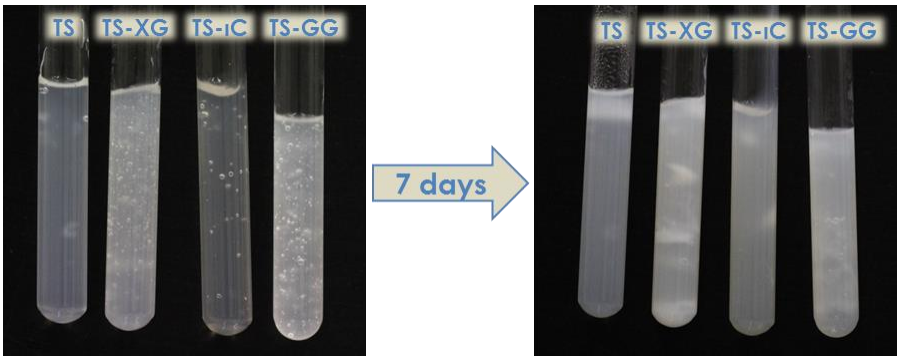

Fig. 8.4 Corresponding pictures of the TS based pastes measured in figure 8.3. The comparison after 7 days was chosen due to a better visualization of long-term stability. After 7 days storage all systems, except TS–ιC, show certain decomposition.

The storage modulus for SDTS–GG decreases significantly after 3 days indicating a strong decomposition. The weak amylose network of SDTS cannot prevent demixing of starch components, which is also visible by a slight increase of G' for the pure SDTS paste after 3 days, similar to the native TS. In the mixture with GG, the separated domains continuously grow which finally result in complete bulk phase separation. The guar gum dominance, even after complete decomposition, provokes lower viscoelastic properties with slight viscous dominating part in this system (cf. 7.3).

To conclude, the mixture of ι-carrageenan and starch forms a well-mixed system with strong intermolecular interaction between the different polymers. On the other hand, the mixture with xanthan gum and guar gum results in a separation into local micro domains and a mutual exclusion of starch and xanthan or guaran, as it has been shown for maize starch [58]. The mechanical properties of the starch-based mixtures can be adjusted and designed by successive addition of hydrocolloids and can be followed analytically by rheological measurements. From the interaction in a composite gel between the investigated hydrocolloids and the native tapioca starch, conclusions can be drawn for the mixed systems with the spray dried starch. The mixtures between spray dried TS and hydrocolloids have hydrocolloid dominated functional properties and by mixing the cold soluble tapioca starch with xanthan gum, ι-carrageenan, or guar gum on dry basis, a thickening effect with a weak gel character can be easily produced by hydration without heat addition. According to the desired application, the mechanical properties and texture can be controlled and tuned by varying the mixture composition.

9 Conclusion and Outlook

The main purpose of this work was to provide a basis for the production of a cold soluble tapioca starch, which disintegrates at room temperature while maintaining the typical characteristics of a tapioca starch paste. To achieve this, a gelatinized starch paste was spray dried and subsequently, by mixing the spray dried starch with appropriate cold soluble thickening agents, it was possible to tune and adjust the mechanical properties of the rehydrated modified starch paste.

Tapioca starch differs from other starches by its low level of residual materials (lipid, protein, ash), lower amylose content (17%), and high molecular weights of amylose and amylopectin. When heated in excess water, starch undergoes an irreversible structural transition and as a result the starch granules lose birefringence and crystallinity. The granules then swell and absorb water, resulting in altered rheological properties of the starch–water suspension. The result is a composite gel of undissolved granule ghosts, embedded in a continuous matrix of entangled amylose polymer chains and separated highly branched amylopectin molecules. The swollen ghosts are at least twice as large as the dry granules, no birefringence is visible and depending on applied shear they remain partially intact. It was shown that these granule ghosts predominantly consist of amylopectin. Ghosts are weak elastic structures and act as soft filler particles which reinforce the surrounding amylose network. It was demonstrated that the viscoelastic properties of a tapioca starch paste result as an interplay of the three different components: entangled amylose polymer chains, highly branched amylopectin polymers, which cannot interpenetrate each other, and the micrometer-sized ghost granules.

The comparison of the viscoelastic properties of the paste made from native tapioca starch with those of the rehydrated paste of the spray dried starch, revealed significant differences. Native TS does not gelatinize without heat application whereas SDTS dissolves completely at room temperature and a viscous paste can be obtained. Results of dynamic and steady rheological measurements showed a decay of the viscoelastic properties mainly caused by weakening of the amylose matrix structure. During the spray drying process, the strong shear and heat conditions represent a nonequilibrium state and are assumed to have a certain degradation effect on the starch components. Given this, the stability and density of amylose polymer chain entanglements would be reduced which in turn forms a weaker transient network structure. Thus, in a paste produced by the spray dried starch, shorter amylose polymer chains deplete the intermolecular association resulting in a decay of the overall elasticity. This assumption was supported by CLSM, LM, different shear and drying experiments, amylase

digestion and in particular by tracer diffusion via DLS. It could be shown that for native TS, the critical concentration upon which the entanglement density starts to influence the diffusion of the tracer particles is reached at an earlier state and hampers their further motion to a more drastic extent.

The functional properties of starch can be modified by the incorporation of nonstarch polysaccharides. The major practical advantages are the enhancement of viscosity, modified flow behavior or mechanical properties, all strongly dependent on the physicochemical properties of the added polymers. Hydrocolloids exhibit a variety of structures, including different branching, flexibility, molecular weight ranges, and ionic charge, all of which influence their behavior and the rheology of their solution. Xanthan gum, ι-carrageenan, and guar gum were thus added systematically in different concentrations to native and spray dried tapioca starch, to study their effect on the mechanical properties of the resulting final pastes. Differing interactions result in different gel structures and determine the mechanical properties of the binary starch-based systems. Differing interaction of the three following hydrocolloids with different types of tapioca starch were studied and compared: (1) a highly charged, but very stiff hydrocolloid, i.e. xanthan gum, (2) a charged hydrocolloid with flexible molecular structure, i.e. ι-carrageenan, and (3) a neutral and flexible polymer chain, i.e. guar gum, in a composite gel. Similar observations were made when comparing the mixtures of native and spray dried tapioca starch with the corresponding hydrocolloids. Although, in this case the composite pastes with SDTS were always hydrocolloid dominated. From the interactions in a composite gel between the investigated hydrocolloids and the native tapioca starch, conclusions can be drawn for the mixed systems with the spray dried starch.

The alteration of the viscoelastic properties of the tapioca starch pastes by the addition of the hydrocolloids was explained using a simple phenomenological model of the network structures describing the molecular interaction in starch–hydrocolloid mixtures. The addition of ι-carrageenan is assumed to form a well-mixed phase with intermolecular crosslinks. Both, ι-carrageenan and amylose consist of linear and flexible polymer chains, and due to the electrostatic elongation of carrageenan molecules the stereochemical approach of the two different polymers is facilitated and enables intermolecular physical interaction. A permanent and stable network of amylose and ι-carrageenan chains is obtained, which strengthens and reinforces the matrix structure of the mixed paste. On the other hand, the addition of guar or xanthan gum causes phase separation where the guaran or xanthan molecules separate into local domains, and thus interaction of the two species is impossible. In contrast to ι-carrageenan, the nonionic guaran molecules favor a flexible nonordered random coil conformation in aqueous solution and separate as dispersed phase within the amylose containing continuous phase. Xanthan gum is very stiff and has a rod-like character, and from a steric point of

view, the large xanthan gum molecules are not able to diffuse into the starch network and vice versa. The addition of the different hydrocolloids leads to changes in gel and network structures, which was monitored by confocal laser scanning microscopy. CLSM observations helped to characterize the continuous and dispersed phases of the composite gels.

Looking ahead, it is worth pursuing this challenging project of producing cold water soluble starch products with enhanced functional properties by the admixture of other cold soluble hydrocolloids, through the spray drying of starch–hydrocolloid mixtures. Investigation of the functional properties of a rehydrated powder produced by spray drying of an already gelatinized paste containing the native TS and varying amounts of hydrocolloid is still to be accomplished. Comparison with the results of SDTS–hydrocolloid mixtures presented here could advance its application range. The greatest challenge would be the practical realization due to the highly viscous character of the TS–hydrocolloid mixtures. Given this, the admixture of ι-carrageenan, in particular, could prevent the degradation of amylose molecules due to the reinforced network structure.

Beyond the scope of this work is the investigation of the impact of low molecular weighted co-solutes such as sugars, salts, or other ingredients. Food gels often contain sugars to enhance sweetness or stability. While dissolving, sugar molecules have strong restructuring effects on the water molecules by the formation of hydrate shells. Consequently, depending on the nature and structure of the added sugar, competition for the available water between sugar molecules and hydrocolloids take place within the system, and may determine their texture and mechanical properties [51] [154]. Recently, the influence of sucrose on thermal and pasting properties of starch–xanthan mixtures was investigated and strong interaction affecting gelatinization and retrogradation of the starch-based composite were found [155]. The use of newly established sweetening agents such as aspartame, stevia, or erythritol as natural sugar replacements would be also of interest. In addition, various salts are often added to food formulations to enhance the taste. Especially in the case of ionic hydrocolloids, this addition plays a significant role due to supplementary charges. Some research has already been done on the effect of different salts on starch–hydrocolloid mixtures [156]. The detailed investigation of all interaction that occurs between starch and different additives furthers our understanding of the role of starch in multicomponent systems, and helps to control the functional behavior of starch-based food formulations. However, regarding the mechanical properties of the bulk, it is still not completely understood how the different structural and physical elements interact with one another.

In conclusion, starch and those food products containing starch form one of the greatest sectors in the food industry. It is not only important to understand the composition of these products, their relevant structural elements and how they mutually interact, but also, it is mandatory for the food sector to provide a comprehensive description of the structural and textural properties of starch and starch-related products.

Appendix A Supporting information to chapter 6

A.1 Granule size native TS

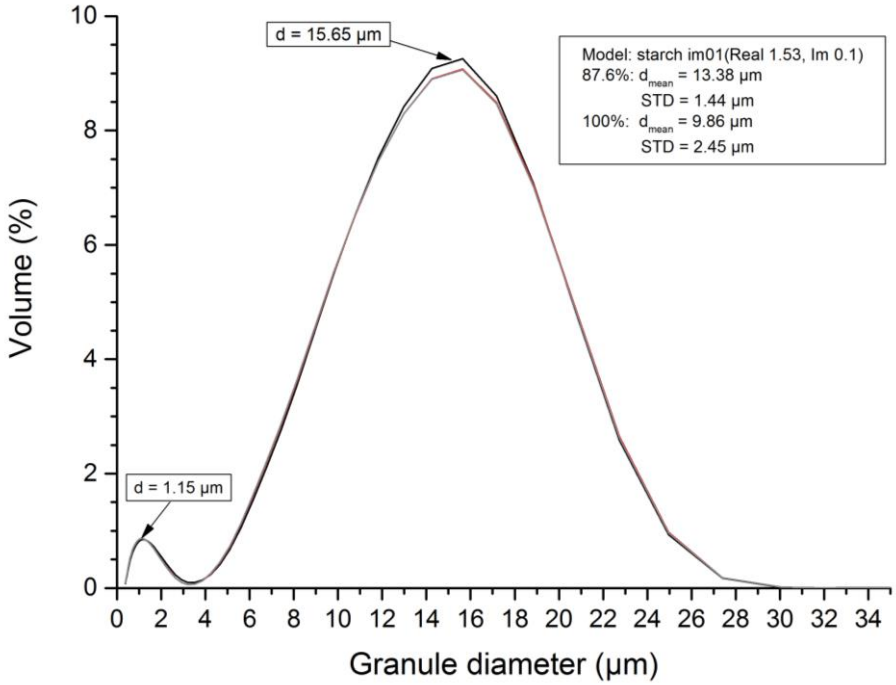

Fig. A0.1 Granule size of native TS measured by laser diffraction with LS 13320 from Beckmann-Coulter. The granule diameter ranges from 4 to 28 µm with a mean value of 13.4 µm, in addition some smaller particles less than 4 µm can be found probably arising from granule remnants.

A.2 Molecular weight distribution

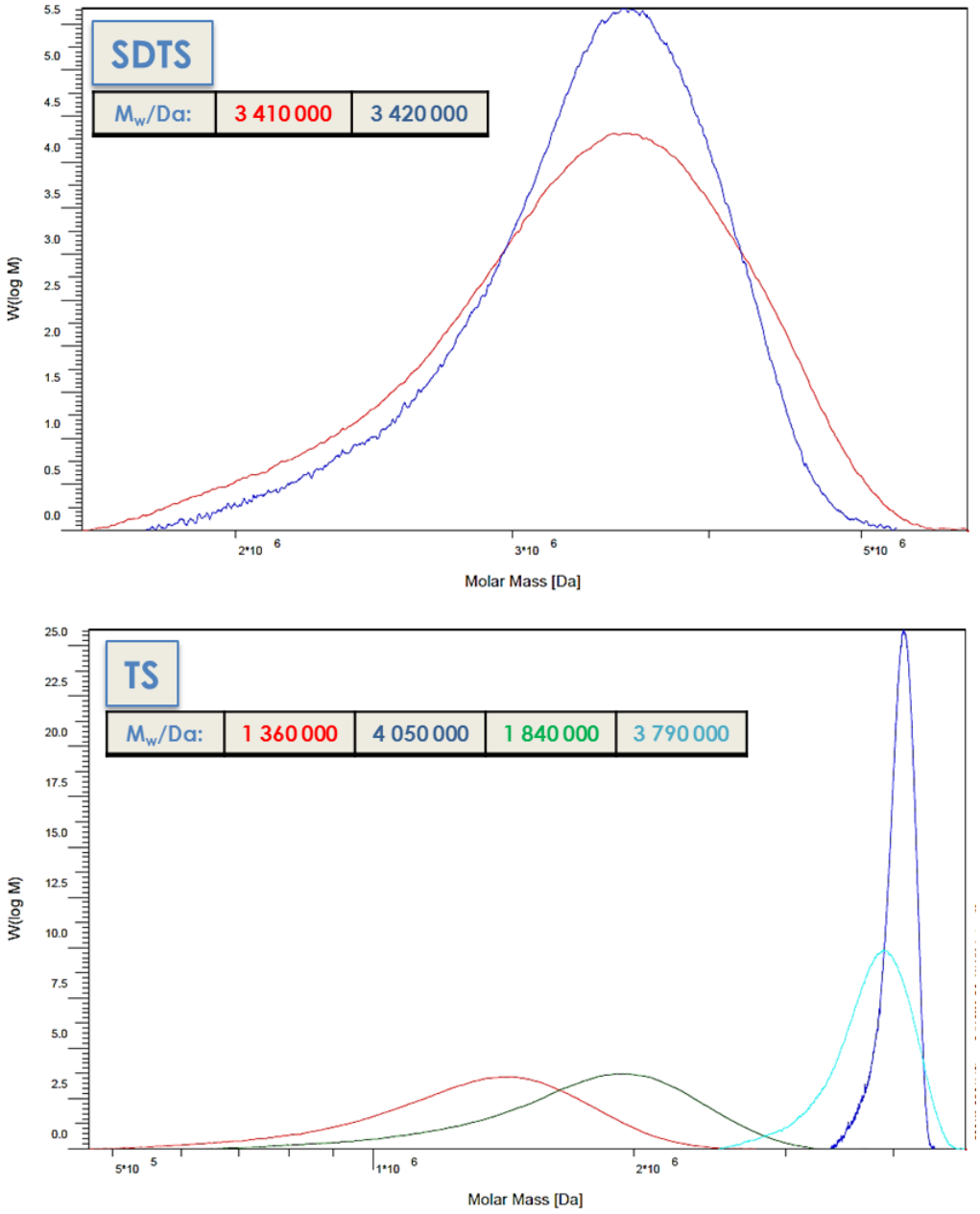

Fig. A0.2 Molecular weight distribution for SDTS and TS via GPC-MALS measured by PSS Polymer Standards Service GmbH; eluent: DMSO/5 g/L LiBr; dn/dc = 0.0559 mL/g. The analysis of the molecular weight and the polydispersity via GPC suggests a molecular degradation after the spray drying process. For the spray dried starch an average molecular weight $\overline{M_w}$ of 3 415 000 Da and a PDI of 2.81 was measured after dissolving in DMSO. In contrast, for the native starch no reproducible results (data ranges from 1 360 000 Da to 4 050 000 Da) could be obtained, due to an inadequate solubility of the sample in DMSO. This hampered dissolution behavior can be interpreted as a high molecular and dense structure.

A.3 Electrophoretic mobility of gold nanoparticles in TS and SDTS pastes

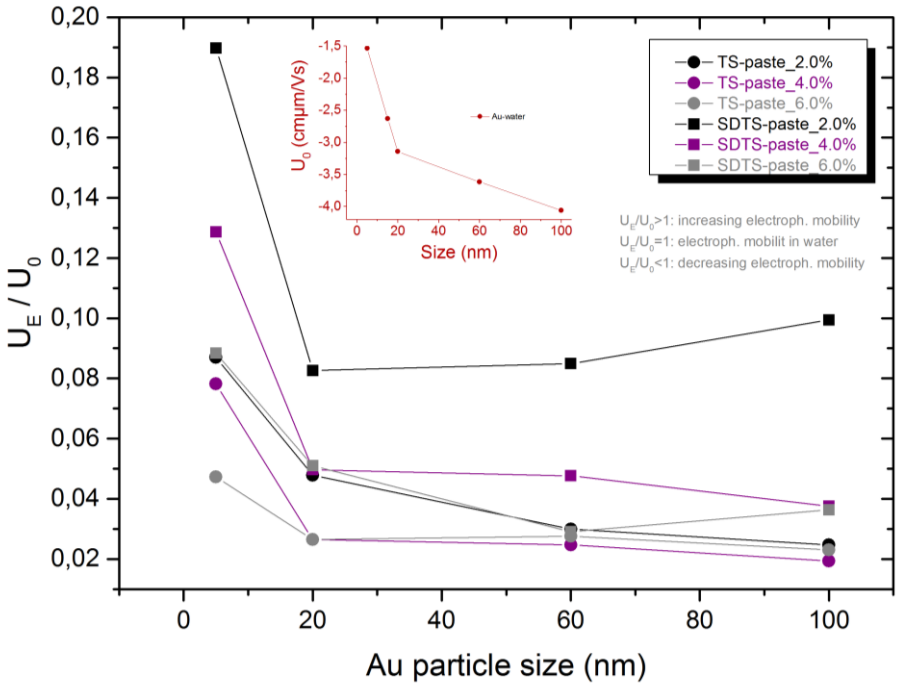

Fig. A0.3 Electrophoretic mobility of gold nanoparticles in different concentrated TS and SDTS pastes; normalized by the mobility in pure water and measured with Zetasizer Nano ZS (Malvern, Germany). Due to an increased surface charge, the electrophoretic mobility of the gold nanoparticles increases with increasing particle size in pure water. For both starch pastes the mobility decreases with increasing starch concentration. With TS paste as surrounding media, the mobility decreases with increasing particle size and converges to zero for 100 nm particles. In the corresponding SDTS pastes a significant faster mobility can be measured indicating the weaker network structures.

Appendix B Supporting information to chapter 7

B.1 VTP and amplitude sweep test of different tapioca starch concentrations

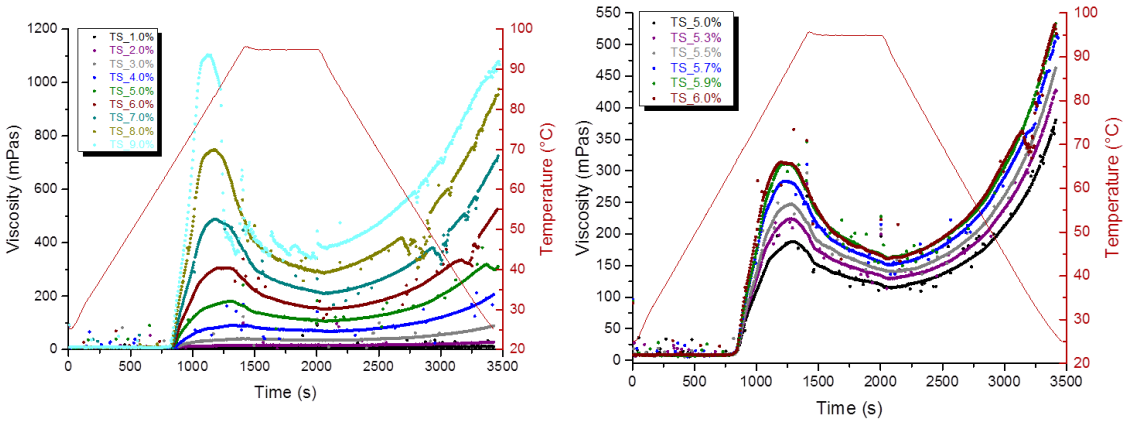

Fig. B0.1 VTP at $\dot{\gamma} = 200\ s^{-1}$ of native TS in different concentrations. Averages of threefold determination, standard deviation not shown. $T_{pasting}$ and T_{peak} are independent of starch concentration.

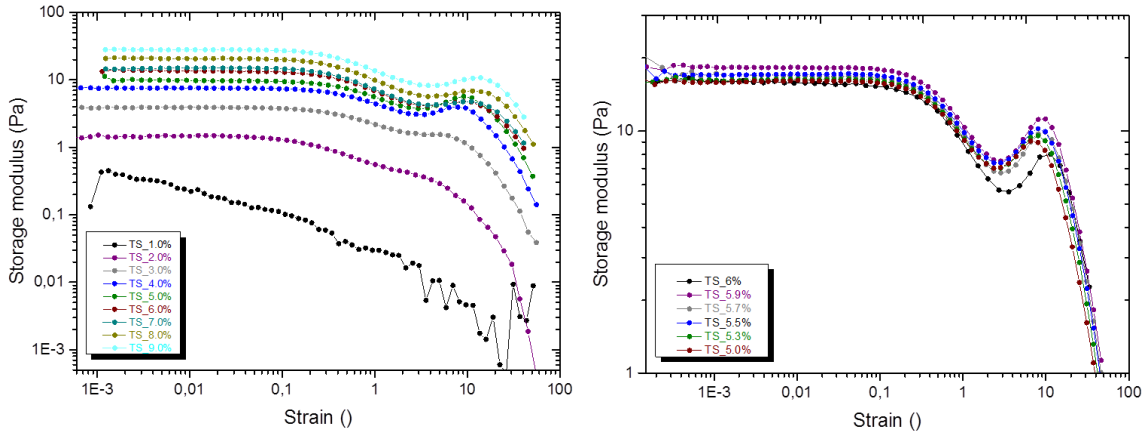

Fig. B0.2 Amplitude sweep tests at f = 1 Hz and T = 25 °C for native TS in different concentration. Averages of threefold determination, standard deviation not shown.

B.2 Temperature sweeps of starch–hydrocolloid mixtures

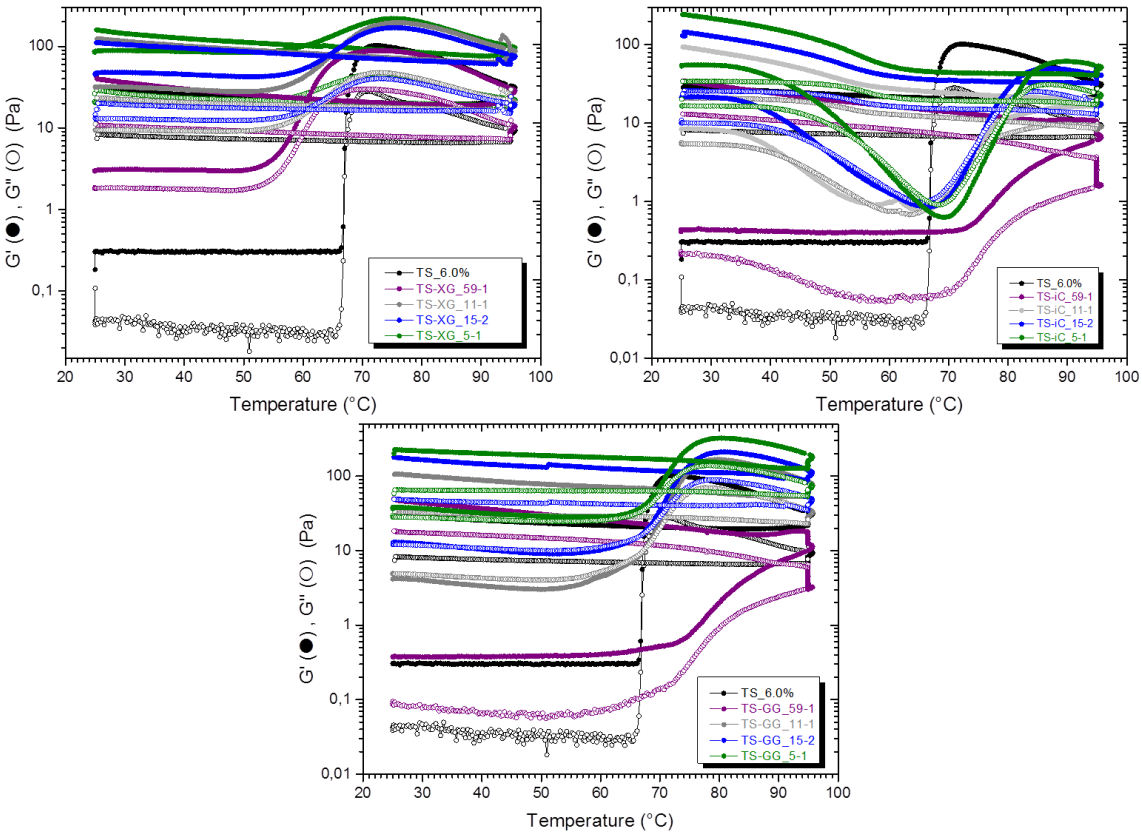

Fig. B0.3 Temperature sweep tests of G' and G'' at γ = 0.01 for the different starch-hydrocolloid mixtures. Averages of threefold determination, standard deviation not shown.

B.3 Viscosity–temperature profiles of starch–hydrocolloid mixtures

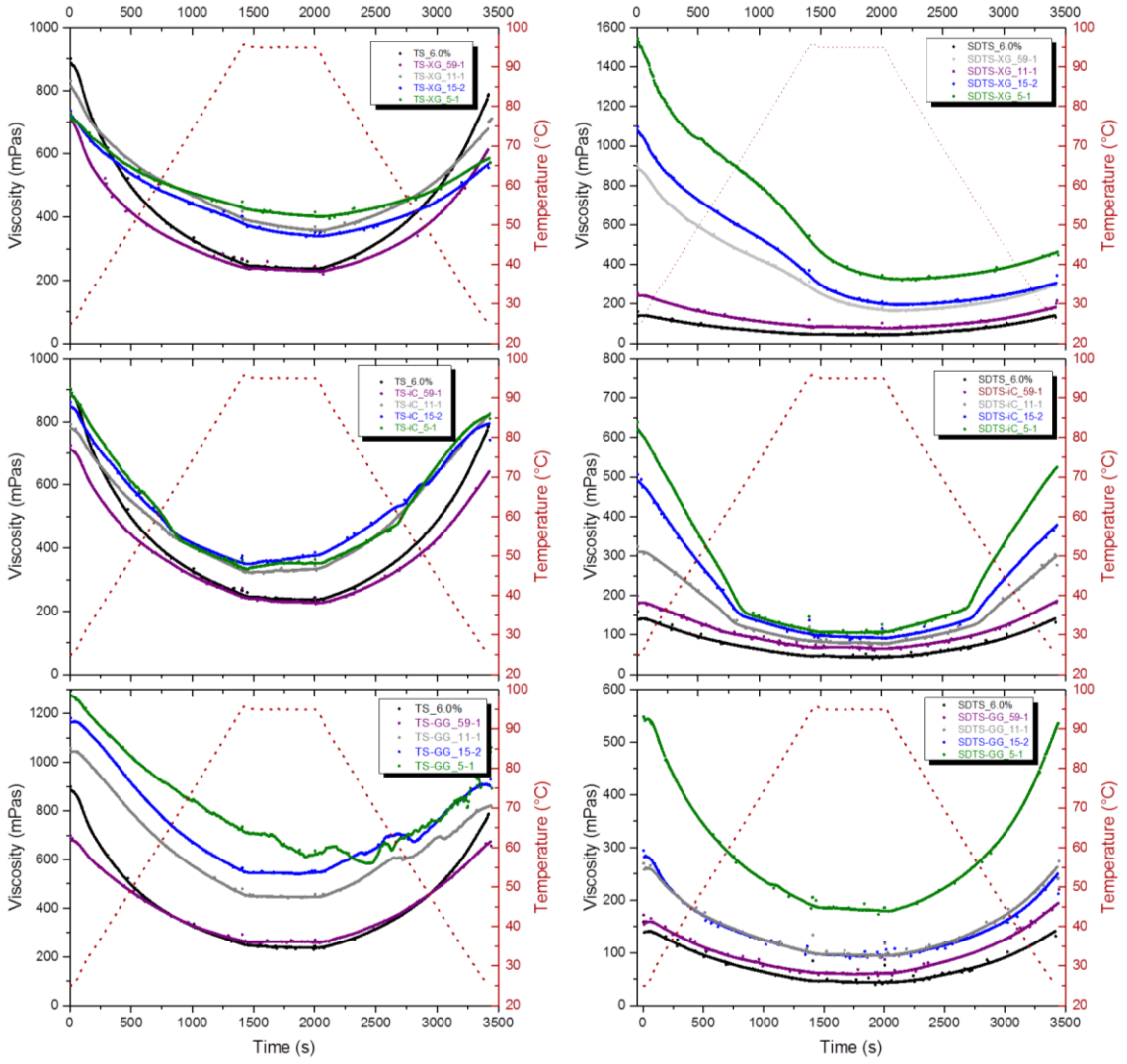

Fig. B0.4 VTP at $\dot{\gamma}$ = 287 s^{-1} (PP 40) of TS–XG, TS–ιC, and TS–GG after gelatinization (left) and SDTS–XG, SDTS–ιC, and SDTS–GG (right) in different mixing ratios. Averages of threefold determination, standard deviation not shown.

B.4 Viscosity in dependence of time during constant stirring of starch–hydrocolloid mixtures

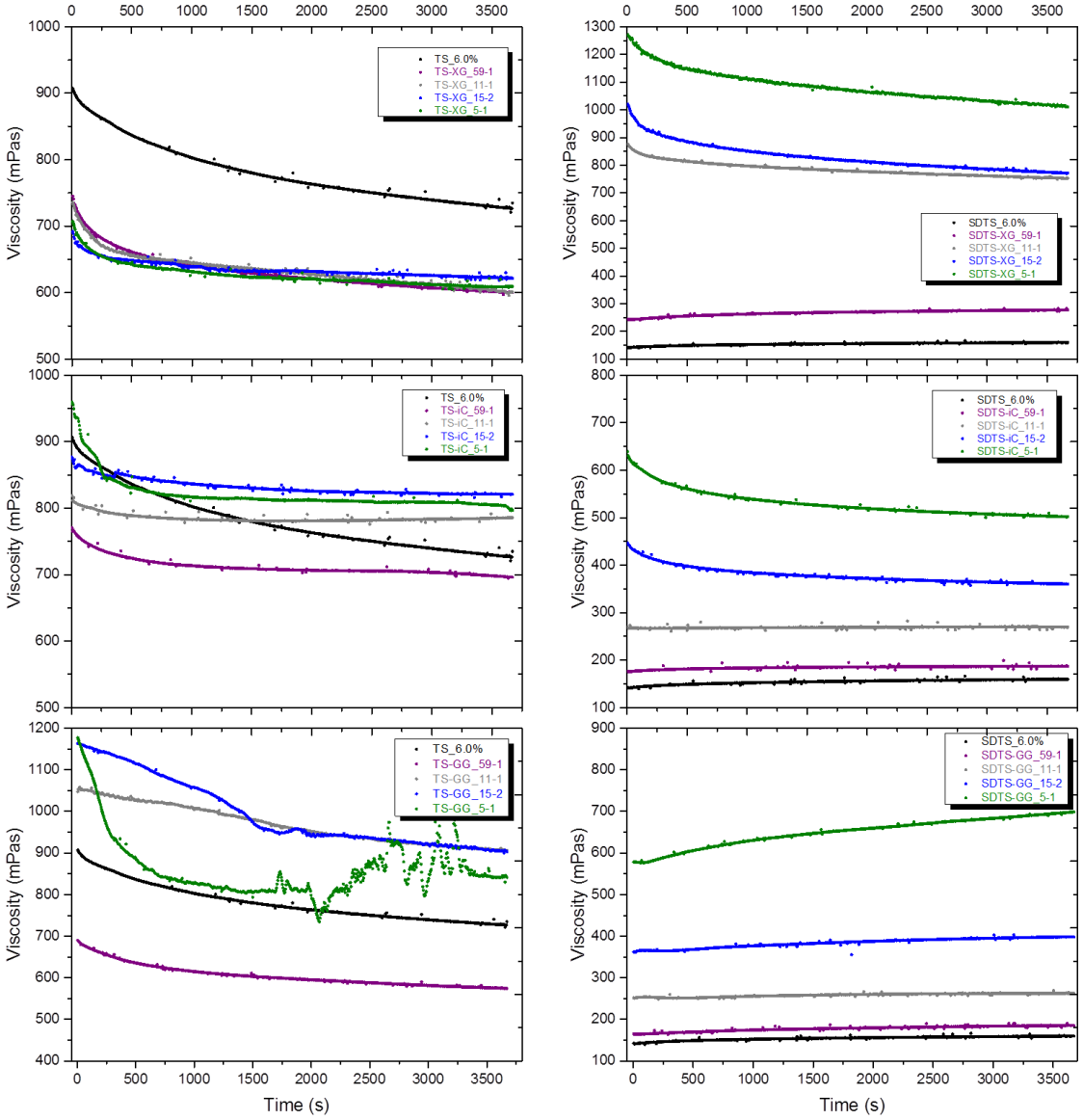

Fig. B0.5 Viscosity as function of time during constant stirring at $\dot{\gamma}$ = 274 s^{-1} (CP 40, 4°) of TS–XG, TS–ιC, and TS–GG after gelatinization (left) and SDTS–XG, SDTS–ιC, and SDTS–GG (right) in different mixing ratios. Averages of threefold determination, standard deviation not shown.

B.5 Creep experiments of starch–hydrocolloid mixtures

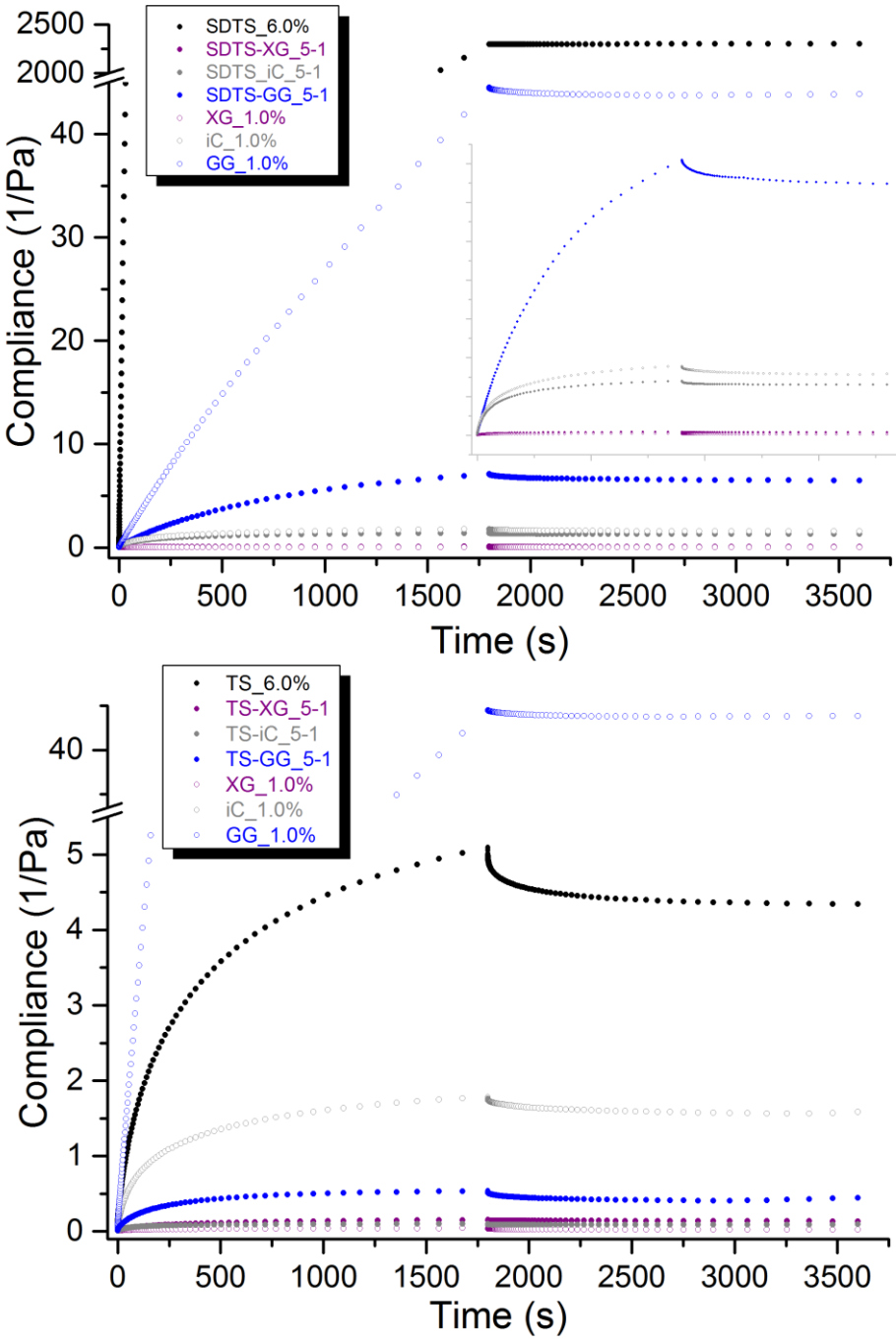

Fig. B0.6 Creep and creep recovery as lin-lin plot of compliance as function of time at constant shear stress σ = 0.15 Pa and T = 25 °C for SDTS (above) and TS (below) in 5–1 mixture as well as for the individual hydrocolloids. Averages of threefold determination, standard deviation not shown.

Bibliography

[1] Schwartz, D.; Whistler, R. L., Chapter 1 - History and Future of Starch. In *Starch (Third Edition)*, BeMiller, J.; Whistler, R., Eds. Academic Press: San Diego, 2009; pp 1-10.

[2] Sheldrake, P., Starch. In *Food stabilisers, thickeners and gelling agents*, Imeson, A., Ed. Wiley-Blackwell: Oxford, 2009; pp 293-324.

[3] Willett, J. L., Chapter 19 - Starch in Polymer Compositions1. In *Starch (Third Edition)*, BeMiller, J.; Whistler, R., Eds. Academic Press: San Diego, 2009; pp 715-743.

[4] BeMiller, J. N., Pasting, paste, and gel properties of starch–hydrocolloid combinations. *Carbohydrate Polymers* **2011,** *86* (2), 386-423.

[5] Breuninger, W. F.; Piyachomkwan, K.; Sriroth, K., Chapter 12 - Tapioca/Cassava Starch: Production and Use. In *Starch (Third Edition)*, BeMiller, J.; Whistler, R., Eds. Academic Press: San Diego, 2009; pp 541-568.

[6] Xie, S. X.; Liu, Q.; Cui, S. W., Starch modification and applications. In *Food carbohydrates: chemistry, physical properties, and applications Cui SW*, Steve, W. C., Ed. CRC Press: Boca Raton, 2005; pp 357-405.

[7] Aguilera, J.; Lillford, P., Structure–Property Relationships in Foods. In *Food Materials Science*, Aguilera, J.; Lillford, P., Eds. Springer New York: 2008; pp 229-253.

[8] Belitz, H.-D.; Grosch, W.; Schieberle, P., *Lehrbuch der Lebensmittelchemie*. Springer DE: 2008.

[9] Pomeranz, Y., *Functional properties of food components*. Academic Press: 2012.

[10] Stephen, A. M.; Phillips, G. O., *Food polysaccharides and their applications*. CRC Press: 2006; Vol. 160.

[11] Tolstoguzov, V., Food Polymers. In *Food Materials Science*, Aguilera, J.; Lillford, P., Eds. Springer New York: 2008; pp 21-44.

[12] Fennema, O. R., Water and ice. In *Food Chemistry*, Fennema, O. R., Ed. Marcel Dekker, Inc.: New York, 1996; pp 17-94.

[13] Saha, D.; Bhattacharya, S., Hydrocolloids as thickening and gelling agents in food: a critical review. *J Food Sci Technol* **2010,** *47* (6), 587-597.

[14] Phillips, G. O.; Williams, P. A., *Handbook of hydrocolloids*. Elsevier: 2009.

[15] Rinaudo, M., Main properties and current applications of some polysaccharides as biomaterials. *Polymer International* **2008,** *57* (3), 397-430.

[16] Morris, V. J., Gels. In *The Chemical Physics of Food*, Belton, P., Ed. Blackwell Science Ltd: 2007; pp 151-198.

[17] Nishinari, K.; Zhang, H.; Ikeda, S., Hydrocolloid gels of polysaccharides and proteins. *Current Opinion in Colloid & Interface Science* **2000,** *5* (3–4), 195-201.

[18] Rao, M. A., Rheological behavior of food gels. In *Rheology of Fluid, Semisolid, and Solid Foods*, Springer: 2014; pp 331-390.

[19] Taggart, P.; Mitchell, J.; Phillips, G.; Williams, P., Starch. In *Handbook of Hydrocolloids*, Phillips, G.; Williams, P., Eds. CRC Press: 2009; pp 108-141.

[20] Manners, D. J., Recent developments in our understanding of amylopectin structure. *Carbohydrate Polymers* **1989,** *11* (2), 87-112.

[21] Zobel, H. F., Molecules to Granules: A Comprehensive Starch Review. *Starch - Stärke* **1988,** *40* (2), 44-50.

[22] Buléon, A.; Colonna, P.; Planchot, V.; Ball, S., Starch granules: structure and biosynthesis. *InternationalJjournal of Biological Macromolecules* **1998,** *23* (2), 85-112.

[23] Hizukuri, S., Relationship between the distribution of the chain length of amylopectin and the crystalline structure of starch granules. *Carbohydrate Research* **1985,** *141* (2), 295-306.

[24] Miguel, Â. S. M.; Lobo, B. W. P.; da Costa Figueiredo, É. V.; Dellamora-Ortiz, G. M.; Martins-Meyer, T. S., Enzymes in bakery: current and future trends. In *Food Industry*, Muzzalupo, I., Ed. INTECH Open Access Publisher: 2013.

[25] Tetlow, I. J., Starch biosynthesis in developing seeds. *Seed Science Research* **2011,** *21* (01), 5-32.

[26] Parker, R.; Ring, S. G., Aspects of the Physical Chemistry of Starch. *Journal of Cereal Science* **2001,** *34* (1), 1-17.

[27] Jane, J.-l., Chapter 6 - Structural Features of Starch Granules II. In *Starch (Third Edition)*, BeMiller, J.; Whistler, R., Eds. Academic Press: San Diego, 2009; pp 193-236.

[28] Jacobs, H.; Delcour, J. A., Hydrothermal Modifications of Granular Starch, with Retention of the Granular Structure: A Review. *Journal of Agricultural and Food Chemistry* **1998,** *46* (8), 2895-2905.

[29] Jenkins, P.; Comerson, R.; Donald, A.; Bras, W.; Derbyshire, G.; Mant, G.; Ryan, A., In situ simultaneous small and wide angle x-ray scattering: A new technique to study starch gelatinization. *Journal of Polymer Science Part B: Polymer Physics* **1994,** *32* (8), 1579-1583.

[30] Buleon, A.; Colonna, P., Physicochemical behaviour of starch in food applications. In *The chemical physics of food*, Belton, P., Ed. Blackwell Publishing Ltd, Oxford: 2007; pp 20-67.

[31] Pérez, S.; Baldwin, P. M.; Gallant, D. J., Chapter 5 - Structural Features of Starch Granules I. In *Starch (Third Edition)*, BeMiller, J.; Whistler, R., Eds. Academic Press: San Diego, 2009; pp 149-192.

[32] Tester, R. F.; Karkalas, J.; Qi, X., Starch—composition, fine structure and architecture. *Journal of Cereal Science* **2004,** *39* (2), 151-165.

[33] Biliaderis, C. G., Chapter 8 - Structural Transitions and Related Physical Properties of Starch. In *Starch (Third Edition)*, BeMiller, J.; Whistler, R., Eds. Academic Press: San Diego, 2009; pp 293-372.

[34] Ratnayake, W. S.; Jackson, D. S., A new insight into the gelatinization process of native starches. *Carbohydrate Polymers* **2007,** *67* (4), 511-529.

[35] Ring, S. G., Some Studies on Starch Gelation. *Starch - Stärke* **1985,** *37* (3), 80-83.

[36] Marchant, J. L.; Blanshard, J. M. V., Studies of the Dynamics of the Gelatinization of Starch Granules Employing a Small Angle Light Scattering System. *Starch - Stärke* **1978,** *30* (8), 257-264.

[37] Swinkels, J. J. M., Composition and Properties of Commercial Native Starches. *Starch - Stärke* **1985,** *37* (1), 1-5.

[38] Bemiller, J. N., Starch modification: challenges and prospects. *Starch-Stärke* **1997,** *49* (4), 127-131.

[39] Chiu, C.-w.; Solarek, D., Chapter 17 - Modification of Starches. In *Starch (Third Edition)*, BeMiller, J.; Whistler, R., Eds. Academic Press: San Diego, 2009; pp 629-655.

[40] Bhandari, B. R.; Patel, K. C.; Chen, X. D., Spray drying of food materials—Process and product characteristics. In *Drying technologies in food processing*, Xiao Dong Chen, A. S. M., Ed. Blackwell Publishing Ltd: Oxford, 2008; pp 113-159.

[41] BüchiLabortechnikAG, Mini Sprühtrockner B-290. 2014.

[42] Atkins, P. W., *Physikalische chemie*. Wiley-VCH Verlag GmbH: Weinheim, 2004.

[43] Urlacher, B.; Noble, O., Xanthan gum. In *Thickening and gelling agents for food*, Imeson, A., Ed. Aspen Publisher: New York, 1999; pp 284-311.

[44] Sworn, G., Xanthan gum. In *Food Stabilisers, Thickeners and Gelling Agents*, Imeson, A., Ed. Wiley-Blackwell: Oxford, 2010; pp 325-342.

[45] Moorhouse, R.; Walkinshaw M, D.; Arnott, S., Xanthan Gum?Molecular Conformation and Interactions. In *Extracellular Microbial Polysaccharides*, AMERICAN CHEMICAL SOCIETY: 1977; Vol. 45, pp 90-102.

[46] Norton, I. T.; Goodall, D. M.; Frangou, S. A.; Morris, E. R.; Rees, D. A., Mechanism and dynamics of conformational ordering in xanthan polysaccharide. *Journal of Molecular Biology* **1984,** *175* (3), 371-394.

[47] Nordqvist, D.; Vilgis, T. A., Rheological study of the gelation process of agarose-based solutions. *Food Biophysics* **2011,** *6* (4), 450-460.

[48] Vilgis, T. A., Hydrocolloids between soft matter and taste: Culinary polymer physics. *International Journal of Gastronomy and Food Science* **2012,** *1* (1), 46-53.

[49] Edwards, S. F.; Vilgis, T., The Dynamics of the Glass Transition. *Physica Scripta* **1986,** *1986* (T13), 7.

[50] Russ, N.; Zielbauer, B. I.; Koynov, K.; Vilgis, T. A., Influence of Nongelling Hydrocolloids on the Gelation of Agarose. *Biomacromolecules* **2013,** *14* (11), 4116-4124.

[51] Russ, N.; Zielbauer, B. I.; Vilgis, T. A., Impact of sucrose and trehalose on different agarose-hydrocolloid systems. *Food Hydrocolloids* **2014,** *41* (0), 44-52.

[52] Blakemore, W. R.; Harpell, A. R., Carrageenan. In *Food stabilisers, thickeners and gelling agents*, Imeson, A. P., Ed. Wiley-Blackwell: Oxford, 2010; p 73.

[53] Piculell, L., Gelling carrageenans. In *Food polysaccharides and their applications*, Stephen, A. M., Phillips, Glyn O., Williams, Peter A., Ed. CRC Press: Boca Raton, FL, 2006; pp 239-287.

[54] Rees, D. A.; Welsh, E. J., Secondary and Tertiary Structure of Polysaccharides in Solutions and Gels. *Angewandte Chemie International Edition in English* **1977,** *16* (4), 214-224.

[55] Fox, J., Seed gums. In *Thickening and gelling agents for food*, Imeson, A. P., Ed. Aspen Publisher: Gaithersburg, 1999; pp 262-283.

[56] Chaisawang, M.; Suphantharika, M., Pasting and rheological properties of native and anionic tapioca starches as modified by guar gum and xanthan gum. *Food Hydrocolloids* **2006,** *20* (5), 641-649.

[57] Conde-Petit, B.; Pfirter, A.; Escher, F., Influence of xanthan on the rheological properties of aqueous starch-emulsifier systems. *Food Hydrocolloids* **1997,** *11* (4), 393-399.

[58] Eidam, D.; Kulicke, W.-M.; Kuhn, K.; Stute, R., Formation of Maize Starch Gels Selectively Regulated by the Addition of Hydrocolloids. *Starch - Stärke* **1995,** *47* (10), 378-384.

[59] Mandala, I.; Michon, C.; Launay, B., Phase and rheological behaviors of xanthan/amylose and xanthan/starch mixed systems. *Carbohydrate Polymers* **2004,** *58* (3), 285-292.

[60] Savary, G.; Handschin, S.; Conde-Petit, B.; Cayot, N.; Doublier, J.-L., Structure of polysaccharide-starch composite gels by rheology and confocal laser scanning microscopy: Effect of the composition and of the preparation procedure. *Food Hydrocolloids* **2008,** *22* (4), 520-530.

[61] Tischer, P. C. S. F.; Noseda, M. D.; de Freitas, R. A.; Sierakowski, M. R.; Duarte, M. E. R., Effects of iota-carrageenan on the rheological properties of starches. *Carbohydrate Polymers* **2006,** *65* (1), 49-57.

[62] Tolstoguzov, V., Thermodynamic considerations of starch functionality in foods. *Carbohydrate Polymers* **2003,** *51* (1), 99-111.

[63] Biliaderis, C. G.; Arvanitoyannis, I.; Izydorczyk, M. S.; Prokopowich, D. J., Effect of Hydrocolloids on Gelatinization and Structure Formation in Concentrated Waxy Maize and Wheat Starch Gels. *Starch - Stärke* **1997,** *49* (7-8), 278-283.

[64] Elias, H., *Macromolecules; Vol. 3: Physical Structures and Properties*. Wiley-VCH: Weinheim, 2008.

[65] Coupland, J. a. E., Rammilie, Polymers. In *An Introduction to the Physical Chemistry of Food*, Coupland, J., Ed. Springer: New-York, 2014; pp 107-130.

[66] Koltzenburg, S.; Maskos, M.; Nuyken, O., *Polymere: Synthese, Eigenschaften und Anwendungen*. Springer: 2014.

[67] Tolstoguzov, V., Phase behavior in mixed polysaccharide systems. In *Food polysaccharides and their applications*, Stephen, A. M.; Phillips, G. O., Eds. CRC Press: Boca Raton, 2006; pp 589-627.

[68] Manias, E. a. U., L.A., Thermodynamics of polymer blends. In *Polymer blends handbook*, Utracki, L. A. a. W., C.A., Ed. Springer: 2014; pp 171-289.

[69] Conde-Petit, B., *Structural features of starch in food: A polymeric and colloidal approach*. Laboratory of Food Chemistry and Food Technology: Zurich, 2001.

[70] De Gennes, P. G., *Scaling concepts in polymer physics*. Cornell University Press: New York, 1979.

[71] Kalichevsky, M. T.; Ring, S. G., Incompatibility of amylose and amylopectin in aqueous solution. *Carbohydrate Research* **1987,** *162* (2), 323-328.

[72] Tolstoguzov, V., Phase behaviour of macromolecular components in biological and food systems. *Food / Nahrung* **2000,** *44* (5), 299-308.

[73] Tolstoguzov, V., Some thermodynamic considerations in food formulation. *Food Hydrocolloids* **2003,** *17* (1), 1-23.

[74] Zasypkin, D.; Braudo, E.; Tolstoguzov, V., Multicomponent biopolymer gels. *Food Hydrocolloids* **1997,** *11* (2), 159-170.

[75] Miles, M. J.; Morris, V. J.; Orford, P. D.; Ring, S. G., The roles of amylose and amylopectin in the gelation and retrogradation of starch. *Carbohydrate research* **1985,** *135* (2), 271-281.

[76] Cairns, P.; Miles, M. J.; Morris, V. J.; Brownsey, G. J., X-Ray fibre-diffraction studies of synergistic, binary polysaccharide gels. *Carbohydrate Research* **1987,** *160* (0), 411-423.

[77] Fischer, P.; Windhab, E. J., Rheology of food materials. *Current Opinion in Colloid & Interface Science* **2011,** *16* (1), 36-40.

[78] Mezger, T., *Das Rheologie Handbuch: Für Anwender von Rotations-und Oszillations-Rheometern*. Vincentz Network GmbH & Company KG: Hannover, 2010.

[79] Ferry, J. D., *Viscoelastic properties of polymers*. John Wiley & Sons: 1980.

[80] Rao, M. A., Introduction: food rheology and structure. In *Rheology of Fluid, Semisolid, and Solid Foods*, Springer: 2014; pp 1-26.

[81] Rao, M. A., Flow and functional models for rheological properties of fluid foods. In *Rheology of Fluid, Semisolid, and Solid Foods*, Springer: 2014; pp 27-61.

[82] Graessley, W., The entanglement concept in polymer rheology. In *The Entanglement Concept in Polymer Rheology*, Springer Berlin Heidelberg: 1974; Vol. 16, pp 1-179.

[83] Vilgis, T. A., Soft matter food physics—the physics of food and cooking. *Reports on Progress in Physics* **2015,** *78* (12), 124602.

[84] (a) Einstein, A., Eine neue Bestimmung der Moleküldimensionen. *Annalen der Physik* **1906,** *324* (2), 289-306; (b) Einstein, A., Berichtigung zu meiner Arbeit: „Eine neue Bestimmung der Moleküldimensionen”. *Annalen der Physik* **1911,** *339* (3), 591-592.

[85] Ross-Murphy, S. B., Rheological methods. In *Physical techniques for the study of food biopolymers*, Ross-Murphy, S. B., Ed. Springer: 1994; pp 343-392.

[86] Lin, Y.-H., *Polymer viscoelasticity: basics, molecular theories and experiments*. World Scientific Publishing Co. Pte. Ltd.: 2003.

[87] Rao, M. A., Rheology of Food Gum and Starch Dispersions. In *Rheology of Fluid, Semisolid, and Solid Foods*, Springer US: 2014; pp 161-229.

[88] Whistler, R. L., Introduction to industrial gums. In *Industrial gums: polysaccharides and their derivatives*, BeMiller, J. N.; Whistler, R. L., Eds. Academic Press: 1993; pp 1-20.

[89] Dickie, R., Heterogeneous polymer–polymer composites. I. Theory of viscoelastic properties and equivalent mechanical models. *Journal of Applied Polymer Science* **1973,** *17* (1), 45-63.

[90] Manson, J. A.; Sperling, L. H., *Polymer blends and composites*. Springer Science & Business Media: 1976.

[91] Nielsen, L.; Landel, R., Particulate-filled polymers. In *Mechanical properties of polymers and composites*, Marcel Dekker Inc New York: 1994; Vol. 2, pp 377-460.

[92] Rao, M. A.; Okechukwu, P. E.; Da Silva, P. M. S.; Oliveira, J. C., Rheological behavior of heated starch dispersions in excess water: role of starch granule. *Carbohydrate Polymers* **1997,** *33* (4), 273-283.

[93] Cardona, J. A. R.; Iriart, C. H.; Herrera, M. L., *Applications of Confocal Laser Scanning Microscopy (CLSM) in Foods*. INTECH Open Access Publisher: 2013.

[94] Dürrenberger, M. B.; Handschin, S.; Conde-Petit, B.; Escher, F., Visualization of Food Structure by Confocal Laser Scanning Microscopy (CLSM). *LWT - Food Science and Technology* **2001,** *34* (1), 11-17.

[95] Claxton, N. S.; Fellers, T. J.; Davidson, M. W., Laser scanning confocal microscopy. *Department of Optical Microscopy and Digital Imaging, Florida State University, Tallahassee, www.olympusconfocal.com/theory/LSCMIntro.pdf* **2006**.

[96] van de Velde, F.; van Riel, J.; Tromp, R. H., Visualisation of starch granule morphologies using confocal scanning laser microscopy (CSLM). *Journal of the Science of Food and Agriculture* **2002,** *82* (13), 1528-1536.

[97] Hans Tromp, R.; van de Velde, F.; van Riel, J.; Paques, M., Confocal scanning light microscopy (CSLM) on mixtures of gelatine and polysaccharides. *Food Research International* **2001,** *34* (10), 931-938.

[98] Höhne, G.; Hemminger, W. F.; Flammersheim, H.-J., *Differential scanning calorimetry*. Springer: 2003.

[99] Schärtl, W., *Light scattering from polymer solutions and nanoparticle dispersions*. Springer Science & Business Media: 2007.

[100] Mukhopadhyay, A.; Granick, S., Micro-and nanorheology. *Current opinion in colloid & interface science* **2001,** *6* (5), 423-429.

[101] Rochas, C.; Geissler, E., Measurement of Dynamic Light Scattering Intensity in Gels. *Macromolecules* **2014,** *47* (22), 8012-8017.

[102] Limbach, T. Tracerdiffusion und Rheologie von Polymerhydrogelen. Johannes-Gutenberg Universität, Mainz, 2015.

[103] Finkelstein, R. S.; Sarko, A., Anisotropic scattering by single starch granules. II. Layered granule structure. *Biopolymers* **1972,** *11* (4), 881-892.

[104] Russ, N.; Zielbauer, B. I.; Ghebremedhin, M.; Vilgis, T. A., Pre-gelatinized tapioca starch and its mixtures with xanthan gum and ι-carrageenan. *Food Hydrocolloids* **2016,** *56*, 180-188.

[105] Fannon, J. E.; BeMiller, J. N., Structure of corn starch paste and granule remnants revealed by low-temperature scanning electron microscopy after cryopreparation. *Cereal chem* **1992,** *69* (4), 456-460.

[106] (a) Atkin, N. J.; Abeysekera, R. M.; Cheng, S. L.; Robards, A. W., An experimentally-based predictive model for the separation of amylopectin subunits

during starch gelatinization. *Carbohydrate Polymers* **1998,** *36* (2–3), 173-192; (b) Atkin, N. J.; Abeysekera, R. M.; Robards, A. W., The events leading to the formation of ghost remnants from the starch granule surface and the contribution of the granule surface to the gelatinization endotherm. *Carbohydrate Polymers* **1998,** *36* (2–3), 193-204.

[107] Flint, O., *Food microscopy: a manual of practical methods, using optical microscopy*. Garland Science: 1994; Vol. 30.

[108] Obanni, M.; BeMiller, J. N., Ghost microstructures of starch from different botanical sources. *Cereal chemistry* **1996,** *73* (3), 333-337.

[109] Zhang, B.; Dhital, S.; Flanagan, B. M.; Gidley, M. J., Mechanism for starch granule ghost formation deduced from structural and enzyme digestion properties. *Journal of agricultural and food chemistry* **2014,** *62* (3), 760-771.

[110] Garcia, V.; Colonna, P.; Lourdin, D.; Buleon, A.; Bizot, H.; Ollivon, M., Thermal transitions of cassava starch at intermediate water contents. *Journal of Thermal Analysis* **1996,** *47* (5), 1213-1228.

[111] Donovan, J. W., Phase transitions of the starch–water system. *Biopolymers* **1979,** *18* (2), 263-275.

[112] Cooke, D.; Gidley, M. J., Loss of crystalline and molecular order during starch gelatinisation: origin of the enthalpic transition. *Carbohydrate research* **1992,** *227*, 103-112.

[113] Morris, V. J., Starch gelation and retrogradation. *Trends in Food Science & Technology* **1990,** *1* (0), 2-6.

[114] Carrillo-Navas, H.; Avila-de la Rosa, G.; Gómez-Luría, D.; Meraz, M.; Alvarez-Ramirez, J.; Vernon-Carter, E. J., Impact of ghosts on the viscoelastic response of gelatinized corn starch dispersions subjected to small strain deformations. *Carbohydrate Polymers* **2014,** *110* (0), 156-162.

[115] Schiedt, B.; Baumann, A.; Conde-Petit, B.; Vilgis, T. A., Short-and Long-Range Interactions Governing the Viscoelastic Properties during Wheat Dough and Model Dough Development. *Journal of Texture Studies* **2013,** *44* (4), 317-332.

[116] Genovese, D. B.; Rao, M. A., Role of Starch Granule Characteristics (volume fraction, rigidity, and fractal dimension) on Rheology of Starch Dispersions With and Without Amylose. *Cereal Chemistry Journal* **2003,** *80* (3), 350-355.

[117] (a) Hyun, K.; Kim, S. H.; Ahn, K. H.; Lee, S. J., Large amplitude oscillatory shear as a way to classify the complex fluids. *Journal of Non-Newtonian Fluid Mechanics* **2002,** *107* (1–3), 51-65; (b) Hyun, K.; Wilhelm, M.; Klein, C. O.; Cho, K. S.; Nam, J. G.; Ahn, K. H.; Lee, S. J.; Ewoldt, R. H.; McKinley, G. H., A review of nonlinear oscillatory shear tests: Analysis and application of large amplitude oscillatory shear (LAOS). *Progress in Polymer Science* **2011,** *36* (12), 1697-1753.

[118] Sikora, M.; Kowalski, S.; Tomasik, P., Binary hydrocolloids from starches and xanthan gum. *Food Hydrocolloids* **2008,** *22* (5), 943-952.

[119] Roger, P.; Bello-Perez, L. A.; Colonna, P., Contribution of amylose and amylopectin to the light scattering behaviour of starches in aqueous solution. *Polymer* **1999,** *40* (25), 6897-6909.

[120] Joosten, J. G.; McCarthy, J. L.; Pusey, P. N., Dynamic and static light scattering by aqueous polyacrylamide gels. *Macromolecules* **1991,** *24* (25), 6690-6699.

[121] LeBel, R. G.; Goring, D. A. I., Density, Viscosity, Refractive Index, and Hygroscopicity of Mixtures of Water and Dimethyl Sulfoxide. *Journal of Chemical & Engineering Data* **1962,** *7* (1), 100-101.

[122] Biliaderis, C. G.; Page, C. M.; Maurice, T. J.; Juliano, B. O., Thermal characterization of rice starches: A polymeric approach to phase transitions of granular starch. *Journal of Agricultural and Food Chemistry* **1986,** *34* (1), 6-14.

[123] Donald, A.; Waigh, T.; Jenkins, P.; Gidley, M.; Debet, M.; Smith, A., Internal structure of starch granules revealed by scattering studies. **1997**.

[124] Zobel, H. F.; Stephen, A. M., Starch: Structure, analysis, and application. In *Food polysaccharides and their applications*, Stephen, A. M.; Phillips, G. O.; Williams, P. A., Eds. 2006; pp 25-85.

[125] Huang, Z.-Q.; Lu, J.-P.; Li, X.-H.; Tong, Z.-F., Effect of mechanical activation on physico-chemical properties and structure of cassava starch. *Carbohydrate Polymers* **2007,** *68* (1), 128-135.

[126] Bahnassey, Y. A.; Breene, W. M., Rapid Visco-Analyzer (RVA) Pasting Profiles of Wheat, Corn, Waxy Corn, Tapioca and Amaranth Starches (A. hypochondriacus and A cruentus) in the Presence of Konjac Flour, Gellan, Guar, Xanthan and Locust Bean Gums. *Starch - Stärke* **1994,** *46* (4), 134-141.

[127] Sajjan, S. U.; Rao, M. R., Effect of hydrocolloids on the rheological properties of wheat starch. *Carbohydrate polymers* **1987,** *7* (5), 395-402.

[128] Liehr, M.; Kulicke, W.-M., Rheological examination of the influence of hydrocolloids on the freeze-thaw-stability of starch gels. *Starch* **1996**.

[129] Shi, X.; BeMiller, J. N., Effects of food gums on viscosities of starch suspensions during pasting. *Carbohydrate Polymers* **2002,** *50* (1), 7-18.

[130] Heyman, B.; De Vos, W. H.; Van der Meeren, P.; Dewettinck, K., Gums tuning the rheological properties of modified maize starch pastes: Differences between guar and xanthan. *Food Hydrocolloids* **2014,** *39*, 85-94.

[131] Giboreau, A.; Cuvelier, G.; Launay, B., Rheological behaviour of three biopolymer/water systems, with emphasis on yield stress and viscoelastic properties. *Journal of Texture Studies* **1994,** *25* (2), 119-138.

[132] Gonera, A.; Cornillon, P., Gelatinization of Starch/Gum/Sugar Systems Studied by using DSC, NMR, and CSLM. *Starch - Stärke* **2002,** *54* (11), 508-516.

[133] Krüger, A.; Ferrero, C.; Zaritzky, N. E., Modelling corn starch swelling in batch systems: effect of sucrose and hydrocolloids. *Journal of Food Engineering* **2003,** *58* (2), 125-133.

[134] Funami, T.; Kataoka, Y.; Omoto, T.; Goto, Y.; Asai, I.; Nishinari, K., Food hydrocolloids control the gelatinization and retrogradation behavior of starch. 2a. Functions of guar gums with different molecular weights on the gelatinization behavior of corn starch. *Food Hydrocolloids* **2005,** *19* (1), 15-24.

[135] Crossland, L.; Favor, H., Starch gelatinization studies. II. A method for showing the stages in swelling of starch during heating in the amylograph. *Cereal Chem* **1948,** *25*, 213-220.

[136] Winter, H. H., Can the gel point of a cross-linking polymer be detected by the G′ – G″ crossover? *Polymer Engineering & Science* **1987,** *27* (22), 1698-1702.

[137] Labropoulos, K. C.; Niesz, D. E.; Danforth, S. C.; Kevrekidis, P. G., Dynamic rheology of agar gels: theory and experiments. Part I. Development of a rheological model. *Carbohydrate Polymers* **2002,** *50* (4), 393-406.

[138] Joseph, D.; Riccius, O.; Arney, M., Shear-wave speeds and elastic moduli for different liquids. Part 2. Experiments. *Journal of Fluid Mechanics* **1986,** *171*, 309-338.

[139] Tester, R.; Sommerville, M., The effects of non-starch polysaccharides on the extent of gelatinisation, swelling and α-amylase hydrolysis of maize and wheat starches. *Food Hydrocolloids* **2003,** *17* (1), 41-54.

[140] Alloncle, M.; Doublier, J.-L., Viscoelastic properties of maize starch/hydrocolloid pastes and gels. *Food Hydrocolloids* **1991,** *5* (5), 455-467.

[141] Kulicke, W.-M.; Eidam, D.; Kath, F.; Kix, M.; Kull, A. H., Hydrocolloids and Rheology: Regulation of Visco-elastic Characteristics of Waxy Rice Starch in Mixtures with Galactomannans. *Starch - Stärke* **1996,** *48* (3), 105-114.

[142] Chaisawang, M.; Suphantharika, M., Effects of guar gum and xanthan gum additions on physical and rheological properties of cationic tapioca starch. *Carbohydrate Polymers* **2005,** *61* (3), 288-295.

[143] Funami, T.; Noda, S.; Hiroe, M.; Asai, I.; Ikeda, S.; Nishinari, K., Functions of iota-carrageenan on the gelatinization and retrogradation behaviors of corn starch in the presence or absence of various salts. *Food Hydrocolloids* **2008,** *22* (7), 1273-1282.

[144] Kim, C.; Yoo, B., Rheological properties of rice starch–xanthan gum mixtures. *Journal of Food Engineering* **2006,** *75* (1), 120-128.

[145] (a) Lai, V.-F.; Huang, A.-L.; Lii, C.-Y., Rheological properties and phase transition of red algal polysaccharide–starch composites. *Food Hydrocolloids* **1999,** *13* (5), 409-418; (b) Lai, V.; Lii, C., influences of starch fillers on the viscoelasticity of agarose and kappa-carrageenan gels. *Food science and agricultural chemistry* **2003**.

[146] Rao, M. A.; Tattiyakul, J., Granule size and rheological behavior of heated tapioca starch dispersions. *Carbohydrate Polymers* **1999,** *38* (2), 123-132.

[147] Quemada, D.; Flaud, P.; Jezequel, P., Rheological properties and flow of concentrated disperse media i-modelling of steady and unsteady behavior. *Chemical Engineering Communications* **1985,** *32* (1-5), 61-83.

[148] Che, L.-m.; Li, D.; Wang, L.-j.; Özkan, N.; Chen, X. D.; Mao, Z.-h., Rheological properties of dilute aqueous solutions of cassava starch. *Carbohydrate Polymers* **2008,** *74* (3), 385-389.

[149] Chen, C. R.; Ramaswamy, H. S., Rheology of tapioca starch. *Food Research International* **1999,** *32* (5), 319-325.

[150] Bhandari, P. N.; Singhal, R. S., Effect of succinylation on the corn and amaranth starch pastes. *Carbohydrate Polymers* **2002,** *48* (3), 233-240.

[151] Closs, C.; Conde-Petit, B.; Roberts, I.; Tolstoguzov, V.; Escher, F., Phase separation and rheology of aqueous starch/galactomannan systems. *Carbohydrate Polymers* **1999,** *39* (1), 67-77.

[152] Mandala, I. G.; Bayas, E., Xanthan effect on swelling, solubility and viscosity of wheat starch dispersions. *Food Hydrocolloids* **2004,** *18* (2), 191-201.

[153] German, M.; Blumenfeld, A.; Guenin, Y. V.; Yuryev, V.; Tolstoguzov, V., Structure formation in systems containing amylose, amylopectin, and their mixtures. *Carbohydrate Polymers* **1992,** *18* (1), 27-34.

[154] Maurer, S.; Junghans, A.; Vilgis, T. A., Impact of xanthan gum, sucrose and fructose on the viscoelastic properties of agarose hydrogels. *Food Hydrocolloids* **2012,** *29* (2), 298-307.

[155] (a) Chantaro, P.; Pongsawatmanit, R., Influence of sucrose on thermal and pasting properties of tapioca starch and xanthan gum mixtures. *Journal of Food Engineering* **2010,** *98* (1), 44-50; (b) Sudhakar, V.; Singhal, R. S.; Kulkarni, P. R., Effect of sucrose on starch—hydrocolloid interactions. *Food Chemistry* **1995,** *52* (3), 281-284.

[156] (a) Sudhakar, V.; Singhal, R. S.; Kulkarni, P. R., Studies on starch-hydrocolloid interactions: effect of salts. *Food Chemistry* **1995,** *53* (4), 405-408; (b) Sudhakar, V.; Singhal, R. S.; Kulkarni, P. R., Effect of salts on interactions of starch with guar gum. *Food Hydrocolloids* **1996,** *10* (3), 329-334.